RESEARCH & REVIEWS IN SCIENCE AND MATHEMATICS

December 2022

Editors

Prof. Dr. Alpaslan DAYANGAÇ

Prof. Dr. Hasan AKGÜL

Doç. Dr. Mustafa SEVİNDİK

gece kitaplığı

İmtiyaz Sahibi / Publisher • Yaşar Hız
Genel Yayın Yönetmeni / Editor in Chief • Eda Altunel
Kapak & İç Tasarım / Cover & Interior Design • Gece Kitaplığı
Editörler / Edıtors • Prof. Dr. Alpaslan DAYANGAÇ
Prof. Dr. Hasan AKGÜL
Doç. Dr. Mustafa SEVİNDİK
Birinci Basım / First Edition • © Aralık 2022
ISBN • 978-625-430-572-6

Gece Kitaplığı / Gece Publishing
Türkiye Adres / Turkey Address: Kızılay Mah. Fevzi Çakmak 1. Sokak Ümit Apt. No: 22/A Çankaya / Ankara / TR
Telefon / Phone: +90 312 384 80 40
web: www.gecekitapligi.com
e-mail: gecekitapligi@gmail.com

Baskı & Cilt / Printing & Volume
Sertifika / Certificate No: 47083

Research & Reviews in Science and Mathematics

December 2022

Editors

Prof. Dr. Alpaslan DAYANGAÇ
Prof. Dr. Hasan AKGÜL
Doç. Dr. Mustafa SEVİNDİK

CONTENTS

CHAPTER 1

COMPLEX SCALAR FIELD IN UNIMODULAR F(R,T) GRAVITY

Melis ULU DOĞRU[1]

Hüseyin AYDIN[2]

1 Assoc. Prof. Dr., Çanakkale Onsekiz Mart University, Science Faculty, Department of Physics. Çanakkale, TURKEY, melisulu@comu.edu.tr

2 Dr., Çanakkale Onsekiz Mart University, School of Graduate Studies, Department of Physics. Çanakkale, TURKEY, huseynaydin@gmail.com

1. INTRODUCTION

Massive bodies tend to move towards each other by accelerating due to their nature (Linde, 1990). The scientific equivalent of this behavior is called “gravity”. Due to mass and energy equivalent situation, energy sources such as light can also be a source which will cause gravitational interaction, even if they are massless (Clifford, 2006). Gravitational force, one of the fundamental interactions which can be measured in nature, is also the weakest of them. Mankind's attempt to understand gravity in an effort to understand nature dates back to the 4th century BC. In the beginning, this effort is mostly about understanding the movements of objects at a certain height from the ground towards the ground surface and movements of celestial objects seen in sky around Earth. Newton's theory of gravitation, which found many applications with its very simple lines, left its place to Einstein's General Relativity (Clifford, 2006). However, it can still be used in calculations that do not require relativity, where it can be used today. Examining the universe from its beginning to its future passes through a set of coordinates that consider time as a coordinate. In this sense, it is necessary to define a non-absolute concept of time, and thus relativity is an indifferent condition for understanding the evolution of the universe. Einstein's theory is a larger-scale theory of gravity that incorporates relativistic effects, including time as a relative coordinate of the coordinate system that expresses the universe and its behavior mathematically (Einstein, 1916). The theory, which successfully provided observational tests of the Solar System, was considered as the strongest gravity theory until the expansion of the universe was discovered by Hubble (Carroll, 2004).

Observations of distant galaxies published by Hubble in 1929 showed that galaxies were moving away from each other at a speed proportional to the distance between them (Hubble, 1929). This result shows that universe has an expanding and dynamic structure. This behavior is called Hubble's Law in the literature. In fact, Lemaître had also dynamically interpreted the cosmological model which describes the universe using Einstein's theory of relativity.

International scientific authorities have decided to refer to this law as “Hubble-Lemaître Law” as of 2018 (Simon, 2020).

Although Einstein's General Relativity can explain the expanding structure of the universe with some assumptions, it has left its place to the search for a consistent and stronger theory of gravity due to the cosmological constant problem and some similar problems (Weinberg, 1989).

The cosmological constant term, which was added manually to the field equations in Einstein's General Relativity to prevent collapsing structure of the universe model and to propose a static universe model, was defined as "my biggest mistake" by Einstein himself. This term, which was added manually, gave rise to the fact that the universe was not static but expanding. Coherent explanations of the expanding universe models required an explanatory note that was naturally added to the field equations from the variation process (Clifton *et al.,* 2012). Therefore, this situation has led scientists to consider the Lagrangian function differences and/or additional field generating factors that would enable such a term to be added.

Unimodular gravitational theories are a group of theories developed to ensure that expanding structure of universe is mathematically and directly related to field equations of cosmological constant according to Einstein's General Relativity (Buffalo *et al.,* 2015). Firstly, Unimodular Gravity was proposed, which solves the cosmological constant origination in Einstein's General Relativity (Rubio *et al.,* 2022). Subsequently, other unimodular modified theories have been developed to consider that geometry-dependent Lagrangian function is not directly dependent on the Ricci scalar, but on a function of this or other cosmological objects. On the other hand, Unimodular f(R,T) theory includes the cosmological constant term added as an integral constant in viable f(R,T) models proposed in f(R,T) theory, with a constraint on metric potentials and its determinant, which is a mathematically natural field (Rajabi and Nozari, 2017). It is theory which incorporates it into its equations. The success of f(R,T) theory makes Unimodular f(R,T) theory more important to research.

In this study, it is aimed to investigate how the complex scalar field is distributed within the scope of Unimodular f(R,T) theory. This study has been organized in the following form: Firstly, the basic equations of the Unimodular f(R,T) theory are remembered in Section 2. The field equations and their solutions of Unimodular f(R,T) theory for cylindrically symmetrical space-time filled with scalar field are obtained in Chapter 3. Finally, obtained solutions and results are discussed by comparing with other results in the literature.

2. UNIMODULAR f(R,T) GRAVITY

The f(R,T) theory of gravity uses Lagrangian, which depends on a general function of Ricci scalar and trace of energy-momentum tensor (Harko *et al.,* 2011). Unimodular f(R,T) theory was developed by Rajabi and Nozari (2017). They studied the Friedmann-Robertson-Walker cosmologies by choosing the energy-momentum tensor as perfect fluid (Rajabi and Nozari, 2017). Although there are many studies in the literature about f(R,T) theory, there are a small number of studies on the Unimodular f(R,T) theory (Alvarenga *et al.,* 2013; Houndjo, 2012; Reddy, *et al.*, 2012; Sharif and Zubair, 2012; Barrientos and Rubilar, 2014; Azizi, 2013; Moraes and Santos, 2016). In unimodular theories, the determinant of the metric tensor satisfies the condition $\sqrt{-g} = \epsilon$ (ϵ is any constant). In Unimodular f(R,T) theory, the action function is defined as:

$$S = \frac{1}{2}\int d^4x\left[\sqrt{-g}\, f(R,T) - 2\lambda\left(\sqrt{-g} - \epsilon\right)\right] + S_m \qquad (1)$$

where λ is Lagrange multiplier and S_m is action function of cosmic matter (Rajabi and Nozari, 2017). From Eq.(1) and principle of variation ($\delta S = 0$), field equation of unimodular f(R,T) theory is obtained as follows:

$$\frac{df(R,T)}{dR}R_{ik} - \frac{1}{2}g_{ik}f(R,T) + (g_{ik}\,\square - \nabla_i\nabla_k)\frac{df(R,T)}{dR} + \lambda g_{ik} - T_{ik} + \frac{df(R,T)}{dT}(T_{ik} + \Theta_{ik}) = 0 \quad (2)$$

where $\Theta_{ik} = g^{ab}\frac{\delta T_{ab}}{\delta g^{ik}}$, $f_{,R}(R,T) = \frac{df(R,T)}{dR}$ and $f_{,T}(R,T) = \frac{df(R,T)}{dT}$ (Rajabi ve Nozari, 2017). Trace of Eq.(2) is obtained as:

$$(R + 3\square)\frac{df(R,T)}{dR} - 2f(R,T) + \lambda - T + \frac{df(R,T)}{dT}(T + \Theta) = 0. \quad (3)$$

From Eqs.(2) and (4), it could be written general form of the field equation in the following form (Rajabi and Nozari, 2017):

$$\left[R_{ik} - \tfrac{1}{3}g_{ik}R - \nabla_i\nabla_k\right]\frac{df(R,T)}{dR} + \tfrac{1}{6}f(R,T)g_{ik} - \tfrac{1}{3}\lambda g_{ik} - \left[T_{ik} - \tfrac{1}{3}g_{ik}T\right] + \frac{df(R,T)}{dT}\left[T_{ik} - \tfrac{1}{3}g_{ik}T\right] + \frac{df(R,T)}{dT}\left[\Theta_{ik} - \tfrac{1}{3}g_{ik}\Theta\right] = 0. \quad (4)$$

3. SCALAR FIELDS IN UMIMODULAR f(R,T) GRAVITY

Line element of cylindrically symmetric space-time is given by

$$ds^2 = B^2(r)dr^2 + r^2d\phi^2 + dz^2 - A^2(r)dt^2. \quad (5)$$

In order to satisfy the unimodularity condition, the metric tensor determinant must be $\sqrt{-g} = \epsilon = 1$ (Rajabi and Nozari, 2017). The condition for the cylindrically symmetrical space-time given by Eq.(5) is possible by considering a modified time coordinate, which is often used in unimodular theories. This transformation is in the form of $d\tau = rA(r)B(r)dt$. From the transformation, unimodular cylindrically symmetric space-time is obtained as follows (Aydın and Ulu Doğru, 2021):

$$ds^2 = B^2(r)dr^2 + r^2d\phi^2 + dz^2 - \frac{1}{B^2(r)r^2}d\tau^2. \quad (6)$$

Energy-momentum tensor of scalar field is given by:

$$T_{ij} = \Phi_{,i}\Phi_{,j} - \frac{1}{2}g_{ij}\left(g^{ab}\Phi_{,a}\Phi_{,b}\right) \quad (7)$$

where $\Phi(r)$ is scalar potential. Non-vanishing components of energy momentum tensor of unimodular and cylindrically symmetric scalar field in Unimodular f(R,T) theory are obtained as follows (Aydın and Ulu Doğru, 2021):

$$T_i^j = diag\left[\frac{(\Phi_{,r})^2}{2B^2(r)}, -\frac{(\Phi_{,r})^2}{2B^2(r)}, -\frac{(\Phi_{,r})^2}{2B^2(r)}, -\frac{(\Phi_{,r})^2}{2B^2(r)}\right]. \quad (8)$$

Trace of the energy-momentum tensor from Eq.(8) is calculated as:

$$T = -\frac{(\Phi_{,r})^2}{B^2(r)}. \quad (9)$$

From Eqs.(4)-(9), we get field equation of unimodular cylindrically symmetric scalar field in the scope of Unimodular f(R,T) theory as follows:

$$\left(-\frac{1}{2} - \frac{df_2}{dT}\right)(\Phi_{,r})^2 - \frac{1}{r}\frac{B_{,r}}{B} + \frac{1}{r^2}(-1 + r^2(\lambda - f_2)B^2) = 0, \quad (10)$$

$$\left(\frac{1}{2} - \frac{df_2}{dT}\right)\frac{(\Phi_{,r})^2 r^2}{B^2} - \frac{B_{,rr}\,r^2}{B^3} + 3\frac{B_{,r}{}^2 r^2}{B^4} + 3\frac{B_{,r}r}{B^3} + \frac{1}{B^2}\left(2 + r^2(\lambda - f_2)B^2\right) = 0, \quad (11)$$

$$\left(\frac{1}{2} - \frac{df_2}{dT}\right)\frac{(\Phi_{,r})^2}{B^2} - \frac{B_{,rr}}{B^3} + 3\frac{B_{,r}{}^2}{B^4} + 3\frac{B_{,r}}{B^3 r} + \frac{1}{B^2 r^2}(1 + r^2(\lambda - f_2)B^2) = 0, \quad (12)$$

$$\left(-\frac{1}{2} + \frac{df_2}{dT}\right)\frac{(\Phi_{,r})^2}{B^4 r^2} + \frac{1}{r^3}\frac{B_{,r}}{B^5} + \frac{1}{B^2 r^2}(\lambda - f_2) = 0. \quad (13)$$

Eqs.(10)-(13) is also taken into account as *f(R, T) = R+2f_2(T)* (Rajabi and Nozari, 2017). There is an exact solution of the field equations given in Eqs.(10)-(13) with complex scalar field as follows:

$$B(r) = \frac{c_2}{\sqrt{r}}, \tag{14}$$

$$\Phi(r) = \pm i \ln(r) + c_1 \tag{15}$$

where c_1 and c_2 are arbitrary constants. As can be seen from Eq.(15), matter source of given space-time curvature according to Unimodular f(R,T) theory can be a complex scalar field. The field which releases *U(1)* symmetry in the quantization of classical theory is complex scalar fields (Srednicki, 2007). On the other hand, the unimodularity condition used in unimodular gravity theories, which restricts the metric, facilitates the investigation of early period of universe. For this reason, we see that unimodular gravitational theories are quantified and used in particle physics studies of the first particles mass gain and nucleosynthesis period (Garcia-Bellido *et al.,* 2011). Also, it is customary to choose $\Phi(r) = \frac{1}{\sqrt{2}}(\Phi_1 + i\Phi_2)$ for scalar field function satisfying the field equations and Klein-Gordon equation. Such scalar fields give rise to *U(1)* symmetry under $\Phi \to e^{-i\alpha}\Phi$, $\Phi^* \to e^{i\alpha}\Phi^*$ transform (Wald, 1995). Thus, complex scalar fields are involved in unification of unimodular gravity and quantum gravity and its investigation as a fundamental theory of particle-gravitation (Einchorn, 2011).

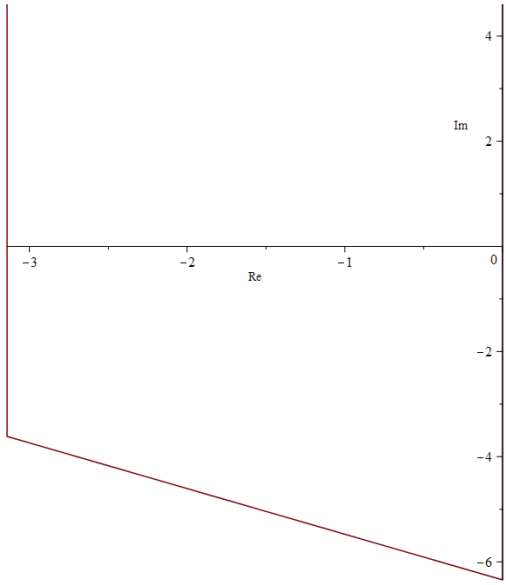

Figure 1. The change of scalar field ($\Phi(r) = i\ln(r)\,, c_1 = 0$).

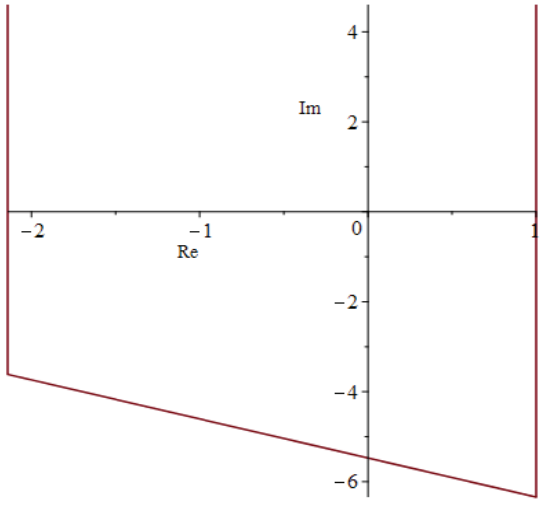

Figure 2. The change of scalar field ($\Phi(r) = i\ln(r) + 1$).

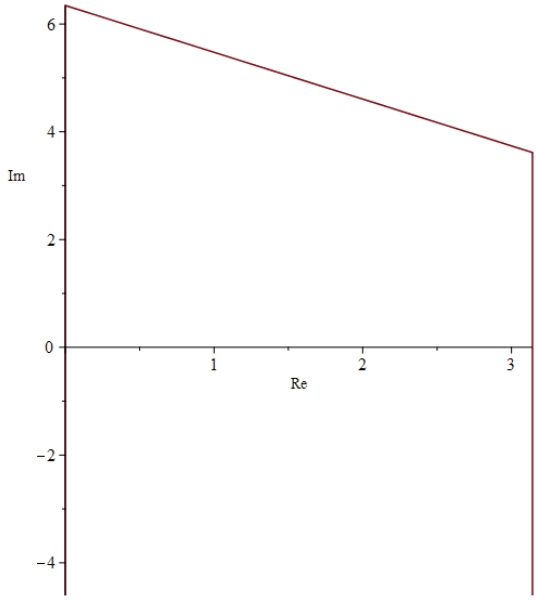

Figure 3. The change of scalar field ($\Phi(r) = -i\ln(r)\,, c_1 = 0$).

The variation of the cylindrical symmetric complex scalar field with the radial coordinate obtained within the scope of Unimodular f(R,T) theory is shown in Figure (1)-(3) for different sign and constant selections.

From Eqs.(10)-(13), important functions of considered *f(R,T)* model are obtained as follows:

$$f_2(r) = \frac{2\lambda B^2 r^2 + 1}{2B^2 r^2}, \tag{16}$$

$$\frac{df_2(T)}{dT} = \frac{1}{2}. \tag{17}$$

Ricci scalar for space-time given in Eq.(6) is

$$R = \frac{2B_{,rr}}{B^3} - 3\frac{{B_{,r}}^2}{B^4} - \frac{B_{,r}}{B^3 r} - \frac{1}{B^2 r^2}. \tag{18}$$

By considering Eq.(14) and (18) together, we get

$$R = -\frac{1}{c_2^2 r}. \tag{19}$$

From Eqs.(16)-(19), it is calculated as

$$f_2(r) = \lambda + \frac{1}{2c_2^2 r}. \tag{20}$$

4. CONCLUSION

In this study, static cylindrically symmetric space-time is unimodularized by cosmic time transformation, and scalar field distribution filling the space-time is investigated within the framework of Unimodular f(R,T) theory. Using $f(R, T) = R+2f_2(T)$ model, field equations and exact solutions for unimodular cylindrically symmetric space-time and scalar field are obtained. As a result, it was seen that the theory allows such a space-time filling with scalar field only if it is complex. The resulting scalar field is compatible with the simple scalar field function, which is frequently used in the literature in canonical quantization and unimodular quantum gravity. In addition, the functions, part of the $f(R, T) = R+2f_2(T)$ model used obtained results in case $T(r)=-R(r)$, reducible to the basic Λ-CDM model. All these results support that Unimodular f(R,T) theory is a consistent field of research for given space-time and matter form.

REFERENCES

Alvarenga, F. G., Houndjo, M. J. S., Monwanou, A. V., and Orou, J. B. C. (2013). Testing some f(R,T) gravity models from energy conditions. Journal of Modern Physics, 4(1), 130-139.

Aydın, H. and Ulu Doğru, M. (2021). "Cylindrically symmetric unimodular f(R) black holes". International Journal of Geometric Methods in Modern Physics, 18(7), 2150101.

Azizi, T. (2013). Wormhole geometries in f(R,T) gravity. International Journal of Theoretical Physics, 52(10), 3486-3493.

Barrientos, J., and Rubilar, G. F. (2014). Comment on "f(R,T) gravity". Physical Review D, 90(2), 028501.

Bufalo, R., Oksanen, M. and Tureanu, A. (2015). How unimodular gravity theories differ from general relativity at quantum level The European Physical Journal C volume 75, 477.

Carballo-Rubio, R., Garay, L. J., García-Moreno, G. (2022) Unimodular Gravity vs General Relativity: A status report Class. Quantum Grav. 39, 243001.

Carroll, Sean M. (2004), Spacetime and Geometry: An Introduction to General Relativity, San Francisco: Addison-Wesley, ISBN 978-0-8053-8732-2.

Clifford, M. W. (2006). The Confrontation between General Relativity and Experiment Living Reviews in Relativity volume 9, 3.

Clifton, T., Pedro, G. F., Antonio, P. And Constantinos, S. (2012). Modified Gravity and Cosmology. Physics Reports. 513 num.3 (1): 1-89. arXiv:1106.2476.

Einstein, A. (1916), Relativity: The Special and the General Theory, Berlin, ISBN 978-3-528-06059-6.

Eichhorn, A. (2011). On unimodular quantum gravity. Classical and Quantum Gravity, Volume 30, Number 11.

García-Bellido, J., Rubio, J., Shaposhnikov, M. and Zenhäusern, D. (2011). Higgs-dilaton cosmology: From the early to the late Universe. Phys. Rev. D 84, 123504.

Harko, T., Lobo, F.S.N., Nojiri, S. and Odintsov, S.D. (2011), f(R,T) gravity, Phys. Rev. D, 84, 024020.

Houndjo, M. J. S. (2012). Reconstruction of f(R,T) gravity describing matter dominated and accelerated phases. International Journal of Modern Physics D, 21(01), 1250003.

Hubble, E.P. (1929) A Relation between Distance and Radial Velocity among Extra-Galactic Nebulae. Proceedings of the National Academy of Sciences of the United States of America, 15, 167-173.

Linde, A.D. (1990). Particle Physics and Inflationary Cosmology (Harwood Academic Publishers, Chur, Switzerland)

Rajabi, F. And Nozari, K. (2017). Unimodular f(R,T) Gravity. Phys. Rev. D 96, 084061.

Reddy, D. R., Santikumar, R. and Naidu, R. L. (2012). Bianchi type-III cosmological model in f(R,T) theory of gravity. Astrophysics and Space Science, 342(1), 249-252.

Sharif, M. and Zubair, M. (2012). Energy conditions constraints and stability of power law solutions in f(R,T) gravity. Journal of the Physical Society of Japan, 82(1), 014002.

Simon A. M. (2020) Georges Lemaitre and the Foundations of Big Bang Cosmology The Antiquarian Astronomer. 2-20, https://arxiv.org/abs/2007.09459.

Srednicki, M. (2007). Quantum Field Theory. Cambridge University Press. ISBN 9780521864497.

Moraes, P. H. R. S., and Santos, J. R. L. (2016). A complete cosmological scenario from f(R,T^{Φ}) gravity theory. The European Physical Journal C, 76(2), 60.

Wald, R. M. (1995). Quantum field theory in curved space-time and black hole thermodynamics. Chicago U. ISBN 0-226-87025-1.

Weinberg, S. (1989). "The cosmological constant problem". Reviews of Modern Physics. 61 (1): 1–23.

CHAPTER 2

STATISTICAL INFERENCE FOR FINITE MIXTURES OF THE POWER MUTH DISTRIBUTIONS

Hayrinisa DEMİRCİ BİÇER[1], Cenker BİÇER[2]

1 Assoc.Prof.Dr., Hayrinisa DEMİRCİ BİÇER, Kırıkkale Univ., Dep. of Statistics. ORCID:0000-0002-1520-5004, hdbicer@kku.edu.tr.
2 Assoc.Prof.Dr., Cenker BİÇER, Kırıkkale Univ., Dep. of Statistics. ORCID: 0000-0003-2222-3208, cbicer@kku.edu.tr.

INTRODUCTION

A heterogeneous structure is encountered in the data observed from many real-world phenomena. As in the analysis of homogeneous data, it is desirable to optimally model heterogeneous data. Although heterogeneous data can be modeled with standard probability distribution models, the modeling performance of these models is often not at the desired level. In order to understand and explain a phenomenon, the modeling performance of the probability model used to model it is important. In this respect, mixture distributions are essential tools in the efficient analysis of heterogeneous data and they have high modeling performance. In its most general form, the probability density function (pdf) of a mixture distribution given by

$$f(x) = \sum_{j=1}^{k} p_j f_j(x, \theta_j), \tag{1}$$

where, X is a random variable, p_j , $\left(\sum_{j=1}^{k} p_j = 1\right)$, is the mixing ratio fort he j^{th} component of the mixture distribution, $f_j(x, \theta_j)$, j. is the pdf of the j^{th} component, and θ_j is the parameter vector of the j^{th} component. The cumulative distribution function (cdf) corresponding to the probability density function given by Equation (1) is

$$F(x) = \sum_{j=1}^{k} p_j F_j(x, \theta_i), \tag{2}$$

where, $F_j(x, \theta_j)$ is the cdf of the j^{th} component distribution. A finite mixture distribution contains a total of three kinds of unknown parameters: the first is the number of components, the second is the mixture ratios, and the third is the parameter or parameters of the component distributions. In the literature, there are many studies on the development of methods that can be used to estimate the parameters of finite mixture distributions. Maximum likelihood, moments, least squares, and maximum spacing estimation methods are some of the methods used in estimating the parameters of the families of standard distributions. These methods can also be used in estimating the mixing ratios and component distribution parameters of a finite mixture distribution. By taking into account the component distribution, one can choose which of these approaches will be applied. However, while applying these estimation methods, analytical solutions cannot be achieved in general and it is inevitable to resort to numerical methods most

of the time in the process of obtaining estimations. The estimate of the parameters of finite mixture distributions has been the subject of numerous studies in the literature. Some of these are (Jewell, 1982), (Elmahdy, & Aboutahoun, 2013), (Erisoglu, & Erisoglu, 2014), (Ali, 2015), (Tahir et al., 2017), (Demirci Biçer, 2018), (Biçer, & Biçer, 2018), (Young et al., 2019), and (Al-Moisheer, 2021). However, the parameter estimation problem for mixtures of many standard distribution families is still among the topics to be investigated. The Power Muth distribution is one of these standard families. In this context, this study's main objective is to address the issue of estimating the parameters of the k-components mixtures of the Power Muth distributions when the component number k is known. The solution to this problem is investigated according to the maximum likelihood and least squares methods in the paper.

Other parts of this study are organized as follows: the section "THE POWER MUTH DISTRIBUTION AND ITS MIXTURES" includes an overview of the Power Muth distribution and the distributions of its finite mixtures. In the "ESTIMATION" section, maximum likelihood and least squares estimators of unknown parameters of k-components mixtures of the Power Muth distributions are investigated. The "SIMULATION" section is devoted to simulation studies that comparatively investigate the performance of the estimators obtained with the study in estimating the unknown parameters of the k-component mixtures of the power Muth distributions. The "CONCLUSION" section concludes the work.

THE POWER MUTH DISTRIBUTION AND ITS MIXTURES

The Power Muth distribution is a probability distribution model that has the potential to model many data from the fields of science, engineering, and health. The probability density function (pdf) of the power Muth distribution is

$$f(x,\beta,\theta)=\frac{\theta}{\beta}\ e^{\left(\frac{x}{\beta}\right)^{\theta}-e^{\left(\frac{x}{\beta}\right)^{\theta}}+1}\left(e^{\left(\frac{x}{\beta}\right)^{\theta}}-1\right)\left(\frac{x}{\beta}\right)^{\theta-1},x>0, \tag{3}$$

and the corresponding cumulative distribution is

$$F(x,\beta,\theta)=1-e^{\left(\frac{x}{\beta}\right)^{\theta}-e^{-\left(\frac{x}{\beta}\right)^{\theta}}+1},x>0, \tag{4}$$

where, $\beta>0$ is the scale parameter and the θ>0 is the scale parameter of the distribution (Jodra et al., 2017). Considering the general form of the

probability density function of a finite mixture distribution given by Equation (1), the probability density function of the k-component mixtures of the power Muth distributions is easily written as

$$f(x)=\sum_{j=1}^{k} p_j \frac{\theta_j}{\beta_j} e^{\left(\frac{x}{\beta_j}\right)^{\theta_j}-e^{\left(\frac{x}{\beta_j}\right)^{\theta_j}}+1}\left(e^{\left(\frac{x}{\beta_j}\right)^{\theta_j}}-1\right)\left(\frac{x}{\beta_j}\right)^{\theta_j-1}, \qquad (5)$$

where $\beta_j > 0$ is the scale parameter of the j^{th} component distribution and θ_j>0 is the scale parameter of the j^{th} component distribution. The distribution has a total of 3k unknown parameters. We present Figures 1-2 to understand the form of the pdf given by equation (5). Figures 1-2 display the plots of the pdf of the two-component mixtures of the power Muth distributions for different parameter values.

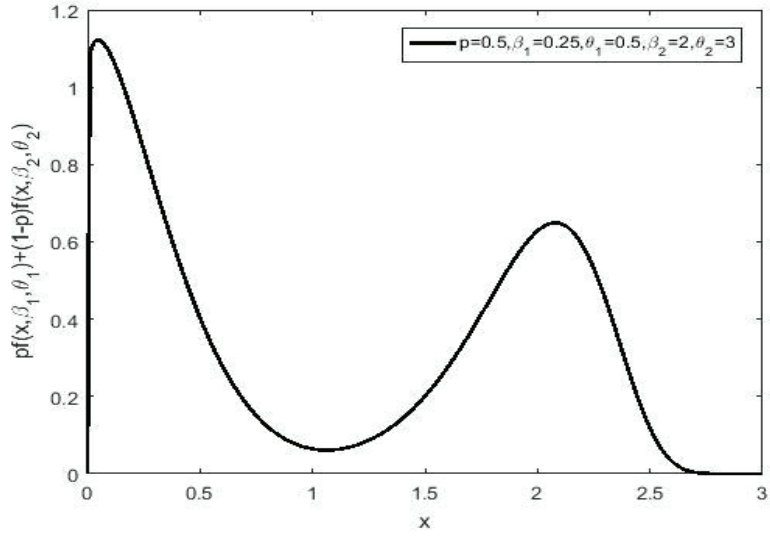

Figure 1. The pdf of the two-component mixtures of the power Muth distributions for $p = 0.50, \beta_1 = 0.25, \theta_1 = 0.5,\ \beta_2 = 2, \theta_2 = 3$

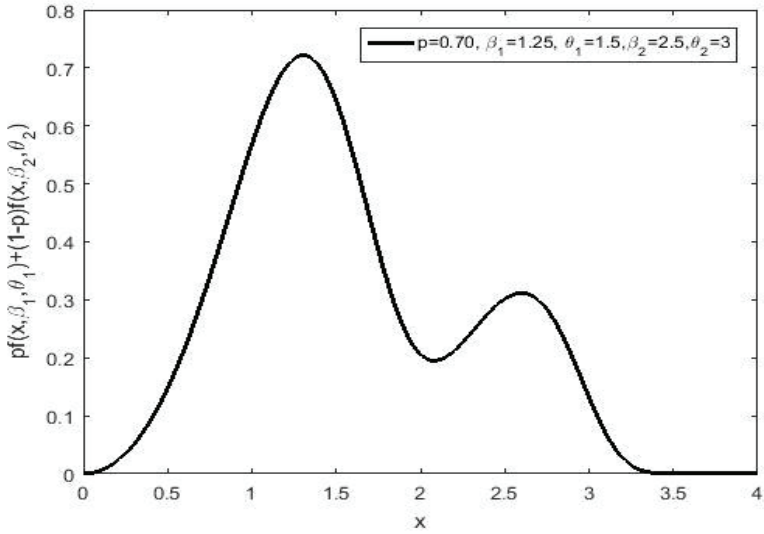

Figure 2. The pdf of the two-component mixtures of the power Muth distributions for $p = 0.50, \beta_1 = 0.25, \theta_1 = 0.5,\ \beta_2 = 2, \theta_2 = 3$

ESTIMATION

In this section, estimators of unknown parameters of the k-component mixtures of the power Muth distributions are investigated using the maximum likelihood and least squares methods.

Suppose the random variables $X_1, X_2, \ldots, X_n$ are a random sample taken from the k-component mixtures of the power Muth distributions and $x_1, x_2, \ldots, x_n$ is a realization of $X_1, X_2, \ldots, X_n$. The likelihood function of k-component mixtures of the power Muth distributions based on random observations $x_1, x_2, \ldots, x_n$ can be written as

$$L(\Lambda; x_1, x_2, \ldots, x_n) = \prod_{i=1}^{n} \sum_{j=1}^{k} p_j \frac{\theta_j}{\beta_j} e^{\left(\frac{x_i}{\beta_j}\right)^{\theta_j} - e^{\left(\frac{x_i}{\beta_j}\right)^{\theta_j}} + 1} \left(e^{\left(\frac{x_i}{\beta_j}\right)^{\theta_j}} - 1 \right) \left(\frac{x_i}{\beta_j}\right)^{\theta_j - 1}, \quad (6)$$

where $\Lambda = (p_1, p_2, \ldots, p_k, \beta_1, \beta_2, \ldots, \beta_k, \theta_1, \theta_2, \ldots, \theta_k)$ implies the parameter vector. We also can write the following logarithmic likelihood function.

$$\ln L(\Lambda; x_1, x_2, \ldots, x_n) = \sum_{i=1}^{n} \ln \sum_{j=1}^{k} p_j \frac{\theta_j}{\beta_j} e^{\left(\frac{x_i}{\beta_j}\right)^{\theta_j} - e^{\left(\frac{x_i}{\beta_j}\right)^{\theta_j}} + 1} \left(e^{\left(\frac{x_i}{\beta_j}\right)^{\theta_j}} - 1 \right) \left(\frac{x_i}{\beta_j}\right)^{\theta_j - 1} \tag{7}$$

Then, by considering the

$$\sum_{j=1}^{k} p_j = 1,$$

the logarithmic likelihood function given by Equation (7) is written as

$$\ln L(\Lambda; x_1, x_2, \ldots, x_n) = \sum_{i=1}^{n} \ln \sum_{j=1}^{k} p_j \frac{\theta_j}{\beta_j} e^{\left(\frac{x_i}{\beta_j}\right)^{\theta_j} - e^{\left(\frac{x_i}{\beta_j}\right)^{\theta_j}} + 1} \left(e^{\left(\frac{x_i}{\beta_j}\right)^{\theta_j}} - 1 \right) \left(\frac{x_i}{\beta_j}\right)^{\theta_j - 1} - n \left(\sum_{j=1}^{k} p_j - 1 \right). \tag{8}$$

By deriving the logarithmic likelihood function given by Equation (8) according to the parameters and equating it to zero, we have the likelihood equations

$$\frac{\partial}{\partial p_j} \ln L(\Lambda; x_1, x_2, \ldots, x_n) = \sum_{i=1}^{n} \frac{p_j \frac{\theta_j}{\beta_j} e^{\left(\frac{x_i}{\beta_j}\right)^{\theta_j} - e^{\left(\frac{x_i}{\beta_j}\right)^{\theta_j}} + 1} \left(e^{\left(\frac{x_i}{\beta_j}\right)^{\theta_j}} - 1 \right) \left(\frac{x_i}{\beta_j}\right)^{\theta_j - 1}}{\sum_{j=1}^{k} p_j f_j(x_i, \theta_j)} \frac{1}{p_j} - n = 0 \tag{9}$$

$$\frac{\partial}{\partial\beta_j}\ln L(\Lambda; x_1, x_2, \dots, x_n) = \sum_{i=1}^{n} \xi(x_i, \beta_j, \theta_j) \times \frac{\theta_j \left(\frac{\left(e^{\left(\frac{x_i}{\beta_j}\right)^{\theta_j}} \left(e^{\left(\frac{x_i}{\beta_j}\right)^{\theta_j}} - 3 \right) + 1 \right) \left(\frac{x_i}{\beta_j}\right)^{\theta_j}}{e^{\left(\frac{x_i}{\beta_j}\right)^{\theta_j}} - 1} - 1 \right)}{\beta_j} = 0 \tag{10}$$

and

$$\frac{\partial}{\partial\theta_j}\ln L(\Lambda; x_1, x_2, \dots, x_n) = \sum_{i=1}^{n} \xi(x_i, \beta_j, \theta_j) \times \left[\left(1 - \frac{\left(e^{\left(\frac{x_i}{\beta_j}\right)^{\theta_j}} \left(e^{\left(\frac{x_i}{\beta_j}\right)^{\theta_j}} - 3 \right) + 1 \right) \left(\frac{x_i}{\beta_j}\right)^{\theta_j}}{e^{\left(\frac{x_i}{\beta_j}\right)^{\theta_j}} - 1} \right) \ln\left(\frac{x_i}{\beta_j}\right) + \frac{1}{\theta_j} \right], \tag{11}$$

where

$$\xi(x_i, \beta_j, \theta_j) = \frac{p_j f_j(x_i, \beta_j, \theta_j)}{\sum_{j=1}^{k} p_j f_j(x_i, \beta_j, \theta_j)}.$$

Now, we solve the equations (9)-(11) according to the parameters. From Equation (9,) p_j can be written as

$$p_j = \frac{1}{n}\sum_{i=1}^{n} \xi(x_i, \beta_j, \theta_j). \tag{12}$$

If Equation (10) is solved with respect to β_j, we have

$$\beta_j = \frac{\sum_{i=1}^{n} \xi(x_i, \beta_j, \theta_j)\theta_j}{\frac{\sum_{i=1}^{n} \xi(x_i, \beta_j, \theta_j)\, \tau_j(x_i, \beta_j, \theta_j)\theta_j}{\beta_j}}. \tag{13}$$

And also, from the solution of Equation (11), we can write

$$\theta_j = \frac{\sum_{i=1}^{n} \xi(x_i, \beta_j, \theta_j)}{\sum_{i=1}^{n} \xi(x_i, \beta_j, \theta_j) \ln\left(\frac{\beta_j}{x_i}\right)\left(1 - \tau_j(x_i, \beta_j, \theta_j)\right)}, \tag{14}$$

where

$$\tau_j(x_i, \beta_j, \theta_j) = \frac{\left(e^{\left(\frac{x_i}{\beta_j}\right)^{\theta_j}}\left(e^{\left(\frac{x_i}{\beta_j}\right)^{\theta_j}} - 3\right) + 1\right)\left(\frac{x_i}{\beta_j}\right)^{\theta_j}}{e^{\left(\frac{x_i}{\beta_j}\right)^{\theta_j}} - 1}.$$

Unfortunately, closed forms of maximum likelihood estimators cannot be obtained by employing these equations since solutions (13) and (14) contain parameters. However, it is possible to reach the maximum likelihood estimates of the parameters using numerical approaches. For this purpose, the equations (12)- (14) can be considered as

$$\hat{p}_j^{(t+1)} = \frac{1}{n}\sum_{i=1}^{n} \xi\left(x_i, \hat{\beta}_j^{(t)}, \hat{\theta}_j^{(t)}\right),$$

$$\hat{\beta}_j^{(t+1)} = \frac{\sum_{i=1}^{n} \xi\left(x_i, \hat{\beta}_j^{(t)}, \hat{\theta}_j^{(t)}\right)\theta_j}{\sum_{i=1}^{n} \xi\left(x_i, \hat{\beta}_j^{(t)}, \hat{\theta}_j^{(t)}\right)\tau_j\left(x_i, \hat{\beta}_j^{(t)}, \hat{\theta}_j^{(t)}\right)\hat{\theta}_j^{(t)}/\hat{\beta}_j^{(t)}} \tag{16}$$

and

$$\hat{\theta}_j^{(t+1)} = \frac{\sum_{i=1}^{n} \xi\left(x_i, \hat{\beta}_j^{(t)}, \hat{\theta}_j^{(t)}\right)}{\sum_{i=1}^{n} \xi\left(x_i, \hat{\beta}_j^{(t)}, \hat{\theta}_j^{(t)}\right)\ln\left(\frac{\hat{\beta}_j^{(t)}}{x_i}\right)\left(1 - \tau_j\left(x_i, \hat{\beta}_j^{(t)}, \hat{\theta}_j^{(t)}\right)\right)}, \tag{17}$$

respectively. Thus we can reach the maximum likelihood estimates of the parameters by applying the fixed point theorem to Equations (15)-(17) by considering an initial estimate of the parameter vector such $\Lambda^{(0)}$.

We now investigate the least squares estimators of the unknown parameters of the mentioned distribution. Advanced researchers can refer to the following study for more details on the least squares estimate methodology: (Swain, 1988).

Let $x_{1:n}, x_{2:n}, \ldots, x_{n:n}$ is an ordered measurements drawn from k-component mixtures of the power Muth distributed population. By considering the cdf of the k-component mixtures of the power Muth distributions given by Equation (4), least squares estimators of the parameter vector Λ are obtained by minimizing utulity function

$$L = \sum_{i=1}^{n} \left(\sum_{\mathrm{j}=1}^{k} p_j F_j\left(x_{(i:n)}, \beta_j, \theta_j\right) - E_i \right)^2$$

$$= \sum_{i=1}^{n} \left(\sum_{\mathrm{j}=1}^{k} p_j \left(1 - e^{\left(\frac{x_{(i:n)}}{\beta_j}\right)^{\theta_j} - e^{-\left(\frac{x_{(i:n)}}{\beta_j}\right)^{\theta_j}} + 1} \right) - E_i \right)^2,$$

with respect to parameters, where $E_i = \frac{i}{n+1}$ implie the value of the empirical distribution function for the measurement i. One can use Octave's (octave manual) fiminsearch function to solve this minimization problem.

SIMULATION STUDY

In this part of the study, the efficiencies of the estimators obtained by the study are compared numerically. Here, we consider the two-component mistures of the power Muth distributions. In the simulation study, two different scenarios, p=0.50 and p=0.75, are considered for the mixing ratio parameter. As two comparison criteria, we use Bias and mean square error (MSE) by given following equations

$$Bias = \sum_{i=1}^{m} (\hat{\eta}_i - \eta)/m$$

$$MSE = \sum_{i=1}^{m} (\eta - \hat{\eta}_i)^2/m,$$

where, m is the simulation repetition. The results are obtained by 1000 iterated simulations throughout the study.

Scenario 1: For case $p = 0.50$, the parameter values are set as $\beta_1 =$ 0.25, 0.50 and 2, $\beta_2 = 2$, $\theta_1 = 0.5$, $\theta_2 = 3$. Simulated results based on sample sizes *n*= 50,100 ve 200 are tabulated by Tables 1-4.

Table 1: Simulated results for p= 0.5, β_1 =0.25, θ_1 =0.5, β_2 =2 ve θ_2 =3

n		50			100			200		
Param.	Met-hod	Est.	Bias	MSE	Est.	Bias	MSE	Est.	Bias	MSE
	MLE									
p		0.503	0.003	0.001	0.502	0.002	0.000	0.502	0.002	0.000
β_1		0.260	0.010	0.003	0.251	0.001	0.001	0.252	0.002	0.001
θ_1		0.537	0.037	0.013	0.519	0.019	0.006	0.509	0.009	0.002
β_2		2.001	0.001	0.006	1.991	-0.009	0.003	2.000	0.000	0.001
θ_2		3.211	0.211	0.440	3.068	0.068	0.150	3.076	0.076	0.094
	LSE									
p		0.504	0.004	0.000	0.505	0.005	0.000	0.503	0.003	0.000
β_1		0.252	0.002	0.000	0.251	0.001	0.000	0.252	0.002	0.000
θ_1		0.505	0.005	0.000	0.506	0.006	0.000	0.507	0.007	0.000
β_2		1.999	-0.001	0.004	1.997	-0.003	0.001	2.003	0.003	0.001
θ_2		3.025	0.025	0.002	3.028	0.028	0.002	3.028	0.028	0.002

Table 2:Simulated results for p= 0.5, β_1 =0.5, θ_1 =0.5, β_2 =2 ve θ_2 =3.

n		50			100			200		
Param.	Met-hod	Est.	Bias	MSE	Est.	Bias	MSE	Est.	Bias	MSE
	MLE									
p		0.479	-0.021	0.006	0.489	-0.011	0.003	0.494	-0.006	0.001
β_1		0.495	-0.005	0.015	0.489	-0.011	0.009	0.490	-0.010	0.003
θ_1		0.618	0.118	0.040	0.541	0.041	0.007	0.521	0.021	0.003
β_2		1.991	-0.009	0.011	1.991	-0.009	0.004	1.993	-0.007	0.002
θ_2		3.228	0.228	1.121	3.090	0.090	0.328	3.063	0.063	0.128
	LSE									
p		0.506	0.006	0.000	0.505	0.005	0.000	0.505	0.005	0.000
β_1		0.502	0.002	0.000	0.503	0.003	0.000	0.501	0.001	0.000
θ_1		0.506	0.006	0.000	0.505	0.005	0.000	0.506	0.006	0.000
β_2		1.997	-0.003	0.003	2.002	0.002	0.002	1.998	-0.002	0.001
θ_2		3.030	0.030	0.003	3.029	0.029	0.001	3.033	0.033	0.002

Table 3:Simulated results for p= 0.5, β_1 =1, θ_1 =0.5, β_2 =2 ve θ_2 =3.

n		50			100			200		
Param.	Met-hod	Est.	Bias	MSE	Est.	Bias	MSE	Est.	Bias	MSE
	MLE									
p		0.498	-0.002	0.014	0.500	0.000	0.008	0.499	-0.001	0.002
β_1		1.011	0.011	0.069	0.983	-0.017	0.041	0.997	-0.003	0.016
θ_1		0.554	0.054	0.021	0.509	0.009	0.007	0.511	0.011	0.003
β_2		2.005	0.005	0.009	2.003	0.003	0.006	1.995	-0.005	0.002
θ_2		3.704	0.704	2.324	3.131	0.131	0.651	3.061	0.061	0.227
	LSE									
p		0.502	0.002	0.000	0.501	0.001	0.000	0.503	0.003	0.000
β_1		1.015	0.015	0.001	1.010	0.010	0.000	1.008	0.008	0.000

θ_1		0.504	0.004	0.000	0.504	0.004	0.000	0.506	0.006	0.000
β_2		2.005	0.005	0.009	2.013	0.013	0.003	2.004	0.004	0.002
θ_2		3.020	0.020	0.004	3.020	0.020	0.002	3.023	0.023	0.001

Table 4:Simulated results for p= 0.5, β_1 =2, θ_1 =0.5, β_2 =2 ve θ_2 =3.

n		50			100			200		
Param.	Met-hod	Est.	Bias	MSE	Est.	Bias	MSE	Est.	Bias	MSE
	MLE									
p		0.488	-0.012	0.007	0.512	0.012	0.004	0.495	-0.005	0.002
β_1		2.145	0.145	0.246	2.040	0.040	0.097	2.056	0.056	0.046
θ_1		0.542	0.042	0.016	0.531	0.031	0.007	0.515	0.015	0.003
β_2		2.001	0.001	0.007	1.994	-0.006	0.004	1.993	-0.007	0.002
θ_2		3.396	0.396	1.611	3.215	0.215	0.517	3.008	0.008	0.203
	LSE									
p		0.514	0.014	0.001	0.512	0.012	0.000	0.512	0.012	0.000
β_1		2.030	0.030	0.004	2.029	0.029	0.003	2.018	0.018	0.002
θ_1		0.502	0.002	0.000	0.500	0.000	0.000	0.499	-0.001	0.000
β_2		1.966	-0.034	0.027	2.001	0.001	0.011	2.001	0.001	0.003
θ_2		3.016	0.016	0.011	3.001	0.001	0.005	3.017	0.017	0.004

When the results presented in Tables 1 – 4 are examined, it is seen that both estimators provide satisfactory results. Additionally, it is seen that LSE estimators have lower Bias and MSE values in the estimation of unknown parameters. In general, in all cases discussed in Tables 1-4, the Bias and MSE values of both MLE and LSE estimators decrease as the number of observations increases.

Scenario 2: For case p =0.70, we set the parameter values as β_1 = 0.50, β_2 = 2, θ_1 = 0.25, 0.5, 1,2 and θ_2 = 3. Simulated results based on sample sizes *n*= 50,100 ve 200 are figured by Tables 5-8.

Table 5:Simulated results for p= 0.7, β_1 =2, θ_1 =0.25, β_2 =2 ve θ_2 =3.

n		50			100			200		
Param	Met-hod	Est.	Bias	MSE	Est.	Bias	MSE	Est.	Bias	MSE
	MLE									
p		0.691	-0.009	0.007	0.698	-0.002	0.002	0.704	0.004	0.001
β_1		0.474	-0.026	0.030	0.509	0.009	0.018	0.506	0.006	0.008
θ_1		0.254	0.004	0.002	0.256	0.006	0.001	0.252	0.002	0.000
β_2		2.018	0.018	0.016	2.013	0.013	0.007	2.014	0.014	0.003
θ_2		3.919	0.919	3.988	3.344	0.344	0.887	3.265	0.265	0.301
	LSE									
p		0.698	-0.002	0.002	0.705	0.005	0.001	0.704	0.004	0.001
β_1		0.508	0.008	0.000	0.505	0.005	0.000	0.503	0.003	0.000
θ_1		0.254	0.004	0.000	0.255	0.005	0.000	0.253	0.003	0.000

β_2	1.979	-0.021	0.018	1.967	-0.033	0.012	1.986	-0.014	0.007
θ_2	3.044	0.044	0.003	3.040	0.040	0.004	3.044	0.044	0.003

Table 6:Simulated results for p= 0.7, β_1 =2, θ_1 =0.5, β_2 =2 ve θ_2 =3.

n		50			100			200		
Param.	Met-hod	Est.	Bias	MSE	Est.	Bias	MSE	Est.	Bias	MSE
	MLE									
p		0.676	-0.024	0.008	0.671	-0.029	0.008	0.681	-0.019	0.002
β_1		0.470	-0.030	0.013	0.476	-0.024	0.009	0.484	-0.016	0.003
θ_1		0.540	0.040	0.014	0.546	0.046	0.008	0.519	0.019	0.002
β_2		1.981	-0.019	0.026	1.972	-0.028	0.017	1.979	-0.021	0.006
θ_2		3.592	0.592	3.035	3.187	0.187	0.941	3.028	0.028	0.358
	LSE									
p		0.701	0.001	0.001	0.704	0.004	0.000	0.704	0.004	0.000
β_1		0.503	0.003	0.000	0.503	0.003	0.000	0.503	0.003	0.000
θ_1		0.506	0.006	0.000	0.505	0.005	0.000	0.505	0.005	0.000
β_2		2.012	0.012	0.004	2.005	0.005	0.003	2.006	0.006	0.002
θ_2		3.038	0.038	0.002	3.038	0.038	0.002	3.038	0.038	0.002

Table 7:Simulated results for p= 0.7, β_1 =2, θ_1 =1, β_2 =2 ve θ_2 =3.

n		50			100			200		
Param.	Met-hod	Est.	Bias	MSE	Est.	Bias	MSE	Est.	Bias	MSE
	MLE									
p		0.702	0.002	0.000	0.700	0.000	0.000	0.701	0.001	0.000
β_1		0.506	0.006	0.002	0.499	-0.001	0.001	0.504	0.004	0.000
θ_1		1.050	0.050	0.032	1.013	0.013	0.011	1.017	0.017	0.005
β_2		1.993	-0.007	0.007	2.000	0.000	0.004	2.001	0.001	0.002
θ_2		3.319	0.319	0.706	3.177	0.177	0.383	3.038	0.038	0.143
	LSE									
p		0.703	0.003	0.000	0.702	0.002	0.000	0.703	0.003	0.000
β_1		0.500	0.000	0.000	0.502	0.002	0.000	0.502	0.002	0.000
θ_1		1.008	0.008	0.000	1.008	0.008	0.000	1.010	0.010	0.000
β_2		2.017	0.017	0.001	2.017	0.017	0.001	2.008	0.008	0.000
θ_2		3.045	0.045	0.003	3.045	0.045	0.003	3.041	0.041	0.002

Table 8:Simulated results for p= 0.7, β_1 =2, θ_1 =2, β_2 =2 ve θ_2 =3.

n		50			100			200		
Param.	Met-hod	Est.	Bias	MSE	Est.	Bias	MSE	Est.	Bias	MSE
p		0.700	0.000	0.000	0.701	0.001	0.000	0.700	0.000	0.000
β_1		0.499	-0.001	0.000	0.499	-0.001	0.000	0.500	0.000	0.000
θ_1		2.103	0.103	0.132	2.025	0.025	0.055	2.004	0.004	0.016
β_2		2.009	0.009	0.008	2.002	0.002	0.003	2.000	0.000	0.002
θ_2		3.451	0.451	0.816	3.187	0.187	0.246	3.039	0.039	0.086

	LSE									
p		0.706	0.006	0.000	0.705	0.005	0.000	0.705	0.005	0.000
β_1		0.499	-0.001	0.000	0.501	0.001	0.000	0.501	0.001	0.000
θ_1		2.014	0.014	0.001	2.013	0.013	0.001	2.017	0.017	0.001
β_2		2.012	0.012	0.001	2.012	0.012	0.001	2.013	0.013	0.001
θ_2		3.039	0.039	0.002	3.040	0.040	0.002	3.043	0.043	0.002

The simulated results for Scenario 2 and presented in Tables 5–8 are consistent with the results given in Tables 1–4. Again, as the number of observations increases, both the Bias and MSE values of both estimators converge to zero. Therefore, it can be said that both estimators are asymptotically consistent and unbiased.

CONCLUSION

In this study, the estimation problem in finite mixtures of power Muth distributions is considered. Two different approaches, maximum likelihood, and least squares are used to examine the solution to the mentioned estimation problem in the paper. Based on the methods considered, estimators for unknown parameters in finite mixtures of the power Muth distributions are obtained and presented in the study. The estimation performances of the presented estimators are compared with simulation studies. Two different criteria, Bias and MSE, are chosen as comparison criteria in simulation studies. With the information obtained from the simulations, it is concluded that the estimators obtained in the study are asymptotically consistent and unbiased estimators. Therefore, it can be said that it is appropriate to use both the maximum likelihood estimators and the least-square estimators to estimate the unknown parameters of the finite mixtures of the power Muth distributions.

REFERENCES

1. Jewell, N. P. (1982). Mixtures of exponential distributions. The annals of statistics, 479-484.

2. Elmahdy, E. E., & Aboutahoun, A. W. (2013). A new approach for parameter estimation of finite Weibull mixture distributions for reliability modeling. Applied Mathematical Modelling, 37(4), 1800-1810.

3. Erisoglu, U., & Erisoglu, M. (2014). L-moments estimations for mixture of Weibull distributions. Journal of data science, 12, 69-85.

4. Ali, S. (2015). Mixture of the inverse Rayleigh distribution: Properties and estimation in a Bayesian framework. Applied Mathematical Modelling, 39(2), 515-530.

5. Tahir, M., Aslam, M., Hussain, Z., & Abbas, N. (2017). On the finite mixture of exponential, Rayleigh and Burr Type-XII distributions: Estimation of parameters in Bayesian framework. Electronic Journal of applied statistical analysis, 10(1), 271-293.

6. Demirci Biçer, H. (2018). Chapter: Parameter Estimation For Finite Mixtures Of Power Lindley Distributions. The Most Recent Studıes In Science And Art, 1659-1669.

7. Biçer, H. D., & Biçer, C. (2018). İki Parametreli Rayleıgh Dağılımlarının Sonlu Karmalarında Parametre Tahmini. Uluslararası İktisadi Ve İdari İncelemeler Dergisi, 383-398.

8. Young, D. S., Chen, X., Hewage, D. C., & Nilo-Poyanco, R. (2019). Finite mixture-of-gamma distributions: estimation, inference, and model-based clustering. Advances in Data Analysis and Classification, 13(4), 1053-1082.

9. Al-Moisheer, A. S. (2021). Mixture of Lindley and lognormal distributions: properties, estimation, and application. Journal of Function Spaces, 2021.

10. Jodra, P., Gomez, H. W., Jimenez-Gamero, M. D., & Alba-Fernandez, M. V. (2017). The power Muth distribution. Mathematical Modelling and Analysis, 22(2), 186-201.

11. Swain, J. J., Venkatraman, S., & Wilson, J. R. (1988). Least-squares estimation of distribution functions in Johnson's translation system. Journal of Statistical Computation and Simulation, 29(4), 271-297.

CHAPTER 3

NUTRIENT AND MINERAL CONTENT AND BIOLOGICAL ACTIVITY OF GENUS PLEUROTUS, WHICH CAUSES WOOD DESTRUCTION IN FORESTS

Emre Cem Eraslan[1], İmran Uysal[2], Mustafa Sevindik[3], Hasan Akgül[4]

1 Akdeniz University, Science Faculty, Department of Biology, Antalya, Türkiye.
2 Osmaniye Korkut Ata University, Bahçe Vocational School, Department of Food Processing, Osmaniye, Turkey.
3 Osmaniye Korkut Ata University, Science and Literature Faculty, Department of Biology, Osmaniye, Turkey.
4 Akdeniz University, Science Faculty, Department of Biology, Antalya, Türkiye. Corresponding author email: hakgul@akdeniz.edu.tr

Introduction

Fungi are ever-present organisms that may be found in a wide variety of ecological settings (Bal et al., 2017; Sevindik, 2019). Depending on whether they are edible, inedible, or toxic, mushrooms may be classified into three broad categories (Sevindik et al., 2018a). Minerals, vitamins, proteins, and carbs are only some of the nutrients found in mushroom structures (Akgül et al., 2017; Bal et al., 2019). In addition to being beneficial to one's health in terms of nutrition, they also have therapeutic value. Various biological effects, such as antioxidant, antibacterial, anticancer, DNA protecting, antiinflammatory, antiproliferative, hepatoprotective, and antiaging, have been attributed to mushrooms in several studies (Weng et al., 2011; Soares et al., 2013; Akgül et al., 2016; Muszyńska et al., 2018; Sevindik et al., 2018b; Barbosa et al., 2020; Krupodorova and Sevindik, 2020; Mushtaq et al., 2020; Selamoğlu et al., 2020). Mushrooms are a valuable organic resource here. One of the most often eaten mushroom types is a *Pleurotus* mushroom. In particular, *P. ostreatus* is a widely eaten and widely grown species of mushroom. Oyster fungus, poplar fungi, abalone fungi, and tree fungi all refer to the same genus, *Pleurotus* (Cohen et al., 2002). Pleurotus species are saprotrophic and wood destroyers as well as high nutritional and medicinal properties for human health (Oei, 1996). There are species of the genus *Pleurotus* in both tropical and temperate regions of the globe. White rot fungus, of which there are many *Pleurotus* species, are the norm on hardwoods. Nutrient and mineral content, as well as the results of previous investigations on the biological activity of species of the genus *Pleurotus*, are discussed.

Nutritional and Mineral Contents

The findings related to the nutritional and mineral contents of the studies on Genus *Pleurotus* species in the literature are shown in Table 1 and Table 2.

Table 1. Nutritional Contents of Genus Pleurotus

Nutritional Composition	**Values (g/100 g)**
Protein	11.95-35.5
Carbohydrate	34-63.03
Ash	2.97-10.7
Mouisture	78-89.1
Fat	1.06-7.50

The nutritional value of *Pleurotus* species has been shown through extensive research (Table 1). The following percentages of various nutrients have been reported: protein (11.95 g/100 g), carbohydrates (34 g/100 g), ash (2.97 g/100 g), moisture (78 g/100 g-89.1 g/100 g), and fat (1.06 g/100

g-7.50 g/100 g) (Bano, 1981; Kıkuchı et al., 1984; Ghosh and Chakravarty, 1990; Yang et al., 2001; Silva et al., 2002; Alam et al., 2008; Kirbag and Akyüz, 2008; Mshandete and Cuff, 2008; Ahmed et al., 2009; Ifeoma et al., 2009; Khan and Tania, 2012; Yehia, 2012; Kortei and Wiafe-Kwagyan, 2015; Gasecka et al., 2016; Jegadeesh et al., 2018).

Table 2. Mineral Contents of genus Pleurotus

Mineral Composition	**Values (mg/kg)**
Zn	0.14-38
K	0.2-2218.33
Na	0.08-686
Fe	0.5-620.7
Ca	0.08-305
Se	0.0025-4.5
Mg	0.4-2593

When it comes to decomposing matter, fungi are crucial players in the environment. Elements are accumulated at varying rates in their bodies depending on the composition of the organic matter they breakdown (Sevindik et al., 2020). Here, we estimated the element compositions of *Pleurotus* species based on a synthesis of the existing literature (Table 2). Specifically, we know the ranges of the following elements: K (0.2 mg/kg -2218.33 mg/kg), Na (0.08 mg/kg -686 mg/kg), Fe (0.5 mg/kg -620.7 mg) /kg, Ca (0.08 mg/kg -305 mg/kg), Se (0.0025 mg/kg -4.5 mg/kg), and Mg (0.4 mg/kg -2593 mg/kg) (Bano, 1981; Ghosh and Chakravarty, 1990; Yang et al., 2001; Silva et al., 2002; Alam et al., 2008; Kirbag and Akyüz, 2008; Mshandete and Cuff, 2008; Ahmed et al., 2009; Ifeoma et al., 2009; Sopanrao et al., 2010; Kortei and Wiafe-Kwagyan, 2015; Gasecka et al., 2016; Jegadeesh et al., 2018).

Biological activity

Fungi create several chemicals with biological activity (Sevindik et al., 2018c). Due to the presence of these bioactive substances, mushrooms are in high demand as therapeutically useful foodstuffs (Korkmaz et al., 2018). This research reviews the available information on the biological activities of *Pleurotus* species. Numerous investigations have been conducted on the biological activities of *Pleurotus* species both *in vitro* and *in vivo*. Ethanol, acetone, diethyl ether, aqueous, hydroalcoholic, methanol, ethyl acetate, butanol, methylene chloride, chloroform, alcoholic, petroleum ether, and carpophore were all utilised as extracts in these experiments. Table 3 displays results from research assessing the biological activity of *Pleurotus* species.

Table 3. Biological activity of genus Pleurotus

Mushroom species	Biological activity	Extraction	References
Pleurotus abalonus	Antitumor, Antioxidant	Ethanol, Acetone, Diethyl ether	(Wang et al., 2011; Shi et al., 2013)
Pleurotus albidus	Antioxidant	Ethanol, Aqueous, hydroalcoholic	(Gambato et al., 2016; Stoffel et al., 2021; Contato et al., 2022)
Pleurotus australis	Antioxidant, Antimicrobial	Aqueous	(Ren et al., 2014)
Pleurotus citrinopileatus	Antioxidant, Antimicrobial, Antitumor	Ethanol, methanol, Diethyl ether, Ethyl acetate, Butanol	(Meng et al., 2011; Gürgen et al., 2020; Wang et al., 2021)
Pleurotus columbinus	Antioxidant, Antimicrobial, Antiviral, Cytotoxic	Methanol, Aqueous	(Angelini et al., 2021; Elhusseiny et al., 2021)
Pleurotus cystidiosus	Antioxidat, Antinociceptive	Ethanol, Methanol, Acetone, Methylene chloride	(Kudahewa et al., 2008; Muruke, 2014; Garcia et al., 2020)
Pleurotus djamor	Antioxidant, Antimicrobial, Anticancer, Antilarvicidal, Hepatoprotective	Ethanol, Methanol, Chloroform, Dimethyl ether, Aqueous, Alcoholic	(Sandeep and Saha, 2011; Zhang et al., 2016; Acharya et al., 2017; Sathyan et al., 2017; Manimaran et al., 2021)
Pleurotus eous	Antimicrobial, Antitumor	Methanol, Aqueous, Petroleum ether, Ethyl acetate	(Sudha et al., 2012; Suseem and Saral, 2013; Gunasekaran et al., 2021)
Pleurotus eryngii	Hypoglycemic, Antihyperlipidaemic, Hepatoprotective, Antioxidant, Antitumor	Water, Butanol, Chloroform, Ethanol, Methanol	(Ma et al., 2014; Zhang et al., 2014; Sun et al., 2017; Zhang et al., 2017; Gong et al., 2022)
Pleurotus flabellatus	Antimicrobial, Antioxidant, Cytotoxic	Methanol, Ethanol	(Pumtes et al., 2016; Klaus et al., 2021; Pandey et al., 2021)
Pleurotus floridanus	Antimicrobial, Anti-inflammatory, Antioxidant	Methanol	(Bains et al., 2021)
Pleurotus giganteus	Antimicrobial, Antioxidant	Aqueous, Ethanol	(Phan et al., 2014; Debnath et al., 2019)
Pleurotus levis	Antimicrobial, Antioxidant	Hydroalcoholic, Methanol Chloroform, Ethanol, Acetone	(Adebayo et al., 2018)
Pleurotus opuntiae	Antimicrobial	Ethanol, Methanol	(Tiwari Pandey et al., 2021)
Pleurotus ostreatoroseus	Antioxidant, Cytotoxic, Antitumor	Aqueous, Water	(de Sousa et al., 2004; Brugnari et al., 2018)
Pleurotus ostreatus	Antioxidant, Antimicrobial, Antitumor, Antiviral, Antiallergic	Water, Ethanol, Acetone, Ethyl acetate	(Silva et al., 2012; Vamanu, 2012; Jesenak et al., 2014; Han et al., 2015; Radzki et al., 2016; Sevindik et al., 2016; Sevindik et al., 2018; Urbancikova et al., 2020; Zhang et al., 2020)
Pleurotus platypus	Antioxidant	Aqueous	(Sathyaprabha et al., 2011)
Pleurotus porrigens	Antioxidant, Cytotoxic	Ethyl acetate, Methanol	(Hasegawa et al., 2007; Ebrahimzadeh et al., 2010)

Pleurotus pulmonarius	Antimicrobial, Anti-inflammatory, Antioxidant, Cytotoxic, Antidiabetic, Anticholinesterase	Hydroalcoholic, Methanol, Water, Acetone	(Adebayo et al., 2012; Nguyen et al., 2016; Balaji et al., 2020; Akyüz et al., 2022)
Pleurotus sajor-caju	Antioxidant, Antimicrobial, Antitumor, Anti-inflammatory	Methanol, Aqueous	(Finimundy et al., 2013; Gogavekar et al., 2014; Kandasamy et al., 2020)
Pleurotus squarrosulus	Antimicrobial	Ethanol, Methanol, Water	(Kalu and Kenneth, 2017)
Pleurotus tuber-regium	Antimicrobial, Antioxidant, Antitumor	Carpophore, Water, Ethanol, Aqueous	(Tao et al., 2009; Anyanwu et al., 2016; Bamigboye et al., 2016; Metsebing et al., 2020)

Antioxidant activity

The metabolic processes of living things and the impact of their environments create molecules known as reactive oxygen species (Sevindik et al., 2017). It is possible for these chemicals to become toxic to living things as their concentrations increase. Beneficial effects of reactive oxygen species are mitigated or suppressed by the antioxidant defence system (Sevindik, 2018). Oxidative stress occurs when the body's natural antioxidants are inadequate. Humans may be susceptible to debilitating illnesses including cancer, cardiovascular disease, Parkinson's, and Alzheimer's due to oxidative stress (Sevindik, 2020). To aid natural antioxidants in mitigating these effects and decreasing oxidative stress, supplemental antioxidants are often used (Baba et al., 2020). Fortified antioxidant levels may be achieved in part by eating mushrooms (Sevindik et al., 2018d). The results of previous research on the antioxidant activity of *Pleurotus* species were gathered in this study (Table 3). In DPPH and hydroxyl radical scavenging assays, *P. abalonus* has been reported to achieve 77.4% and 71.1% maximum scavenging efficiency, respectively (Wang et al., 2011). DPPH (159%, 11.98 mg/mL) and ABTS (73%) findings of *P. albidus* have been published (Gambato et al., 2016; Stoffel et al., 2021). In the DPPH assay, the IC50 value for *P. australis* has been reported as 4.03 mg/mL (Ren et al., 2014). It has been reported that *P. citrinopileatus* had the greatest results in the DPPH, ORAC, and SOD assays, with IC50=7.9 mg/mL, 0.250.009 mgTE/mg, and 2.70.59 U/mg, respectively (Meng et al., 2011). An IC50 value for DPPH activity has been observed between 2.25 and 4.98 g/mL for several *P. columbinus* extracts (Angelini et al., 2021). In another study on *P. columbinus*, IC50 µg/mL values were reported to be 35.13 ± 3.27 for the DPPH test, 13.97 ± 4.91 for the ABTS test, and 29.42 ± 3.21 for the ORAC (Elhusseiny et al., 2021). The DPPH effect of *P. cystidiosus* has been reported to be 79.1%, with an IC50 value of 0.035-0.150 mg/mL, and an iron chelating action of 98.3%,

across a variety of tests and solvents (Muruke, 2014; Garcia et al., 2020). The IC50 value for the DPPH impact of *P. djamor* has been reported to be 0.653 mg/mL, with a corresponding value of 38.095%. (Acharya et al., 2017; Sathyan et al., 2017). It has been reported that the highest effect in the DPPH, Reducing power, Chelation, β-Bleaching, ABTS, FRAP and OH tests of *P. eous* was observed as 43.0±0.21 mg/mL in the β-Bleaching test of the methanol extract (Sudha et al., 2012). It has been reported that the greatest effect of *P. eryngii* in DPPH, reducing power and superoxide anion radical capture tests was obtained from the superoxide anion radical capture test, while the lowest effect was achieved in reducing power (Zhang et al., 2014). In a separate investigation of *P. eous*, it was stated that DPPH, O2−, and OH assays revealed an effect between 0.2-1 mg/mL (Sun et al., 2017). Lipid peroxidation test IC50 value of *P. flabellatus* 1.71 ± 0.02 mg/mL, CUPRAC test IC50 value 2.91 ± 0.01 mg TE/g, iron chelation test IC50 value 4.96 ± 0.08 mg/mL and ABTS test IC50 value 3.36 ± 0.03 mg TE /g has been reported (Klaus et al., 2021). The highest DPPH and ABTS value recorded in a different research was 13.33 mg/mL, which is the IC50 value for ABTS (Pumtes et al., 2016). The DPPH test of *P. floridanus* has been found to be 80.65% (Bains et al., 2021). The best findings of DPPH, FRAP and lipid peroxidation of *P. giganteus* are correspondingly; It has been reported that the IC50 value is 16.18 mg/mL, 2.69 µM, 49.80% (Phan et al., 2014). It has been reported that *P. levis* has a DPPH value of 0.51 µg/mL, a-carotene bleaching value of 0.59 µg/mL, an ABTS value of 0.50 µg/mL, and an ORAC value of 5080.8 mol of trolox equivalent mL^{-1} (Adebayo et al., 2018). Results from an ABTS assay showed that the IC50 value for *P. ostreatoroseus* was 0.057 0.002 mg/mL (Brugnari et al., 2018). The ABTS and FRAP assays have demonstrated antioxidant activity in *P. ostreatus* (Radzki et al., 2016). In a separate investigation, the best findings in DPPH, ABTS, Reducing power and Ferrous ion chelation of *P. ostreatus* were; It has been reported to be 7.2 mg/mL, 10.3%, 1.25 and 19.79% at 10 mg/mL extract concentrations (Vamanu, 2012). In another research, it was revealed that the total antioxidant level of *P. ostreatus* samples collected from the natural environment was 2.023, and the culture sample was 1.153 mmol/L (Sevindik et al., 2018). The DPPH test has shown that *P. platypus* has an effect value of 95.2%, according to previous studies (Sathyaprabha et al., 2011). It has been reported that the best DPPH activity of *P. porrigens* is 21.9±0.9 µg/mL in methanol extract (Ebrahimzadeh et al., 2010). *P. pulmonarius* had a DPPH value of 68.09% at a concentration of 25 mg extract (Akyüz et al., 2022). There are conflicting reports on the DPPH test results for *P. sajor-caju*, with some studies reporting 67.42% and others reporting 88.0%. (Gogavekar et al., 2014; Kandasamy et al., 2020). Most hybrids of *P. tuber-regium* and its parent strain have been found to have DPPH and hydroxyl clearance values below 1 mg/mL. (Bamigboye

et al., 2016). Another research found that the total antioxidant levels of *P. citrinopileatus* cultured in various culture conditions varied between 2.316 and 3.125 mmol/L (Gürgen et al., 2020).

Antimicrobial activity

There has been a rise in the incidence of infectious illnesses in recent years (Eraslan et al., 2021). Considering the rise in antibiotic-resistant microbes and the potential side effects of synthetic medications, researchers are increasingly interested in exploring natural alternatives (Sevindik and Bal, 2021). Fungi are regarded as one of the most valuable natural antibacterial resources. Our research examined the antimicrobial properties of *Pleurotus* species previously described in the literature (Table 3). Disc diffusion experiments looked examined the effects of *P. albidus* on several bacterial species, including *Bacillus cereus*, *Bacillus subtilis*, *Pseudomonas aeruginosa*, and *Staphylococcus aureus*. The most promising results have been shown against *Bacillus* species, according to the literature (Contato et al., 2022). Against *Streptococcus epidermidis*, *P. australis* has been shown to have a considerable impact (Ren et al., 2014). *P. citrinopileatus* has been shown to suppress *Escherichia coli* by 87.0%, according to a study (Meng et al., 2011). While *P. columbinus* was shown to be the least effective against one of the fungus strains, *Candida albicans*, it was found to be the most effective against *E. coli* (Angelini et al., 2021).

P. djamor has been shown to be very effective against *Klebsiella pneumoniae* and *Escherichia coli* (Sathyan et al., 2017). Diameters of inhibition for *Pseudomonas fluorescens*, *Staphylococcus aureus*, *Corynebacterium diphtheriae*, *Magnaporihe grisea* and *Ralstonia solanacearum* were 33 mm, 32 mm, 22.4 mm, and 18.3 mm, respectively, in a separate investigation on (Sandeep and Saha, 2011; *P. djamor* Manimaran et al., 2021). Among the different extracts of *P. eous*, petroleum ether shows the strongest effect and against microorganisms 4.4 µg/mL for *S. aureus*, *B. subtilis* 3.1 µg/mL, *B. cereus* 4.2 µg/mL, *P. aeruginosa* 8.8 µg/mL, MIC values of *E. coli* 3.1 µg/mL and *K. pneumoniae* 4.4 µg/mL have been reported (Suseem and Saral, 2013). Methanol extract of *P. flabellatus* has been reported to exhibit a mean growth inhibition of 10.3±0.3 to 17.6±0.3 mm against *Shigella fexneri*, *Moraxella catarrhalis*, *Serratia marcescens*, *Proteus vulgaris*, *Proteus mirabilis*, *Pseudomonas aeruginosa* and *Staphylococcus aureus* (Pandey et al., 2021). The fungus *P. flabellatus* was shown to be very effective against many distinct strains of *Candida albicans*, according to a separate investigation (Klaus et al., 2021). The reported inhibitory state of *P. floridanus* against *S. aureus*, *P. aeruginosa*, *K. pneumoniae* and *E. coli* ranges from 24.25 to 28.35 mm (Bains et al., 2021). It has been reported that *P. giganteus* acts against *E.*

coli, *P. aeruginosa*, *B. subtilis* and *S. aureus* at concentrations of 12, 10, 14 and 15 µg/mL, respectively (Debnath, et al., 2019). The effectiveness of *P. levis* extracts against *E. coli* and *P. aeruginosa* has been observed to range from 3.33 to 145.52 µg/mL (Adebayo et al., 2018). Also, *Staphylococcus aureus*, *Pseudomonas aeruginosa*, *Proteus mirabilis*, *Proteus vulgaris*, *Serratia marcescens*, *Shigella flexneri* and *Moraxella* sp. are only few of the microorganisms that *P. opuntiae* has been shown to be successful against (Tiwari Pandey et al., 2021). It has been reported that the acetone extract of *P. ostreatus* is 8.33 mm and 7.33 mm on *E. coli* and *B. subtilis*, respectively, while the ethyl acetate extract is 7.67 mm and 8.33 mm on *E. coli* and *B. subtilis*, respectively (Han et al., 2015). *P. ostreatus* was shown to be effective against *Staphylococcus aureus*, *Enterococcus faecalis*, *Escherichia coli*, *Pseudomonas aeruginosa*, *Candida albicans* and *Candida tropicalis* in a separate investigation, but at lower doses (Sevindik et al., 2016). Several bacteria, including *Proteus mirabilis*, *Pseudomonas aeruginosa*, *Salmonella typhi*, *Staphylococcus aureus*, *Escherichia coli*, *Shigella* species and *Klebsiella pneumoniae* have been shown to be vulnerable to *P. pulmonarius* potent antibacterial properties (Adebayo et al., 2012). *Bacillus cereus*, *Staphylococcus aureus*, *Micrococcus luteus*, *Escherichia coli* and *Salmonella typhimurium* were all tested to see how they fared against *P. sajor-caju*. Results showed that *Salmonella typhimurium* had the largest inhibitory zone at 29 2.34 mm, whereas *B. cereus* had the smallest at 18 2.02 mm (Gogavekar et al., 2014). *E. coli*, *B. cereus*, *S. aureus*, *P. aeruginosa*, *C. albicans* and *C. glabrata* bacteria have all been found to be inhibited by *P. squarrosulus* at concentrations between 125 and 500 mg/mL in various extracts (Kalu and Kenneth, 2017). It has been reported that *P. tuber-regium* was effective against *B. subtilis* and *K. aerogenes* at 12.5 mg/mL, *Enterococcus faecalis*, *S. aureus*, *S. epidermidis*, *Enterobacter cloacae*, *E. coli*, *Mycobacterium smegmatis*, *Proteus mirabilis*, *P. vulgaris* and *K. oxytoca* at 6.25 mg/mL and against *C. albicans*, *Aspergillus fumigatus* and *A. ochraceus* at an extract concentration of 3.13 mg/mL (Metsebing et al., 2020). The ethanolic extract of *P. tuber-regium* has been reported to be effective against *Streptococcus* sp. at 50 mg/mL, *E. coli* at 6.25 mg/mL, *P. aeruginosa* at 3.13 mg/mL, *S. aureus* at 12.5 mg/mL and against *Aspergillus* sp. at 25 mg/mL. In addition, aqueous extracts were reported to be effective against *S. auerus*, *E. coli* and *P. aeruginosa* at extract concentrations of 50 mg/mL, 25 mg/mL and 12.5 mg/mL, respectively (Anyanwu et al., 2016). In this regard, according to the literature findings, it is found that Genus *Pleurotus* species exhibit considerable antimicrobial activity. Therefore, it is possible that species of the genus *Pleurotus* provide a significant supply of antimicrobial compounds.

Other activity

Fungi produce secondary metabolites that show significant biological activity in their bodies. These bioactive compounds are responsible for many biological activities (Krupodorova et al., 2022). In our study, the biological activities of Genus *Pleurotus* species reported in the literature were emphasized (Table 3). Among these studies, the antitumor effect of MCF-7, a human breast cancer cell, was investigated in the study on *P. abalonus*. In the study, it was reported that the best antitumor IC50 result was 193 µg/mL (Shi et al., 2013). In another study, the effect of *P. abalonus* against MCF-7 and HepG2, a human liver cell line, was investigated. According to the results obtained, it was reported that the best effect result was 65.2% and 34.7%, respectively (Wang et al., 2011). It has been reported that *P. citrinopileatus* has an effect in the treatment of liver cancer using H22 tumor-bearing mice (Wang et al., 2021). It has been reported that the selectivity index of *P. columbinus* against adenovirus is 4.2. It has also been reported to show moderate cytotoxicity against normal human peripheral blood mononuclear cells (PBMC) and prostate (PC3, DU-145). In addition, colorectal (Colo-205), cecum carcinoma (LS-513), liver cancer (HepG2), cervical cancer (HeLa), breast adenocarcinoma (MDA-MB-231 and MCF-7), leukemia (CCRF-CEM), acute monocytic leukemia (THP1), acute promyelocytic leukemia (NB4), and lymphoma (U937) cell lines have been reported to have low toxicity (Elhusseiny et al., 2021). To determine the antinociceptive potential of *P. cystidiosus*, standard hot plate and tail flick tests were used during oestrus in male rats (doses used: 125, 500 and 1000 mg/kg) and female rats. In male rats, 18% medium dose and 93% high dose were administered and prolongation was observed after 2 hours of administration. It has been reported that estrus female rats showed a significant prolongation in reaction time of 22% in the hot plate test (Kudahewa et al., 2008). It has been reported that *P. djamor* has anticancer effects against A549 cancer cells in the concentration range of 6.25–100 µg/mL. It has also been reported that it has a larvicidal effect against *Aedes aegypti* and *Culex quinquefasciatus* at IC50 (5.88 and 4.84 mg/L) and IC90 (22.80 and 19.33 mg/L) values (Manimaran et al., 2021). For hepatoprotective activity in a different study of *P. djamor*, 800 mg/kg MZPS-3 administration significantly decreased AST, ALT, MDA and LPO levels, increased TC, TG and ALB levels significantly, and significantly increased SOD and GSH- activities. It has been reported that it recovers in a way (Zhang et al., 2016).

The IC50 potency of *P. eous* against HT29 and PC3 cell lines has been reported to be 233.50 µg/mL and 230.80 µg/mL, respectively (Gunasekaran et al., 2021). It has been reported that *P. eryngii* exhibits a high hypoglycemic activity by promoting the expression of the PI3K-

AKT signaling pathway based on in vitro assay and cell experiments (Gong et al., 2022). In a different study of *P. eryngii*, EPS, EEPS and AEPS supplementation increased blood lipid levels (TC, TG, HDL-C and LDL-C), hepatic lipid levels (TC and TG), hepatic enzyme activities (ALP, ALT and AST) can significantly improve its condition (GSH-Px, SOD, T-AOC, MDA and LPO), it has been reported that these polysaccharides are effective in reducing hepatocyte damage in histopathological observations (Zhang et al., 2017). It has been reported that *P. eryngii* exerts a significant effect against HepG-2 at a concentration of 400 μg/mL (Ma et al., 2014). It has been reported that *P. flabellatus* exerts cytotoxic effects against colorectal carcinoma HCT116 cells and normal lung MRC-5 fibroblasts (Klaus et al., 2021). The anti-inflammatory activity of *P. floridanus* was reported to be the highest at 92.58% by HRBC membrane stabilization and albumin denaturation assay (Bains et al., 2021). The uncooked basidiocarp extract of *P. ostreatoroseus* was reported to be cytotoxic to Vero cells, but decreased cytotoxicity of the extracts after cooking and subsequent in vitro digestion (Brugnari et al., 2018). Another study of *P. ostreatoroseus* reported a 41.96% reduction in NCI-H292 cell lines and *in vivo* Sarcoma 180 cell lines (de Sousa et al., 2004). In a study on human carcinoma cell lines of *P. ostreatus*, it was reported that both intracellular and extracellular polysaccharides exhibit antitumor activity (Silva et al., 2012). In another study for the antitumor property of *P. ostreatus*, a new selenium polysaccharide fraction (Se-POP-3) produced by *P. ostreatus* was characterized. It has been reported that Se-POP-3 can induce apoptosis and inhibit the migration of cancer cells as a result of in vitro experiments with cancer and normal cell lines (Zhang et al., 2020). It has been reported that β-glucan pleuran (insoluble β-1,3/1.6-D-glucan) isolated from *P. ostreatus* has a beneficial effect for respiratory tract symptoms and infections in a study on herpes simplex virus type-1 (Urbancikova et al., 2020). In another study, it was observed that β-glucan isolated from *P. ostreatus* significantly decreased peripheral blood eosinophilia and stabilized the total IgE levels in the serum. It has been reported that *P. ostreatus* has an antiallergic effect (Jesenak et al., 2014). It has been reported that conjugated ketonic fatty acid and porrigenic acid isolated from *P. porrigens* exhibit cytotoxic activity against myeloma THP-1 cells, but do not show any significant toxicity against B16F1 melanoma (Hasegawa et al., 2007). *P. pulmonarius* has been reported to show significant inhibition of formalin-induced paw edema in mice (Adebayo et al., 2012). It has been reported that *P. pulmonarius* significantly reduces the percentage of viability in MDA-MB-231 cell lines (Akyüz et al., 2022). In a different study, it was reported that *P. pulmonarius* had an antidiabetic status in a study administered orally to diabetic wistar albino rats induced with 200 and 400 mg/kg of STZ-NA for 4 weeks (Balaji et al., 2020). In another study, it was reported

that *P. pulmonarius* showed slightly lower but moderate inhibitory activity against acetylcholinesterase (AChE) and butyrylcholinesterase compared to galantamine, a standard AChE inhibitor (Nguyen et al., 2016). The cytotoxic activity results of aqueous extracts of *Pleurotus sajor-caju* were reported to be at half-maximum inhibitory concentrations of 0.64±0.02% for Hep-2 and 0.25±0.02% for HeLa (Finimundy et al., 2013). It was observed that β-d-glucan from *Pleurotus sajor-caju* inhibited the inflammatory phase of formalin-induced nociception in mice and reduced the total leukocyte count and myeloperoxidase levels induced by LPS, and with these results, β-d-glucan had a significant anti-inflammatory activity (Silveira et al., 2014). Polysaccharide-protein complex, sulfated and carboxymethylated derivatives of the aqueous extract of *P. tuber-regium* have been reported to have antitumor effects (Tao et al., 2009). According to these literature results, it is seen that Genus *Pleurotus* species show important biological activities. As a result, it is thought that Genus *Pleurotus* species can be used as an important natural resource in pharmacological designs.

Conclusion

For their usefulness as a functional food, mushrooms have garnered a lot of attention. Many biological activity, beyond its nutritional benefits, have been attributed to it. The biological activities of the members of the genus *Pleurotus*, which cause destruction in forest and forest products, were investigated in the literature. The nutritional value, mineral content, and biological activity of *Pleurotus* species were collated in this research. The biological activities of *Pleurotus* species were found to be rather high in the research literature. The nutritional value is another selling point. As a consequence, wood destroyer *Pleurotus* species are being considered as potential key natural materials in pharmaceutical designs.

REFERENCES

Acharya, K., Khatua, S., Ray, S. (2017). Quality assessment and antioxidant study of *Pleurotus djamor* (Rumph. ex Fr.) Boedijn. *Journal of Applied Pharmaceutical Science*, 7(6), 105-110.

Adebayo, E. A., Martínez-Carrera, D., Morales, P., Sobal, M., Escudero, H., Meneses, M. E., Bonilla, M. (2018). Comparative study of antioxidant and antibacterial properties of the edible mushrooms *Pleurotus levis*, *P. ostreatus*, *P. pulmonarius* and *P. tuber-regium*. *International Journal of Food Science & Technology*, 53(5), 1316-1330.

Adebayo, E. A., Oloke, J. K., Majolagbe, O. N., Ajani, R. A., Bora, T. C. (2012). Antimicrobial and anti-inflammatory potential of polysaccharide from *Pleurotus pulmonarius* LAU 09. *African Journal of Microbiology Research*, 6(13), 3315-3323.

Ahmed, S. A., Kadam, J. A., Mane, V. P., Patil, S. S., Baig, M. M. V. (2009). Biological efficiency and nutritional contents of *Pleurotus florida* (Mont.) Singer cultivated on different agro-wastes. *Nature and science*, 7(1), 44-48.

Akgül, H., Sevindik, M., Coban, C., Alli, H., & Selamoglu, Z. (2017). New approaches in traditional and complementary alternative medicine practices: *Auricularia auricula* and *Trametes versicolor*. *J Tradit Med Clin Natur*, *6*(2), 239.

Akgül, H., Sevindik, M., Akata, I., Altuntaş, D., Bal, C., & Doğan, M. (2016). *Macrolepiota procera* (Scop.) Singer. Mantarının Ağır Metal İçeriklerinin ve Oksidatif Stres Durumunun Belirlenmesi. *Süleyman Demirel Üniversitesi Fen Bilimleri Enstitüsü Dergisi*, *20*(3), 504-508.

Akyüz, M., İnci, Ş., Kırbağ, S. (2022). Evaluation of Antimicrobial, Antioxidant, Cytotoxic and DNA Protective Effects of Oyster Mushroom: *Pleurotus pulmonarius* (Fr.) Quel. *Arabian Journal for Science and Engineering*, 1-11.

Alam, N., Amin, R., Khan, A., Ara, I., Shim, M. J., Lee, M. W., Lee, T. S. (2008). Nutritional analysis of cultivated mushrooms in Bangladesh–*Pleurotus ostreatus*, *Pleurotus sajor-caju*, *Pleurotus florida* and *Calocybe indica*. *Mycobiology*, 36(4), 228-232.

Angelini, P., Pellegrino, R. M., Tirillini, B., Flores, G. A., Alabed, H. B., Ianni, F., Ferrante, C. (2021). Metabolomic profiling and biological activities of *Pleurotus columbinus* Quél. Cultivated on different agri-food byproducts. *Antibiotics*, 10(10), 1245.

Anyanwu, N. G., Mboto, C. I., Solomon, L., Frank-Peterside, N. (2016). Phytochemical, proximate composition and antimicrobial potentials of *Pleurotus tuber-regium* sclerotium. *NY Sci J*, 9(1), 35-42.

Baba, H., Sevindik, M., Dogan, M., & Akgül, H. (2020). Antioxidant, Antimicro-

bial Activities and Heavy Metal Contents of Some Myxomycetes. *Fresenius Environmental Bulletin*, *29*(09), 7840-7846.

Bains, A., Chawla, P., Tripathi, A., Sadh, P. K. (2021). A comparative study of antimicrobial and anti-inflammatory efficiency of modified solvent evaporated and vacuum oven dried bioactive components of *Pleurotus floridanus*. *Journal of Food Science and Technology*, 58(9), 3328-3337.

Bal, C., Akgül, H., Sevindik, M., Akata, I., & Yumrutas, O. (2017). Determination of The Anti-Oxidative Activities of Six Mushrooms. *Fresenius Envir Bull*, *26*(10), 6246-6252.

Bal, C., Sevindik, M., Akgül, H., & Selamoglu, Z. (2019). Oxidative Stress Index and Antioxidant Capacity of *Lepista nuda* Collected from Gaziantep/Turkey. *Sigma Journal of Engineering and Natural Sciences*, *37*(1), 1-5.

Balaji, P., Madhanraj, R., Rameshkumar, K., Veeramanikandan, V., Eyini, M., Arun, A., Kim, H. J. (2020). Evaluation Of Antidiabetic Activity of *Pleurotus pulmonarius* Against Streptozotocin-nicotinamide Induced Diabetic Wistar Albino Rats. *Saudi Journal of Biological Sciences*, 27(3), 913-924.

Bamigboye, C. O., Oloke, J. K., Dames, J. F. (2016). Biological Activity of Extracellular and Intracellular Polysaccharides from *Pleurotus tuber-regium* Hybrid and Mutant Strains. *Journal of Food and Nutrition Research*, 4(7), 422-428.

Bano, Z. (1981). Essential Amino Acid Composition and Proximate Analysis of The Mushroom *Pleurotus eous* and *P. florida. Mushroom Newsl. Trop*., 1(3), 6-10.

Barbosa, J. R., dos Santos Freitas, M. M., da Silva Martins, L. H., & de Carvalho Junior, R. N. (2020). Polysaccharides of Mushroom *Pleurotu*s spp.: New Extraction Techniques, Biological Activities and *Carbohydrate Polymers* Development of New Technologies., 229, 115550.

Brugnari, T., da Silva, P. H. A., Contato, A. G., Inácio, F. D., Nolli, M. M., Kato, C. G., de Souza, C. G. M. (2018). Effects of Cooking and in Vitro Digestion on Antioxidant Properties and Cytotoxicity of The Culinary-Medicinal Mushroom *Pleurotus ostreatoroseus* (Agaricomycetes). *International Journal of Medicinal Mushrooms*, 20(3),259-270.

Cohen, R., Persky, L., & Hadar, Y. (2002). Biotechnological Applications and Potential of Wood-Degrading Mushrooms of The Genus *Pleurotus*. *Applied microbiology and biotechnology*, *58*(5), 582-594.

Contato, A. G., de Araújo, C. A. V., Zanzarin, D. M., Aranha, G. M., Sybuia, P. A., Pilau, E. J., de Souza, C. G. M. (2022). Biological Characterization and Antimicrobial Bioactives of Mycelium Extracts from Medicinal Mushrooms *Phellinus linteus* and *Pleurotus albidus* (Agaricomycetes). *International Journal of Medicinal Mushrooms*, 24(6).

de Sousa, M. R. Q., do Nascımento, S. C., Correia, M. J. (2004). Evaluation of Antitumoral Activity of a Fraction of Water-Soluble Components of the

Edible Mushroom *Pleurotus ostreato-roseus*. *Acta Farmaceutıca Bonaerense*, 23(2), 165-168.

Debnath, G., Das, P., Saha, A. K. (2019). Green Synthesis of Silver Nanoparticles Using Mushroom Extract of *Pleurotus giganteus*: Characterization, Antimicrobial, and α-amylase Inhibitory Activity. *Bionanoscience*, 9(3), 611-619.

Ebrahimzadeh, M. A., Nabavi, S. M., Nabavi, S. F., Eslami, S. (2010). Antioxidant and Free Radical Scavenging Activities of Culinary-Medicinal Mushrooms, Golden Chanterelle *Cantharellus cibarius* and Angel's Wings *Pleurotus porrigens*. *International Journal of Medicinal Mushrooms*, 12(3), 265-272.

Elhusseiny, S. M., El-Mahdy, T. S., Awad, M. F., Elleboudy, N. S., Farag, M. M., Aboshanab, K. M., Yassien, M. A. (2021). Antiviral, Cytotoxic and Antioxidant Activities of Three Edible Agaricomycetes Mushrooms: *Pleurotus columbinus*, *Pleurotus sajor-caju* and *Agaricus bisporus*. *Journal of Fungi*, 7(8), 645.

Eraslan, E. C., Altuntas, D., Baba, H., Bal, C., Akgül, H., Akata, I., & Sevindik, M. (2021). Some Biological Activities and Element Contents of Ethanol Extract of Wild Edible Mushroom *Morchella esculenta*. *Sigma Journal of Engineering and Natural Sciences*, *39*(1), 24-28.

Finimundy, T. C., Gambato, G., Fontana, R., Camassola, M., Salvador, M., Moura, S., Roesch-Ely, M. (2013). Aqueous Extracts of *Lentinula edodes* and *Pleurotus sajor-caju* Exhibit High Antioxidant Capability and Promising *in vitro* Antitumor Activity. *Nutrition Research*, 33(1), 76-84.

Gambato, G., Todescato, K., Pavão, E. M., Scortegagna, A., Fontana, R. C., Salvador, M., Camassola, M. (2016). Evaluation of Productivity and Antioxidant Profile of Solid-State Cultivated Macrofungi *Pleurotus albidus* and *Pycnoporus sanguineus*. *Bioresource Technology*, 207, 46-51.

Garcia, K., Garcia, C. J., Bustillos, R., Dulay, R. M. (2020). Mycelial Biomass, Antioxidant, and Myco-Actives of Mycelia of Abalone Mushroom *Pleurotus cystidiosus* in Liquid Culture. *Journal of Applied Biology and Biotechnology*, 8(2), 9-7.

Gasecka, M., Mleczek, M., Siwulski, M., Niedzielski, P. (2016). Phenolic Composition and Antioxidant Properties of *Pleurotus ostreatus* and *Pleurotus eryngii* Enriched with Selenium and Zinc. *European Food Research and Technology*, 242(5), 723-732.

Ghosh, N., Chakravarty, D. K. (1990). Predictive Analysis of The Protein Quality of *Pleurotus citrinopileatus*. *Journal of Food Science and Technology*, 27(4), 236-238.

Gogavekar, S. S., Rokade, S. A., Ranveer, R. C., Ghosh, J. S., Kalyani, D. C., & Sahoo, A. K. (2014). Important Nutritional Constituents, Flavour Components, Antioxidant and Antibacterial Properties of *Pleurotus sajor-ca-*

ju. *Journal of food science and technology*, *51*(8), 1483-1491.

Gong, P., Long, H., Guo, Y., Wang, S., Chen, F., Chen, X. (2022). Isolation, Structural Characterization, and Hypoglycemic Activities of Polysaccharides *in vitro* from *Pleurotus eryngii. Molecules*, 27(20), 7140.

Gunasekaran, S., Govindan, S., Ramani, P. (2021). Investigation of Chemical and Biological Properties of an Acidic Polysaccharide Fraction from *Pleurotus eous* (Berk.) Sacc. *Food Bioscience,* 42, 101209.

Gürgen, A., Sevindik, M., Yıldız, S., & Akgül, H. (2020). Determination of Antioxidant and Oxidant Potentials of *Pleurotus citrinopileatus* Mushroom Cultivated on Various Substrates. *Kahramanmaraş Sütçü İmam Üniversitesi Tarım ve Doğa Dergisi*, *23*(3), 586-591.

Han, S. R., Kim, K. H., Lim, K. O., Oh, T. J. (2015). Biological Activity Analysis of Different Solvent Extracts from *Pleurotus ostreatus*. *Indian Journal of Science and Technology*, 8(26), 1-8.

Hasegawa, T., Ishibashi, M., Takata, T., Takano, F., Ohta, T. (2007). Cytotoxic Fatty Acid from *Pleurocybella porrigens*. *Chemical and Pharmaceutical Bulletin*, 55(12), 1748-1749.

Ifeoma, I., Ikechukwu, A., Princess, C., Henry, I. (2009). Phytochemical Composition of *Pleurotus tuber regium* and Effect of its Dietary Incorporation on Body/Organ Weights and Serum Triacylglycerols in Albino Mice. *Journal of Medicinal Plants Research*, 3(11), 939-943.

Jegadeesh, R., Lakshmanan, H., Kab-Yeul, J., Sabaratnam, V. & Raaman, N. (2018). Cultivation of Pink Oyster mushroom *Pleurotus djamor* var. roseus on Various Agro-residues by Low Cost Rechnique. *J Mycopathol Res*, 56(3), 213-220.

Jesenak, M., Hrubisko, M., Majtan, J., Rennerova, Z., Banovcin, P. (2014). Anti-allergic Effect of Pleuran (β-glucan from Pleurotus ostreatus) in Children with Recurrent Respiratory Tract Infections. *Phytotherapy Research*, 28(3), 471-474.

Kalu, A., Kenneth, O. (2017). Antimicrobial Activity of *Pleurotus squarrosulus* on Clinical Pathogenic Bacteria and Fungi. *Journal of Advances in Microbiology*, 4(3), 1-9.

Kandasamy, S., Chinnappan, S., Thangaswamy, S., Balakrishnan, S., Khalifa, A. Y. (2020). Assessment of Antioxidant, Antibacterial Activities and Bioactive Compounds of The Wild Edible Mushroom *Pleurotus sajor-caju*. *International Journal of Peptide Research and Therapeutics*, 26(3), 1575-1581.

Khan, M. A., Tania, M. (2012). Nutritional and Medicinal Importance of *Pleurotus* Mushrooms: an Overview. *Food Reviews International*, 28(3), 313-329.

Kıkuchı, M., Tamakawa, K., Hıroshıma, K., Aıhara, Y., Mıshıma, Y., Sekı, T., Tsunoda, A. (1984). Survey on Contents of Metals in Edible Mush-

rooms. *Food Hygiene and Safety Science* (Shokuhin Eiseigaku Zasshi), 25(6), 534-542.

Kirbag, S., Akyüz, M. (2008). Evaluation of Agricultural Wastes for The Cultivation of *Pleurotus eryngii* (DC. ex Fr.) Quel. var. ferulae Lanzi. *African Journal of Biotechnology*, 7(20).

Klaus, A., Wan-Mohtar, W., Nikolić, B., Cvetković, S., Vunduk, J. (2021). Pink Oyster Mushroom *Pleurotus flabellatus* Mycelium Produced by an Airlift Bioreactor—the Evidence of Potent *in vitro* Biological Activities. *World Journal of Microbiology and Biotechnology*, 37(1), 1-14.

Korkmaz, A. I., Akgğl, H., Sevindik, M., & Selamoglu, Z. (2018). Study on Determination of Bioactive Potentials of Certain Lichens. *Acta Alimentaria*, *47*(1), 80-87.

Kortei, N. K., Wiafe-Kwagyan, M. (2015). Comparative Appraisal of The Total Phenolic Content, Flavonoids, Free Radical Scavenging Activity and Nutritional Qualities of *Pleurotus ostreatus* (EM-1) and *Pleurotus eous* (P-31) Cultivated on Rice (Oryzae sativa) Straw in Ghana. *Journal of Advances in Biology and Biotechnology*, 3(4), 153-164.

Krupodorova, T., & Sevindik, M. (2020). Antioxidant Potential and Some Mineral Contents of Wild Edible Mushroom *Ramaria stricta*. *AgroLife Scientific Journal*, 9(1), 186-191.

Krupodorova, T., Barshteyn, V., & Sevindik, M. (2022). Antioxidant and Antimicrobial Potentials of Mycelial Extracts of *Hohenbuehelia myxotricha* Grown in Different Liquid Culture Media. BioTechnologia. *Journal of Biotechnology Computational Biology and Bionanotechnology*, 103(1), 19-28

Kudahewa, D. D., Abeytunga, D. T. U., Ratnasooriya, W. D. (2008). Antinociceptive Activity of *Pleurotus cystidiosus*, an Edible Mushroom in Rats. *Pharmacognosy Magazine* , 4(13), 37.

Ma, G., Yang, W., Mariga, A. M., Fang, Y., Ma, N., Pei, F., Hu, Q. (2014). Purification, Characterization and Antitumor Activity of Polysaccharides from *Pleurotus eryngii* Residue. *Carbohydrate Polymers*, 114, 297-305.

Manimaran, K., Murugesan, S., Ragavendran, C., Balasubramani, G., Natarajan, D., Ganesan, A., Seedevi, P. (2021). Biosynthesis of TiO2 Nanoparticles Using Edible Mushroom (*Pleurotus djamor*) Extract: Mosquito Larvicidal, Histopathological, Antibacterial and Anticancer Effect. *Journal of Cluster Science*, 32(5), 1229-1240.

Meng, T. X., Furuta, S., Fukamizu, S., Yamamoto, R., Ishikawa, H., Arung, E. T., Kondo, R. (2011). Evaluation of Biological Activities of Extracts from The Fruiting Body of *Pleurotus citrinopileatus* for Skin Cosmetics. *Journal of wood science*, 57(5), 452-458.

Metsebing, B. P., Oba, R., Mossebo, D. C., Fonkui, T. Y., Tsigain, F. T., Fotsing, M. C. D., Ndinteh, D. N. (2020). Comparative Assessment of Antifungal

and Antibacterial Activities of Crude Extracts of The King Tuber Culinary-Medicinal Mushroom, *Pleurotus tuber-regium* (Agaricomycetes) from Cameroon. *International Journal of Medicinal Mushrooms*, 22(4), 359-366.

Mshandete, A. M., Cuff, J. (2008). Cultivation of Three Types of İndigenous Wild Edible Mushrooms: *Coprinus cinereus*, *Pleurotus flabellatus* and *Volvariella volvocea* on Composted Sisal Decortications Residue in Tanzania. *African Journal of Biotechnology*, 7(24).

Muruke, M. H. (2014). Evaluation of Antioxidant and Iron Chelating Activities of a Wild Edible Oyster Mushroom *Pleurotus cystidiosus* from Tanzania. *Evaluation*, 29, 18-28.

Mushtaq, W., Baba, H., Akata, I., & Sevindik, M. (2020). Antioxidant Potential and Element Contents of Wild Edible Mushroom *Suillus granulatus*. *Kahramanmaraş Sütçü İmam Üniversitesi Tarım ve Doğa Dergisi*, 23(3), 592-595.

Muszyńska, B., Grzywacz-Kisielewska, A., Kała, K., & Gdula-Argasińska, J. (2018). Anti-inflammatory Properties of Edible Mushrooms: A review. *Food Chemistry*, *243*, 373-381.

Nguyen, T. K., Im, K. H., Choi, J., Shin, P. G., Lee, T. S. (2016). Evaluation of Antioxidant, Anti-Cholinesterase, and Anti-İnflammatory Effects of Culinary Mushroom *Pleurotus pulmonarius*. *Mycobiology*, 44(4), 291-301.

Oei, P. (1996). Mushroom cultivation. Tool Publications, Leiden, The Netherlands

Pandey, A. T., Pandey, I., Kerkar, P., Singh, M. P. (2021). Antimicrobial Activity and Mycochemical Profile of Methanol Extract from *Pleurotus flabellatus*. *Vegetos*, 34(3), 619-629.

Phan, C. W., David, P., Tan, Y. S., Naidu, M., Wong, K. H., Kuppusamy, U. R., Sabaratnam, V. (2014). Intrastrain Comparison of The Chemical Composition and Antioxidant Activity of an Edible Mushroom, *Pleurotus giganteus*, and its Potent Neuritogenic Properties. *The Scientific World Journal*, 1-10.

Pumtes, P., Rojsuntornkitti, K., Kongbangkerd, T., Jittrepotch, N. (2016). Effects of Different Extracting Conditions on Antioxidant Activities of *Pleurotus flabellatus*. *International Food Research Journal*, 23(1), 173.

Radzki, W., Ziaja-Sołtys, M., Nowak, J., Rzymowska, J., Topolska, J., Sławińska, A., Kuczumow, A. (2016). Effect of Processing on The Content and Biological Activity of Polysaccharides from *Pleurotus ostreatus* Mushroom. *LWT-Food Science and Technology*, 66, 27-33.

Ren, L., Hemar, Y., Perera, C. O., Lewis, G., Krissansen, G. W., Buchanan, P. K. (2014). Antibacterial and Antioxidant Activities of Aqueous Extracts of Eight Edible Mushrooms. *Bioactive carbohydrates and dietary fibre*, 3(2), 41-51.

Sandeep, A., Saha, A. K. (2011). Antimicrobial Activity of *Pleurotus djamor*. *Journal of Mycopathological Research,* 49(2), 329-332.

Sathyan, A., Majeed, K. A., Majitha, V. K., Rajeswary, K. R. (2017). A Comparative Study of Antioxidant and Antimicrobial Activities of *Pleurotus ostreatus*, *Pleurotus eryngii* and *Pleurotus djamor*. *Int. J. Agric. Innov. Res*, 5, 907-912.

Sathyaprabha, G., Kumaravel, S., Panneerselvam, A. (2011). Analysis of Antioxidant Activity, Total Phenol, Total Flavonoid and Screening of Phyto-Components in *Pleurotus platypus* and *Pleuro tuseous*. *Journal of Chemical and Pharmaceutical Research*, 3(6), 1-6.

Selamoglu, Z., Sevindik, M., Bal, C., Ozaltun, B., Sen, İ., & Pasdaran, A. (2020). Antioxidant, Antimicrobial and DNA Protection Activities of Phenolic Content of *Tricholoma virgatum* (Fr.) P. Kumm. *Biointerface Research in Applied Chemistry*, Volume 10, Issue 3, 2020, 5500 – 5506

Sevindik, M. (2018). Investigation of Antioxidant/Oxidant Status and Antimicrobial Activities of *Lentinus tigrinus*. *Advances in pharmacological sciences*, *2018*.

Sevindik, M. (2019). The Novel Biological Tests on Various Extracts of *Cerioporus varius*. *Fresenius Environmental Bulletin*, *28*(5), 3713-3717.

Sevindik, M. (2020). Antioxidant and Antimicrobial Capacity of *Lactifluus rugatus* and its Antiproliferative Activity on A549 Cells. *Indian Journal of Traditional Knowledge (IJTK)*, *19*(2), 423-427.

Sevindik, M., & Bal, C. (2021). Antioxidant, Antimicrobial and Antiproliferative Activities of Wild Mushroom *Laeticutis cristata* (Agaricomycetes) from Turkey. *International Journal of Medicinal Mushrooms*, *23*(11), 85-90

Sevindik, M., Akgül, H., Akata, I., Alli, H., & Selamoglu, Z. (2017). *Fomitopsis pinicola* in Healthful Dietary Approach and Their Therapeutic Potentials. *Acta alimentaria*, *46*(4), 464-469.

Sevindik, M., Akgül, H., Bal, C., & Selamoglu, Z. (2018a). Phenolic Contents, Oxidant/Antioxidant Potential and Heavy Metal Levels in *Cyclocybe cylindracea*. *Indian Journal of Pharmaceutical Education and Research*, *52*(3), 437-441.

Sevindik, M., Akgül, H., Selamoglu, Z., & Braidy, N. (2020). Antioxidant and Antigenotoxic Potential of *Infundibulicybe geotropa* Mushroom Collected from Northwestern Turkey. *Oxidative medicine and cellular longevity*, *2020*.

Sevindik, M., Akgül, H., Dogan, M., Akata, I., & Selamoglu, Z. (2018b). Determination of Antioxidant, Antimicrobial, DNA Protective Activity and Heavy Metals Content of *Laetiporus sulphureus*. *Fresenius Environmental Bulletin*, *27*(3), 1946-1952

Sevindik, M., Akgül, H., Günal, S., & Doğan, M. (2016). *Pleurotus ostreatus*'

un Doğal ve Kültür Formlarının Antimikrobiyal Aktiviteleri ce Mineral Madde İçeriklerinin Belirlenmesi. *Kastamonu University Journal of Forestry Faculty*, *16*(1) 153-156

Sevindik, M., Bal, C. & Akgül, H. (2018). Comparison of Antioxidant Potentials of The Wild and Cultivated Forms of Edible *Pleurotus ostreatus* and *Agaricus bisporus* Mushrooms. *Turkish Journal of Life Sciences*, *3*(2), 263-266.

Sevindik, M., Rasul, A., Hussain, G., Anwar, H., Zahoor, M. K., Sarfraz, I., ... & Selamoglu, Z. (2018c). Determination of Anti-Oxidative, Anti-Microbial Activity and Heavy Metal Contents of *Leucoagaricus leucothites*. *Pakistan journal of pharmaceutical sciences*, *31*(5 (Supplementary)), 2163-2168.

Shi, X., Zhao, Y., Jiao, Y., Shi, T., Yang, X. (2013). ROS-dependent Mitochondria Molecular Mechanisms Underlying Antitumor Activity of *Pleurotus abalonus* Acidic Polysaccharides in Human Breast Cancer MCF-7 Cells. *PLoS One*, 8(5), e64266.

Silva, S. O., Costa, S. M. G. D., Clemente, E. (2002). Chemical Composition of *Pleurotus pulmonarius* (Fr.) Quél., Substrates and Residue After Cultivation. *Brazilian Archives of Biology and Technology*, 45, 531-535.

Silva, S., Martins, S., Karmali, A., Rosa, E. (2012). Production, Purification and Characterisation of Polysaccharides from *Pleurotus ostreatus* with Antitumour Activity. *Journal of the Science of Food and Agriculture*, 92(9), 1826-1832.

Silveira, M. L., Smiderle, F. R., Moraes, C. P., Borato, D. G., Baggio, C. H., Ruthes, A. C., Iacomini, M. (2014). Structural Characterization and Anti-İnflammatory Activity of a Linear B-D-Glucan Isolated from *Pleurotus sajor-caju. Carbohydrate polymers*, 113, 588-596.

Soares, A. A., de Sá-Nakanishi, A. B., Bracht, A., da Costa, S. M. G., Koehnlein, E. A., de Souza, C. G. M. & Peralta, R. M. (2013). Hepatoprotective Effects of Mushrooms. *Molecules*, *18*(7), 7609-7630.

Sopanrao, P. S., Abrar, A. S., Manoharrao, T. S., Vaseem, B. M. M. (2010). Nutritional Value of *Pleurotus ostreatus* (Jacq: Fr) Kumm Cultivated on Different Lignocellulosic Agro-Wastes. *Innovative Romanian food biotechnology*, (7), 66-76.

Stoffel, F., de Oliveira Santana, W., Fontana, R. C., Camassola, M. (2021). Use of *Pleurotus albidus* Mycoprotein Flour to Produce Cookies: Evaluation of Nutritional Enrichment and Biological Activity. *Innovative Food Science & Emerging Technologies*, 68, 102642.

Sudha, G., Vadivukkarasi, S., Shree, R. B. I., Lakshmanan, P. (2012). Antioxidant Activity of Various Extracts from an Edible Mushroom *Pleurotus eous. Food Science and Biotechnology*, 21(3), 661-668.

Sun, Y., Hu, X., Li, W. (2017). Antioxidant, Antitumor and Immunostimulatory

Activities of The Polypeptide from *Pleurotus eryngii* Mycelium. *International Journal of Biological Macromolecules*, 97, 323-330.

Suseem, S. R., Saral, A. M. (2013). Analysis on Essential Fatty Acid Esters of Mushroom *Pleurotus eous* and its Antibacterial Activity. *Asian J Pharm Clin Res*, 6(1), 188-91.

Tao, Y., Zhang, Y., Zhang, L. (2009). Chemical Modification and Antitumor Activities of Two Polysaccharide–Protein Complexes from *Pleurotus tuber-regium*. *International Journal of Biological Macromolecules*, 45(2), 109-115.

Tiwari Pandey, A., Pandey, I., Kanase, A., Verma, A., Garcia-Canibano, B., Dakua, S. P., Singh, M. P. (2021). Validating Anti-Infective Activity of Pleurotus Opuntiae via Standardization of Its Bioactive Mycoconstituents through Multimodal Biochemical Approach. *Coatings*, 11(4), 484.

Urbancikova, I., Hudackova, D., Majtan, J., Rennerova, Z., Banovcin, P., Jesenak, M. (2020). Efficacy of Pleuran (β-glucan from *Pleurotus ostreatus*) in the Management of *Herpes simplex* Virus Type 1 Infection. *Evidence-Based Complementary and Alternative Medicine*, https://doi.org/10.1155/2020/8562309.

Vamanu, E. (2012). Biological Activities of The Polysaccharides Produced in Submerged Culture of Two Edible *Pleurotus ostreatus* Mushrooms. *Journal of Biomedicine and Biotechnology*, https://doi.org/10.1155/2012/565974.

Wang, C. R., Ng, T. B., Li, L., Fang, J. C., Jiang, Y., Wen, T. Y., Liu, F. (2011). Isolation of a Polysaccharide with Antiproliferative, Hypoglycemic, Antioxidant and HIV-1 Reverse Transcriptase Inhibitory Activities from The Fruiting Bodies of The Abalone Mushroom *Pleurotus abalonus*. *Journal of Pharmacy and Pharmacology*, 63(6), 825-832.

Wang, Q., Niu, L. L., Liu, H. P., Wu, Y. R., Li, M. Y., Jia, Q. (2021). Structural Characterization of a Novel Polysaccharide from *Pleurotus citrinopileatus* and its Antitumor Activity on H22 Tumor-bearing Mice. *International Journal of Biological Macromolecules*, 168, 251-260.

Weng, Y., Lu, J., Xiang, L., Matsuura, A., Zhang, Y., Huang, Q., & Qi, J. (2011). Ganodermasides C and D, Two New Anti-aging Ergosterols from Spores of The Medicinal Mushroom *Ganoderma lucidum*. *Bioscience, biotechnology, and biochemistry*, *75*(4), 800-803.

Yang, J. H., Lin, H. C., Mau, J. L. (2001). Non-Volatile Taste Components of Several Commercial Mushrooms. *Food chemistry*, 72(4), 465-471.

Yehia, R. S. (2012). Nutritional Value and Biomass Yield of The Edible Mushroom *Pleurotus ostreatus* Cultivated on Different Wastes in Egypt. *Innovative Romanian Food Biotechnology*, 11, 9.

Zhang, A., Li, X., Xing, C., Yang, J., Sun, P. (2014). Antioxidant Activity of Polysaccharide Extracted from *Pleurotus eryngii* Using Response Surface Methodology. *International Journal of Biological Macromolecules*, 65, 28-32.

Zhang, C., Li, J., Wang, J., Song, X., Zhang, J., Wu, S., Jia, L. (2017). Antihyperlipidaemic and Hepatoprotective Activities of Acidic and Enzymatic Hydrolysis Exopolysaccharides from *Pleurotus eryngii* SI-04. *BMC Complementary and Alternative Medicine,* 17(1), 1-11.

Zhang, J., Liu, M., Yang, Y., Lin, L., Xu, N., Zhao, H., Jia, L. (2016). Purification, Characterization and Hepatoprotective Activities of Mycelia Zinc Polysaccharides by *Pleurotus djamor*. *Carbohydrate Polymers*, 136, 588-597.

Zhang, Y., Zhang, Z., Liu, H., Wang, D., Wang, J., Deng, Z., Zhong, S. (2020). Physicochemical Characterization and Antitumor Activity *in vitro* of a Selenium Polysaccharide from *Pleurotus ostreatus*. *International Journal of Biological Macromolecules*, 165, 2934-2946.

CHAPTER 4

IMMOBILIZATION OF CANDIDA RUGOSA LIPASE ONTO MAGNETIC SUPPORTS

Ozge CAGLAR[1], Mediha GUMUS[2], Elif OZYILMAZ[3]

1 Selçuk University, Institute of Sciences, Department of Chemistry, Konya/Turkey, E-mail: ozgecaglar07@gmail.com, ORCID ID: https://orcid.org/0000-0002-6595-1582
2 Selçuk University, Institute of Sciences, Department of Biochemistry, Konya/Turkey, E-mail: medihagms00@gmail.com, ORCID ID: https://orcid.org/0000-0001-8462-6307
3 Corresponding Author: Selçuk University, Faculty of Science, Department of Biochemistry, Konya/Turkey, E-mail: eyilmaz80@gmail.com, ORCID ID: https://orcid.org/0000-0003-4360-4165

Introduction

Great advances have been made in biotechnology and biocatalysis in the last 20 years. The use of whole living cells or separate components (e.g. enzymes, metabolites) for chemical changes is known as bioprocess technology (Mesbah, 2022). The rapid growth in the number of chemical reactions that are currently accessible has been largely credited with the success of biocatalysis (Bell et al., 2021). The biotechnology industry has made major efforts in the last decade years to raise the productivity and half-life of biocatalysts (Soni, 2022). Modern enzyme discovery tools and high-throughput laboratory evolution techniques for biocatalyst optimization have made the utilization of biocatalysis possible (Bell et al., 2021). Since enzymatic reactions enable the production of value-added products with less waste generation, enzymatic technology has speed significantly across a wide range of industrial sectors, supporting sustainability (Soni, 2022).

Enzymes are an indispensable part of our lives. For numerous decades, enzymes are used in a variety of chemical processes (Bell et al., 2021). Enzymes are natural biocatalysts with a variety of applications playing a significant role, including biotechnology, bioprocessing, health, food, and the textile industry (Carballares, Fernandez-Lafuente, & Rocha-Martin, 2022; Hummel & Gröger, 2014; Kaur & Jana, 2022; Ozyilmaz, Caglar, & Yilmaz, 2021; Ozyilmaz & Sayin, 2013; Sayin, Yilmaz, & Yilmaz, 2011; Soni, 2022; Zhu, Song, Wang, & Zhang, 2022)

Enzymes are efficient molecules compared to conventional organic and inorganic catalysts. At the same time, enzymes' excellent qualities include their enantio-, stereo-, chemo-, regio-, and selectivity, moderate reaction conditions, ease of removal from contaminated streams, non-toxicity, and environmental friendliness (Rafiee & Rezaee, 2021). They exhibit high catalytic efficiency, specificity, enantioselectivity and stereoselectivity (Carballares et al., 2022; Gröger & Hummel, 2014; Li, Zhang, & Du, 2022; Ozyilmaz, Caglar, Sargin, & Arslan, 2022; Shanmugasundaram & Pandit, 2022; Wei et al., 2022). The advantages of a directing group governing selectivity and a catalyst are combined by enzymes into a single reagent that can be employed alone or in a one-pot reaction with other enzymes (Bell et al., 2021). An enzyme's specific amino acid structural configuration determines its catalytic activity. However, reaction parameters like temperature, pH, and the concentration of salts, surfactants, or other agents might affect it (Almeida, Prata, & Forte, 2022; Damodaran & Parkin, 2018; Nelson & Cox, 2022).

Lipases (EC 3.1.1.3), are the third numerous utilized enzymes after proteases and amylases because of their miscellaneous application areas (Javed et al., 2018; Ülker, Özel, Colak, & Karaoğlu, 2011). Lipases can

be derived from microorganisms, plants, or animals; however, microbial lipases are the most often used type of enzymes in organic chemistry and biotechnology (Javed et al., 2018). The most often utilized enzymes for the catalysis of a wide variety of enantio- and regioselective processes, including interesterification, C-C bond formation, aminolysis, acidolysis, and fat hydrolysis, are lipases (Ozyilmaz et al., 2022; Ozyilmaz & Eski, 2020; Verdasco-Martin et al., 2016; Yilmaz, 2012). At the same time, with their high catalytic activity, high selectivity, and tolerance to a wide range of environmental conditions, lipases are the most important biocatalysts in biotechnology (Ozyilmaz, Ascioglu, & Yilmaz, 2021a; Soni, 2022; Yilmaz, Sezgin, & Yilmaz, 2009). Lipases are sustainable and beneficial to the environment compared to other chemical compounds (Soni, 2022). Therefore, it has an enormous amount of potential in a variety of industries, including biomedical sciences, bioenergy, paper, textiles, food, detergents, and the chemical industry (Domingues et al., 2022; Ozyilmaz, Cetinguney, & Yilmaz, 2019; Pandey, 2022; Soni, 2022; Wei et al., 2022; Yang et al., 2022).

Lipases from *Candida rugosa* were first discovered as early as the sixties. They are by isolating the yeast from natural soils due to its powerful lipase production capacity (De Maria, Sánchez-Montero, Sinisterra, & Alcántara, 2006). The *Candida rugosa* lipase has a lid including a catalytic triple of glutamine, histidine, and serine and an active site of 31 amino acids (Glu-His-Ser) (Ozyilmaz et al., 2022; Ozyilmaz & Eski, 2020) Lid surfaces can have two different conformations, open and closed, with the inner surface hydrophilic and the outer surface is hydrophobic (Mathesh et al., 2016; Ozyilmaz et al., 2022; Ozyilmaz et al., 2019; Ozyilmaz & Eski, 2020). Due to its poor stability, difficulties in recycling, and high vulnerability to environmental variables, free CRL cannot be used in large-scale production (Wang et al., 2022). A hydrophobic carrier is opened using various methods, and its active conformation is preserved. It's also common practice to immobilize or use of surfactants the open form of lipase in order to activate it (Wang et al., 2022). One of the methods designed to address these issues is enzyme immobilization (J. Xie, Zhang, & Simpson, 2022).

Enzyme immobilization is a method developed to address issues with enzyme recovery and reuse. This technique is defined as the retention of one or more enzymes in a particular area (Bolivar, Woodley, & Fernandez-Lafuente, 2022; DiCosimo, McAuliffe, Poulose, & Bohlmann, 2013; Hanefeld, Gardossi, & Magner, 2009; Liese & Hilterhaus, 2013; Sheldon & van Pelt, 2013). Three factors such as enzyme type, support type, and immobilization technique,

are critical in the enzyme immobilization process to produce an immobilized derivative with high enzyme activity retention and improved properties (Costa-Silva et al., 2021; Costa-Silva et al., 2022). Having adequate functional groups, enough porosity, surface area, solubility, high loading capacity, and the potential for microbial growth, high biocompatibility, high affinity toward proteins, biodegradability, flexibility for preparation in different geometrical configurations to contribute permeability to the system, minimal product-inhibition and the ability to preserve the enzymatic activity are other characteristics of an ideal support (Lorenz & Eck, 2005; Mesbah, 2022; Rafiee & Rezaee, 2021).

There are numerous techniques for immobilizing enzymes. They can first be separated into two categories physical methods and chemical techniques (Rafiee & Rezaee, 2021) (Fig. 1).

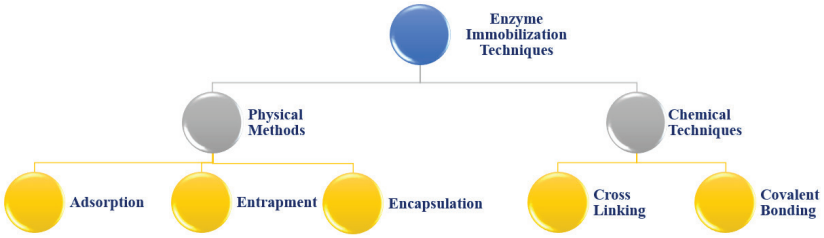

Fig. 1. *Enzyme immobilization techniques (Rafiee & Rezaee, 2021).*

Enzymes can be immobilized in one of two ways: directly onto the transducer surface, or first with a carrier, then set with the support material (Nemiwal, Zhang, & Kumar, 2022; Nguyen, Lee, Lee, Fermin, & Kim, 2019).

Support materials are mainly categorized as organic/inorganic or natural/synthetic depending on their origin. They must have a few qualities regardless of how they are classified, including biocompatibility, availability, nontoxicity, enzyme-high surface area, high porosity, and suitable particle size (Almeida et al., 2022; Rinaudo, 2008; Thangaraj & Solomon, 2019; Torres-Salas et al., 2011; Zdarta, Meyer, Jesionowski, & Pinelo, 2018; Zhang, Yuwen, & Peng, 2013; Zucca, Fernandez-Lafuente, & Sanjust, 2016).

A high surface area to volume ratio, adjustable size, biocompatibility, importance in targeted therapy, simplicity in separation under external

magnetic fields, and superparamagnetic are just a few of the special qualities of nanomaterials (Çağlar, Özyılmaz & Erbaş 2021; Ding, Zeng, Xiao, Chen, & Pan, 2021; Izci, Maksoudian, Manshian, & Soenen, 2021; Ozyilmaz, Alhiali, Caglar, & Yilmaz, 2021). Nanosized materials have a significant surface area, high catalytic efficacy, and high surface reaction activity, which results in low mass transfer resistance and superior loading capacity, making them ideal to play a key role in enzyme immobilization (Asmat & Husain, 2019). Due to their multifunctional properties, nanoparticles are generally the focus of active study in various sectors, including energy, drug release, medicinal research, and the immobilization process (Jamkhande, Ghule, Bamer, & Kalaskar, 2019; Ozyilmaz, Alhiali, et al., 2021; Tran et al., 2022; Yildiz, Ozyilmaz, Bhatti, & Yilmaz, 2017). Under the influence of external magnetic fields, magnetite nanoparticles (MNPs) can be easily removed from the reaction medium due to their large surface area, low toxicity, and high surface-to-volume ratio (Onoja, Chandren, Razak, & Wahab, 2018; Ozyilmaz, Alhiali, et al., 2021; Sayin, Ozyilmaz, Oguz, Yusufoglu, & Yilmaz, 2020).

MNPs have unique characteristics, and in recent years, they have gained a lot of popularity as an inorganic support for enzyme immobilization (Ding et al., 2021; Kaur & Jana, 2022; Onoja et al., 2018; Ozyilmaz, Alhiali, et al., 2021; Wang et al., 2022). It has been indicated that MNPs can be utilized to immobilize enzymes, either as a single support or in combination with other inorganic/organic polymers to build a hybrid support matrix (Onoja et al., 2018).

Research on the application of MNP as a support material for enzyme immobilization is still extremely interesting. The investigations using MNP as a support material on CRL immobilization are listed in the Table 1.

Tablo 1. *CRL immobilization onto magnetic supports*

Magnetic Supports	Immobilization Method	References
Fe_3O_4-CS-DAC-SDS	Cross-Linking	(Wang et al., 2022)
Maghemite (ɣ Fe_2O_3)	Covalent Binding	(Domingues et al., 2022)
Fe_3O_4@Calix-ZIF-8	Encapsulation	(Ozyilmaz, Ascioglu, & Yilmaz, 2021b)
ALG/NC/MMT	Covalent Binding	(Hussin, Attan, & Wahab, 2020)
mZIF-8	Physical adsorption	(Xiao, Chen, Lu, Wang, & Wang, 2021)
SiO_2/Fe_3O_4/GO	Co-precipitation	(Jacob, Wahab, & Misson, 2021)
Magnetic sporopollenin	Encapsulation	(Ozyilmaz, Etci, & Sezgin, 2018)
Graphene oxide Fe_3O_4 nanocomposite	Encapsulation	(W. Xie & Huang, 2018)
MWCNTs	Covalent Binding	(Asmat, Anwer, & Husain, 2019)
MWCNTs	Covalent Binding	(Kaur & Jana, 2022)

SMRs $Ca_3(PO_4)2$	cation exchange adsorption	(Wan, Tian, Li, Li, & Zhang, 2018)
oil palm leaves (OPL) Gl-A-SiO2-MNPs	Co-precipitation	(Onoja et al., 2018)
Fe_3O_4@Calix-2 and Fe_3O_4@ Calix-3	Encapsulation	(Ozyilmaz et al., 2019)
Cellulose Hydrogel beads	Physical adsorption	(Jo et al., 2019)
magnetic poly(styrene-co-divinylbenzene)	Physical adsorption	(Silva, Aguiar, Rosa, De Castro, & Freitas, 2020)
Fe_3O_4/P(GMA-DVB-St) microspheres	Covalent Binding	(Liu, 2018)
$MgFe_{2O}4$	Surface modification	(Romero et al., 2018)
Magnetic Graphene Oxide	Surface modification	(Pinto et al., 2021)
Fe_3O_4@Calix-ZIF-8	Encapsulation	(Ozyilmaz, Ascioglu, et al., 2021a)
Gl-A-SiO2-MNPs	Co-precipitation	(Onoja & Wahab, 2020)
Fe_3O_4@POT	Cross-linking	(Asmat & Husain, 2019)
magnetic PVA-Fe_3O_4	cross-linking	(Jia et al., 2016)

ALG: *alginate,* **CS:** *chitosan* **DAC:** *dialdehyde cellulose* **GO:** *graphene oxide* **Fe_3O_4:** *magnetite* **ɣFe_2O_3:** *Maghemite,* **$MgFe_2O_4$:** *magnetic magnesium spinel nanoparticles* **MNPs***: magnetic nanoparticles* **MMT:** *montmorillonite* **MWCNTs***: magnetic multiwalled carbon nanotubes,* **mZIF-8:** *magnetic ZIF-8,* **NC***: nanocellulose,* **OPL:** *oil palm leaves* **OPLA:** *oil palm leaves ash* **POT:** *poly(o-toluidine),* **SDS:** *sodium dodecyl sulfate* **St:** *styrene*

Conclusion and Suggestions:

Lipases are significant enzymes. Because of their numerous application areas, they are the third most often used enzymes after proteases and amylases. Compared to other enzymes, lipases are versatile and without co-factor. Lipases can't be used in mass production due to their poor stability, challenges with recycling, and greater vulnerability to environmental factors. The creation of novel techniques is crucial to ensuring their robustness, recyclable nature, and structural safety. A technique called enzyme immobilization is use to overcome problems with enzyme recovery and reuse. Purposing to overcome their defficients, immobilization of lipases onto iron oxide nanoparticles have arisen. The selection and application of support materials are important. Due to their special properties, magnetic nanoparticles are excellent support materials for immobilizing enzymes. In recent years, bionanotechnology applications involving bioseparation, tumor hyperthermia, magnetic resonance imaging, diagnostic tools, magnetically guided site-specific drug delivery agents, and biomolecule immobilization have made extensive use of iron oxide magnetic nanoparticles. This review article summarizes the current uses of immobilized enzymes based on iron oxide magnetic nanoparticles and shows their increasing use in the future.

REFERENCES:

Almeida, F. L., Prata, A. S., & Forte, M. B. (2022). Enzyme immobilization: what have we learned in the past five years? *Biofuels, Bioproducts and Biorefining, 16*(2), 587-608.

Asmat, S., Anwer, A. H., & Husain, Q. (2019). Immobilization of lipase onto novel constructed polydopamine grafted multiwalled carbon nanotube impregnated with magnetic cobalt and its application in synthesis of fruit flavours. *International journal of biological macromolecules, 140*, 484-495.

Asmat, S., & Husain, Q. (2019). A robust nanobiocatalyst based on high performance lipase immobilized to novel synthesised poly (o-toluidine) functionalized magnetic nanocomposite: Sterling stability and application. *Materials Science and Engineering: C, 99*, 25-36.

Bell, E. L., Finnigan, W., France, S. P., Green, A. P., Hayes, M. A., Hepworth, L. J., . . . Romero, E. (2021). Biocatalysis. *Nature Reviews Methods Primers, 1*(1), 1-21.

Bolivar, J. M., Woodley, J. M., & Fernandez-Lafuente, R. (2022). Is enzyme immobilization a mature discipline? Some critical considerations to capitalize on the benefits of immobilization. *Chemical Society Reviews*.

Carballares, D., Fernandez-Lafuente, R., & Rocha-Martin, J. (2022). Immobilization-stabilization of the dimeric D-amino acid oxidase from porcine kidney. *Process Biochemistry, 122*, 120-128.

Costa-Silva, T., Carvalho, A., Souza, C., De Castro, H., Bachmann, L., Said, S., & Oliveira, W. (2021). Immobilized enzyme-driven value enhancement of lignocellulosic-based agricultural byproducts: Application in aroma synthesis. *Journal of Cleaner Production, 284*, 124728.

Costa-Silva, T., Carvalho, A., Souza, C., Freitas, L., De Castro, H., & Oliveira, W. (2022). Highly effective Candida rugosa lipase immobilization on renewable carriers: Integrated drying and immobilization process to improve enzyme performance. *Chemical Engineering Research and Design, 183*, 41-55.

Çağlar, O., Özyılmaz E & Erbaş O. (2021). Superparamagnetic iron oxide nanoparticles use in the temporal lobe epilepsy model. *D J Tx Sci* 6(1-2):66-72.

Damodaran, S., & Parkin, K. L. (2018). *Química de alimentos de Fennema*: Artmed editora.

De Maria, P. D., Sánchez-Montero, J. M., Sinisterra, J. V., & Alcántara, A. R. (2006). Understanding Candida rugosa lipases: an overview. *Biotechnology advances, 24*(2), 180-196.

DiCosimo, R., McAuliffe, J., Poulose, A. J., & Bohlmann, G. (2013). Industrial use of immobilized enzymes. *Chemical Society Reviews, 42*(15), 6437-6474.

Ding, Y., Zeng, L., Xiao, X., Chen, T., & Pan, Y. (2021). Multifunctional magnetic nanoagents for bioimaging and therapy. *ACS Applied Bio Materials, 4*(2), 1066-1076.

Domingues, O., Remonatto, D., Dos Santos, L. K., Galán, J. P. M., Flumignan, D. L., & de Paula, A. V. (2022). Evaluation of Candida rugosa Lipase Immobilized on Magnetic Nanoparticles in Enzymatic/Chemical Hydroesterification for Biodiesel Production. *Applied biochemistry and biotechnology, 194*(11), 5419-5442.

Gröger, H., & Hummel, W. (2014). Combining the 'two worlds' of chemocatalysis and biocatalysis towards multi-step one-pot processes in aqueous media. *Current opinion in chemical biology, 19*, 171-179.

Hanefeld, U., Gardossi, L., & Magner, E. (2009). Understanding enzyme immobilisation. *Chemical Society Reviews, 38*(2), 453-468.

Hummel, W., & Gröger, H. (2014). Strategies for regeneration of nicotinamide coenzymes emphasizing self-sufficient closed-loop recycling systems. *Journal of biotechnology, 191*, 22-31.

Hussin, F. N. N. M., Attan, N., & Wahab, R. A. (2020). Taguchi design-assisted immobilization of Candida rugosa lipase onto a ternary alginate/nanocellulose/montmorillonite composite: Physicochemical characterization, thermal stability and reusability studies. *Enzyme and Microbial Technology, 136*, 109506.

Izci, M., Maksoudian, C., Manshian, B. B., & Soenen, S. J. (2021). The use of alternative strategies for enhanced nanoparticle delivery to solid tumors. *Chemical reviews, 121*(3), 1746-1803.

Jacob, A. G., Wahab, R. A., & Misson, M. (2021). Operational stability, regenerability, and thermodynamics studies on biogenic silica/magnetite/graphene oxide nanocomposite-activated candida rugosa lipase. *Polymers, 13*(21), 3854.

Jamkhande, P. G., Ghule, N. W., Bamer, A. H., & Kalaskar, M. G. (2019). Metal nanoparticles synthesis: An overview on methods of preparation, advantages and disadvantages, and applications. *Journal of drug delivery science and technology, 53*, 101174.

Javed, S., Azeem, F., Hussain, S., Rasul, I., Siddique, M. H., Riaz, M., . . . Nadeem, H. (2018). Bacterial lipases: a review on purification and characterization. *Progress in biophysics and molecular biology, 132*, 23-34.

Jia, H., Huang, F., Gao, Z., Zhong, C., Zhou, H., Jiang, M., & Wei, P. (2016). Immobilization of ω-transaminase by magnetic PVA-Fe3O4 nanoparticles. *Biotechnology reports, 10*, 49-55.

Jo, S., Park, S., Oh, Y., Hong, J., Kim, H. J., Kim, K. J., . . . Lee, S. H. (2019). Development of cellulose hydrogel microspheres for lipase immobilization. *Biotechnology and Bioprocess Engineering, 24*(1), 145-154.

Kaur, P., & Jana, A. K. (2022). Amino functionalization of magnetic multiwalled carbon nanotubes with flexible hydrophobic spacer for immobilization of Candida rugosa lipase and application in biocatalytic production of fruit flavour esters ethyl butyrate and butyl butyrate. *Applied Nanoscience*, 1-21.

Li, Q., Zhang, G., & Du, G. (2022). Production of food enzymes. In *Current Developments in Biotechnology and Bioengineering* (pp. 139-155): Elsevier.

Liese, A., & Hilterhaus, L. (2013). Evaluation of immobilized enzymes for industrial applications. *Chemical Society Reviews, 42*(15), 6236-6249.

Liu, X. (2018). Preparation of porous hollow Fe3O4/P (GMA–DVB–St) microspheres and application for lipase immobilization. *Bioprocess and biosystems engineering, 41*(6), 771-779.

Lorenz, P., & Eck, J. (2005). Metagenomics and industrial applications. *Nature Reviews Microbiology, 3*(6), 510-516.

Mathesh, M., Luan, B., Akanbi, T. O., Weber, J. K., Liu, J., Barrow, C. J., . . . Yang, W. (2016). Opening lids: modulation of lipase immobilization by graphene oxides. *ACS Catalysis, 6*(7), 4760-4768.

Mesbah, N. M. (2022). Industrial Biotechnology Based on Enzymes From Extreme Environments. *Frontiers in Bioengineering and Biotechnology, 10*.

Nelson, D. L., & Cox, M. M. (2022). *Princípios de bioquímica de Lehninger*: Artmed Editora.

Nemiwal, M., Zhang, T. C., & Kumar, D. (2022). Enzyme immobilized nanomaterials as electrochemical biosensors for detection of biomolecules. *Enzyme and Microbial Technology*, 110006.

Nguyen, H. H., Lee, S. H., Lee, U. J., Fermin, C. D., & Kim, M. (2019). Immobilized enzymes in biosensor applications. *Materials, 12*(1), 121.

Onoja, E., Chandren, S., Razak, F. I. A., & Wahab, R. A. (2018). Extraction of nanosilica from oil palm leaves and its application as support for lipase immobilization. *Journal of biotechnology, 283*, 81-96.

Onoja, E., & Wahab, R. A. (2020). Robust magnetized oil palm leaves ash nanosilica composite as lipase support: Immobilization protocol and efficacy study. *Applied biochemistry and biotechnology, 192*(2), 585-599.

Ozyilmaz, E., Alhiali, A., Caglar, O., & Yilmaz, M. (2021). Preparation of regenerable magnetic nanoparticles for cellulase immobilization: Improvement of enzymatic activity and stability. *Biotechnology Progress, 37*(4), e3145.

Ozyilmaz, E., Ascioglu, S., & Yilmaz, M. (2021a). Calix [4] arene tetracarboxylic acid-treated lipase immobilized onto metal-organic framework: Biocatalyst for ester hydrolysis and kinetic resolution. *International journal of biological macromolecules, 175*, 79-86.

Ozyilmaz, E., Ascioglu, S., & Yilmaz, M. (2021b). Preparation of One-Pot Immobilized Lipase with Fe3O4 Nanoparticles Into Metal-Organic Framework

For Enantioselective Hydrolysis of (R, S)-Naproxen Methyl Ester. *ChemCatChem, 13*(16), 3687-3694.

Ozyilmaz, E., Caglar, O., Sargin, I., & Arslan, G. (2022). Synergistic role of carbon quantum dots in the activity and stability of Candida rugosa lipase encapsulated within metal–organic frameworks (ZIF-8). *Materials Today Communications, 30*, 103066.

Ozyilmaz, E., Caglar, O., & Yilmaz, M. (2021). L-proline modified inactivated lipase and its immobilization on cellulose-based material: stability and enantioselectivity. *Journal of Chemical Technology & Biotechnology, 96*(10), 2909-2915.

Ozyilmaz, E., Cetinguney, S., & Yilmaz, M. (2019). Encapsulation of lipase using magnetic fluorescent calix [4] arene derivatives; improvement of enzyme activity and stability. *International journal of biological macromolecules, 133*, 1042-1050.

Ozyilmaz, E., & Eski, F. (2020). Effect of cyclic and acyclic surfactants on the activity of Candida rugosa lipase. *Bioprocess and biosystems engineering, 43*(11), 2085-2093.

Ozyilmaz, E., Etci, K., & Sezgin, M. (2018). Candida rugosa lipase encapsulated with magnetic sporopollenin: design and enantioselective hydrolysis of racemic arylpropanoic acid esters. *Preparative Biochemistry and Biotechnology, 48*(10), 887-897.

Ozyilmaz, E., & Sayin, S. (2013). A magnetically separable biocatalyst for resolution of racemic naproxen methyl ester. *Bioprocess and biosystems engineering, 36*(11), 1803-1806.

Ozyilmaz, E., Sayin, S. & Yilmaz, M. (2021). Iron Oxides Nanoparticles as Versatile Carriers for Biocatalysts. *Iron Oxide Nanoparticles and Their Applications*, Nova Science Publishers, pp 55-116.

Pandey, M. D. (2022). Perspective of nanomaterials for sustainable biofuel and bioenergy production. *Materials Letters, 313*, 131686.

Pinto, G. C., Brandt, J. V., Piazza, R. D., Dos Santos, C. C., Lucena, G. N., De Paula, A. V., . . . Marques, R. F. C. (2021). Magnetic Graphene Oxide as a Carrier for Lipases Immobilization: An Approach for Hydrolysis of Olive Oil Emulsion. *ECS Journal of Solid State Science and Technology, 10*(6), 065008.

Rafiee, F., & Rezaee, M. (2021). Different strategies for the lipase immobilization on the chitosan based supports and their applications. *International journal of biological macromolecules, 179*, 170-195.

Rinaudo, M. (2008). Main properties and current applications of some polysaccharides as biomaterials. *Polymer International, 57*(3), 397-430.

Romero, C. M., Spuches, F. C., Morales, A. H., Perotti, N. I., Navarro, M. C., & Gómez, M. I. (2018). Design and characterization of immobilized biocatalyst with lipase activity onto magnetic magnesium spinel nanoparticles:

A novel platform for biocatalysis. *Colloids and Surfaces B: Biointerfaces, 172*, 699-707.

Sayin, S., Ozyilmaz, E., Oguz, M., Yusufoglu, R., & Yilmaz, M. (2020). Calixarenes functionalised water-soluble iron oxide magnetite nanoparticles for enzyme immobilisation. *Supramolecular Chemistry, 32*(5), 334-344.

Sayin, S., Yilmaz, E., & Yilmaz, M. (2011). Improvement of catalytic properties of Candida Rugosa lipase by sol–gel encapsulation in the presence of magnetic calix [4] arene nanoparticles. *Organic & biomolecular chemistry, 9*(11), 4021-4024.

Shanmugasundaram, O., & Pandit, P. (2022). Conclusion on biotechnology in textile production and future scope. In *Applications of Biotechnology for Sustainable Textile Production* (pp. 241-249): Elsevier.

Sheldon, R. A., & van Pelt, S. (2013). Enzyme immobilisation in biocatalysis: why, what and how. *Chemical Society Reviews, 42*(15), 6223-6235.

Silva, M. V., Aguiar, L. G., Rosa, C. M., De Castro, H. F., & Freitas, L. (2020). Kinetic study of isopropyl palmitate synthesis catalyzed by lipases immobilized on a magnetic copolymer support. *Chemical Engineering Communications, 207*(9), 1329-1336.

Soni, S. (2022). Trends in lipase engineering for enhanced biocatalysis. *Biotechnology and Applied Biochemistry, 69*(1), 265-272.

Thangaraj, B., & Solomon, P. R. (2019). Immobilization of lipases–a review. Part II: carrier materials. *ChemBioEng Reviews, 6*(5), 167-194.

Torres-Salas, P., del Monte-Martinez, A., Cutiño-Avila, B., Rodriguez-Colinas, B., Alcalde, M., Ballesteros, A. O., & Plou, F. J. (2011). Immobilized biocatalysts: Novel approaches and tools for binding enzymes to supports. In: Wiley Online Library.

Tran, H.-V., Ngo, N. M., Medhi, R., Srinoi, P., Liu, T., Rittikulsittichai, S., & Lee, T. R. (2022). Multifunctional iron oxide magnetic nanoparticles for biomedical applications: A review. *Materials, 15*(2), 503.

Ülker, S., Özel, A., Colak, A., & Karaoğlu, Ş. A. (2011). Isolation, production, and characterization of an extracellular lipase from Trichoderma harzianum isolated from soil. *Turkish Journal of Biology, 35*(5), 543-550.

Verdasco-Martin, C. M., Villalba, M., dos Santos, J. C., Tobajas, M., Fernandez-Lafuente, R., & Otero, C. (2016). Effect of chemical modification of Novozym 435 on its performance in the alcoholysis of camelina oil. *Biochemical Engineering Journal, 111*, 75-86.

Wan, D., Tian, L., Li, X., Li, B., & Zhang, Q. (2018). A versatile strategy for enzyme immobilization: Fabricating lipase/inorganic hybrid nanostructures on macroporous resins with enhanced catalytic properties. *Biochemical Engineering Journal, 139*, 101-108.

Wang, S., Li, S., Liu, R., Zhang, W., Xu, H., & Hu, Y. (2022). Immobilization

of Interfacial Activated Candida rugosa Lipase Onto Magnetic Chitosan Using Dialdehyde Cellulose as Cross-Linking Agent. *Frontiers in Bioengineering and Biotechnology, 10*.

Wei, X., Li, J., Yang, X., Dong, B., Geng, B., Li, Z., . . . Yan, M. (2022). An enzyme-activated two-photon ratiometric fluorescent probe with lysosome targetability for imaging β-glucuronidase in colon cancer cells and tissue. *Analytica Chimica Acta, 1192*, 339354.

Xiao, Y., Chen, Y., Lu, R., Wang, Y., & Wang, C. (2021). Immobilization of Candida rugosa lipase (CRL) on a hierarchical magnetic zeolitic imidazole framework-8 for efficient biocatalysis. *Biochemical Engineering Journal, 175*, 108120.

Xie, J., Zhang, Y., & Simpson, B. (2022). Food enzymes immobilization: novel carriers, techniques and applications. *Current Opinion in Food Science, 43*, 27-35.

Xie, W., & Huang, M. (2018). Immobilization of Candida rugosa lipase onto graphene oxide Fe3O4 nanocomposite: Characterization and application for biodiesel production. *Energy Conversion and Management, 159*, 42-53.

Yang, B., Jia, R., Fang, M., Wang, S., Lv, Z., & Wang, J. (2022). Probing the interaction of superparamagnetic iron oxide nanoparticles with lipase and their interacting consequences at the molecular level. *Toxicology Research, 11*(4), 654-661.

Yildiz, H., Ozyilmaz, E., Bhatti, A. A., & Yilmaz, M. (2017). Enantioselective resolution of racemic flurbiprofen methyl ester by lipase encapsulated mercapto calix [4] arenes capped Fe 3 O 4 nanoparticles. *Bioprocess and biosystems engineering, 40*(8), 1189-1196.

Yilmaz, E. (2012). Enantioselective enzymatic hydrolysis of racemic drugs by encapsulation in sol–gel magnetic sporopollenin. *Bioprocess and biosystems engineering, 35*(4), 493-502.

Yilmaz, E., Sezgin, M., & Yilmaz, M. (2009). Immobilized copper-ion affinity adsorbent based on a cross-linked β-cyclodextrin polymer for adsorption of Candida rugosa lipase. *Biocatalysis and Biotransformation, 27*(5-6), 360-366.

Zdarta, J., Meyer, A. S., Jesionowski, T., & Pinelo, M. (2018). A general overview of support materials for enzyme immobilization: characteristics, properties, practical utility. *Catalysts, 8*(2), 92.

Zhang, D.-H., Yuwen, L.-X., & Peng, L.-J. (2013). Parameters affecting the performance of immobilized enzyme. *Journal of chemistry, 2013*.

Zhu, Z., Song, H., Wang, Y., & Zhang, Y.-H. P. (2022). Protein engineering for electrochemical biosensors. *Current opinion in biotechnology, 76*, 102751.

Zucca, P., Fernandez-Lafuente, R., & Sanjust, E. (2016). Agarose and its derivatives as supports for enzyme immobilization. *Molecules, 21*(11), 1577.

CHAPTER 5

EXPONENTIATED UNIT TEISSIER DISTRIBUTION

Cenker BİÇER[1], Hayrinisa DEMİRCİ BİÇER[2],

1 Assoc.Prof.Dr., Cenker BİÇER, Kırıkkale Univ., Dep. of Statistics. ORCID: 0000-0003-2222-3208, cbicer@kku.edu.tr.
2 Assoc.Prof.Dr., Hayrinisa DEMİRCİ BİÇER, Kırıkkale Univ., Dep. of Statistics. ORCID:0000-0002-1520-5004, hdbicer@kku.edu.tr.

INTRODUCTION

Technological developments have allowed us to access a greater amount of data today. Therefore, we better understand and describe our nature and the events taking place around us by modeling them more effectively. Creating accurate interpretations from the analysis of phenomena around us requires using accurate or appropriate models to statistically model the data compiled over the phenomena. Since these data compiled from more phenomena exhibit different formal behaviors, the researchers presented many new probability models to optimize their modeling performance in recent years. These new probability models generally originate as a more generalized form of a fundamental distribution. Among the most widely used methods for this purpose are exponentiation, alpha power transformation, and quadratic transmutation rank mapping. Studies Exponentiated exponential distribution (Gupta & Kundu, 2001), Transmuted Weibull distribution (Aryal & Tsokos, 2011), Transmuted Lindley distribution (Merovci, 2013), Exponentiated power Lindley distribution (Ashour & Eltehiwy, 2015), alpha power exponential distribution (Mahdavi & Kundu, 2017), transmuted wrapped exponential distribution (Yilmaz, & Biçer, 2018), alpha power generalized Rayleigh distribution (Demirci Biçer, 2019), transmuted XGamma distribution (Demirci Biçer, 2019), and wrapped two-sided Lindley distribution (Biçer & Yılmaz, 2022) exemplify new probability models derived by using these methods on the positive semi-real line. In addition, some researchers have considered deriving new probability models over the unit interval to produce an alternative to the Beta distribution. Some of these distributions recently added to the literature are log-Lindley (Gómez-Déniz et al., 2014), exponentiated Topp–Leone (Pourdarvish et al., 2015), flexible skew Laplace distribution (Yilmaz, 2016), log- Xgamma (Altun & Hamedani, 2018), unit Lindley (Mazucheli et al, 2019), unit inverse Gaussian (Ghitany, et al., 2019), unit Weibull (Mazucheli et al., 2020), unit Burr-III (Modi & Gill, 2020), unit Ishita distribution (Demirci Biçer & Biçer, 2022), and unit Teissier distribution (Krishna et al., 2022), which are recently added to the literature. The importance of introducing more flexible probability distribution models defined over the unit interval has been studied in detail by these researchers. The novelty of this article is to derive a new probability model with support set $(0,1)$ by using the unit Teissier model as a starting point.

The remainder of the paper is organized as follows. The EUT model is derived from the section "Exponentiated Unit Teissier Distribution." In the section "Basic Features of EUT Distribution," essential characteristics of EUT model such as survival, hazard, reserved hazard quantile functions, as well as its moments, and the distribution of its order statistics, are

investigated. The "Inference" section investigates various estimators of the EUT parameters. Some comprehensive numerical studies are carried out as part of the Section "Simulation Study" to assess how well the estimators obtained in the paper perform. The Section "Conclusions" brings the work to a close.

EXPONENTIATED UNIT TEISSIER DISTRIBUTION

Assume that X comes from the unit Teissier distribution and has the parameter θ >0. Then the probability density function (pdf) and the corresponding cumulative distribution function (cdf) of X are, respectively, given as:

$$g(x,\theta) = \theta\left(x^{-\theta} - 1\right)x^{-(\theta+1)}\left(e^{-x^{-\theta}+1}\right), x > 0 \quad (1)$$

$$G(x,\theta) = e^{1-x^{-\theta}}x^{-\theta}, 0 < x < 1, \quad (2)$$

where θ is the unit Teissier distribution's shape parameter. The unit Teissier distribution was first introduced by (Krishna et al., 2022),. The distribution is, at its core, a modified form of the Teissier distribution. Additionally, the authors looked into a few particular statistical characteristics of the distribution. Table 1 summarizes some of these characteristics.

Table 1. Essential characteristics of the unit Teissier distribution

r.th Moment μ_r	$e\left\{\Gamma\left(-\frac{r}{\theta}+2,1\right)-\Gamma\left(-\frac{r}{\theta}+1,1\right)\right\}$
Expectation $E(X)$	$e\left\{\Gamma\left(-\frac{1}{\theta}+2,1\right)-\Gamma\left(-\frac{1}{\theta}+1,1\right)\right\}$
Variance $Var(X)$	$e\left(\Gamma\left(2-\frac{2}{\theta},1\right)-\Gamma\left(1-\frac{2}{\theta},1\right)\right) - e^2\left(\Gamma\left(2-\frac{1}{\theta},1\right) - \Gamma\left(1-\frac{1}{\theta},1\right)\right)^2$
Survival Function $S_X(x)$	$1 - e^{1-x^{-\theta}}x^{-\theta}$
Hazard Function $H_X(x)$	$\frac{e\theta x^{-\theta-1}\left(x^{\theta}-1\right)}{e^{x^{-\theta}}x^{\theta}-e}$

Where, $\Gamma(a,b)$ implies the incompleted gamma function, see (Abramowitz et al, 1988). Considering the cdf of the unit Teissier distribution given by the equation (2), the cdf of the EUT distribution can

be derived by empploying the conversion $F(x,\theta,\alpha) = [G(x,\theta)]^{\alpha}$. By the Definition 1, we formalize the description of it.

Definition 1. Let the random variable Y follow an EUT disribution. The pdf and the cdf of Y are, respectively, given by

$$f(y,\theta) = \alpha\theta\left(-y^{-\theta-1}\right)\left(y^{\theta}-1\right)\left(e^{1-y^{-\theta}}y^{-\theta}\right)^{\alpha}, 0 < y < 1 \qquad (3)$$

and

$$F(y;\theta,\alpha) = \left(\mathrm{e}^{\left(1-\mathrm{y}^{-\theta}\right)}\mathrm{y}^{-\theta}\right)^{\alpha}, \qquad (4)$$

where, $\theta > 0$ is the shape parameter and $\alpha > 0$ is the scale parameter of the EUT distribution. Figure 1 demonstrates the formal behaviors of the EUT distribution's pdf . From the figure 1, it clear that the EUT distribution is a suitable probability model to use in modeling right or left-skewed measurements over the unit interval.

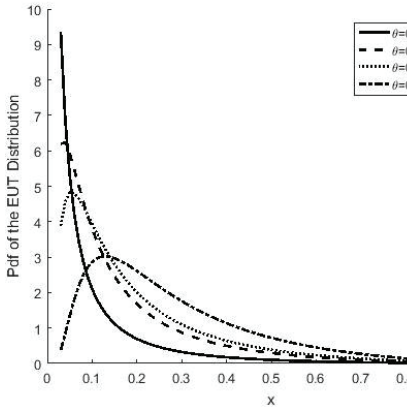

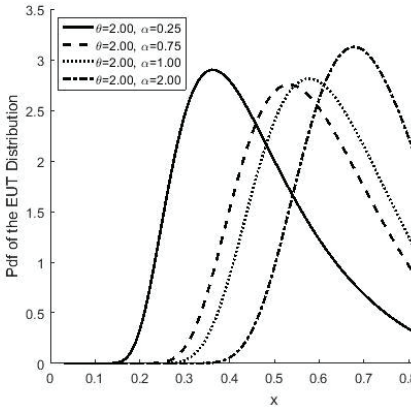

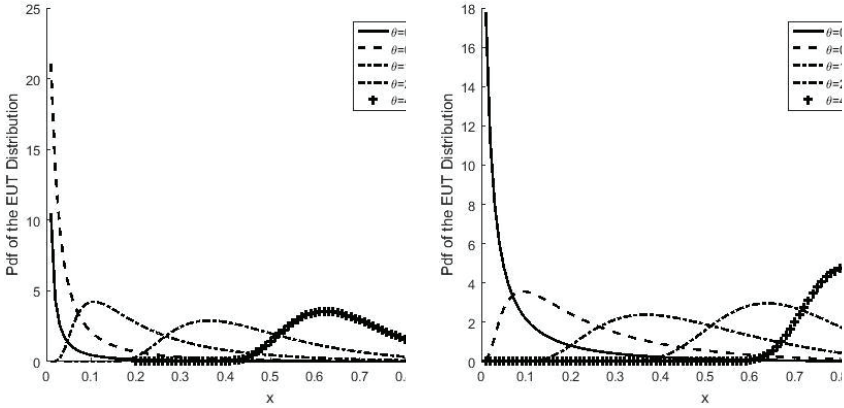

Figure 1. EUT distribution's pdf for different values of θ and α.

BASIC FEATURES OF EUT DISTRIBUTION

A variety of statistical characteristics of EUT the distribution are examined in this section, such as survival, hazard, reserved hazard, quantile functions, moments, variance, and distribution of the order statistics.

Consider Y to be an EUT distributed random variable with the parameters θ and α, and also $t \in (0,1)$. By taking into account these assumptions with together the (3) and (4), the survival function of the EUT distribution, let us call $S_Y(t;\theta,\alpha)$, can be written as

$$\begin{aligned} S_Y(t,\theta,\alpha) &= 1 - F_Y(t,\theta,\alpha) \\ &= 1 - \left(e^{1-t^{-\theta}}t^{-\theta}\right)^{\alpha}. \end{aligned} \tag{5}$$

Now we obtain the hazard and reserved hazard funcitons of the EUT distribution. According to formal definitions of hazard and the reserved hazard functions, EUT distribution's hazard rate, let us call $H_Y(t;\theta,\alpha)$, and reserved hazard rate function, let us call $\xi_Y(t;\theta,\alpha)$, are, respectively, obtained as

$$H(t;\theta,\alpha) = \frac{\alpha\theta t^{-\theta-1}\left(t^{\theta}-1\right)\left(e^{1-t^{-\theta}}t^{-\theta}\right)^{\alpha}}{\left(e^{1-t^{-\theta}}t^{-\theta}\right)^{\alpha}-1} \tag{6}$$

and

$$\xi(t;\theta,\alpha) = \alpha\theta\left(-t^{-\theta-1}\right)\left(t^{\theta}-1\right), \tag{7}$$

Based on various values of the patrameters θ and α , in Figure 2 The EUT distribution's hazard rate function is depicted.

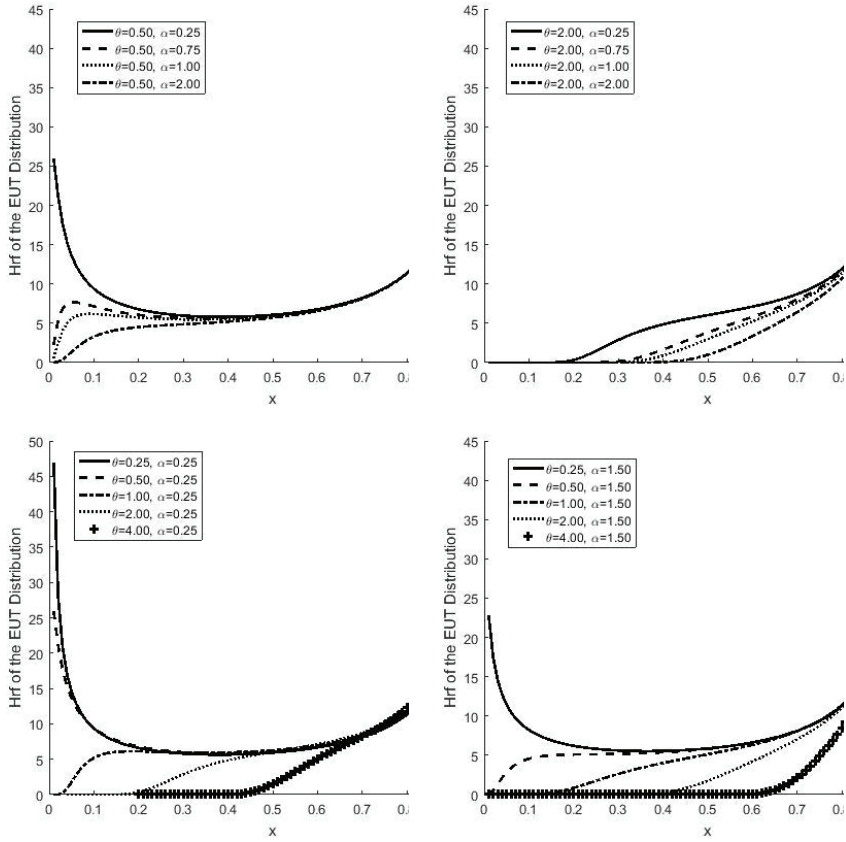

Figure 2. EUT distribution's Hazard function for different values of θ and α.

Figure 2 shows that shapes of the EUT distribution's hazard function follow either increasing or bathtub forms.

The EUT distribution's quantile function is

$$Q(p) = \left(-\frac{1}{W_{-1}\left(-\frac{p^{1/\alpha}}{e}\right)} \right)^{1/\theta}, \qquad (8)$$

where $p \in (0,1)$ and $W_{-1}(a)$ implies Lambert function. One can find further information about this function from (Corless et al., 1996). Thus,

we can write the median of the EUT distribution selecting $p = \frac{1}{2}$ as

$$Median = Q\left(\frac{1}{2}\right) = \left(-\frac{1}{W_{-1}\left(-\frac{\left(\frac{1}{2}\right)^{1/\alpha}}{e} \right)} \right)^{1/\theta}, \tag{9}$$

Based on the formal definition of the r^{th}, $r \in Z^+$, moment of a random variable, r^{th} moment of the EUT distribution is easily obtained as

$$\mu_r = E(Y^r) = \int_{-\infty}^{\infty} y^r f(y,\theta,\alpha)dy$$
$$= \int_0^1 y^r \alpha\theta\left(-y^{-\theta-1}\right)\left(y^\theta - 1\right)\left(e^{1-y^{-\theta}}y^{-\theta}\right)^\alpha dy$$
$$= e^\alpha \alpha\left(E_{\frac{r}{\theta}-\alpha}(\alpha) - E_{\frac{r}{\theta}-\alpha+1}(\alpha)\right), \tag{10}$$

where $E_a(\mathrm{b}) = \int_1^\infty \frac{e^{-bt}}{t^a}dt$.

Thus, the EUT distribution's first and second moments can be expressed as

$$\mu_1 = E(Y) = e^\alpha \alpha\left(E_{\frac{1}{\theta}-\alpha}(\alpha) - E_{-\alpha+\frac{1}{\theta}+1}(\alpha)\right)$$

and

$$\mu_2 = E(Y^2) = \frac{\alpha\left(\theta - 2e^\alpha E_{\frac{2}{\theta}-\alpha}(\alpha)\right)}{\alpha\theta - 2},$$

respectively, by taking equation (10) into consideration. Also, the variance of the EUT distribution is

$$Var(Y) = E(Y^2) - \left(E(Y)\right)^2$$
$$= \mu_2 - \mu_1^2$$

$$= e^{\alpha}\alpha\left(-e^{\alpha}\alpha\left(E_{\frac{1}{\theta}-\alpha}(\alpha) - E_{-\alpha+\frac{1}{\theta}+1}(\alpha)\right)^{2} + E_{\frac{2}{\theta}-\alpha}(\alpha) - E_{-\alpha+\frac{2}{\theta}+1}(\alpha)\right).$$

Now, we explore the distribution of the order statistics of the EUT distribution. Let $Y_1, Y_2, \ldots, Y_n$ is a set of random variables drawn EUT distribution and $Y_{(1)} \cdots Y_{(n)}, \left(Y_{(1)} < \cdots < Y_{(n)}\right)$ displays its orders. By following the formal calculation method of the distribution of an order statistics, the pdf of the i^{th}order statistic is given by

$$f_{Y_{(i)}}(y) = \frac{n!}{(i-1)!\,(n-i)!}F(y)^{i-1}f(y)(1 - F(y))^{n-i}$$

$$= \frac{n!}{(i-1)!\,(n-i)!}\alpha\theta\left(-y^{-\theta-1}\right)\left(y^{\theta}-1\right)\left(e^{1-y^{-\theta}}y^{-\theta}\right)^{\alpha}\left(\left(e^{1-y^{-\theta}}y^{-\theta}\right)^{\alpha}\right)^{i-1} \times \left(1-\left(e^{1-y^{-\theta}}y^{-\theta}\right)^{\alpha}\right)^{n-i} \quad (11)$$

Based on equation (11), we can write the pdf of 1^{st} and n^{th} order statistics as

$$f_{Y_{(1)}}(y) = \alpha\theta(-n)y^{-\theta-1}\left(y^{\theta} - 1\right)\left(e^{1-y^{-\theta}}y^{-\theta}\right)^{\alpha}\left(1-\left(e^{1-y^{-\theta}}y^{-\theta}\right)^{\alpha}\right)^{n-1}$$

and

$$f_{Y_{(n)}}(y) = \alpha\theta(-n)y^{-\theta-1}\left(y^{\theta}-1\right)\left(\left(e^{1-y^{-\theta}}y^{-\theta}\right)^{\alpha}\right)^{n},$$

respectively.

INFERENCE

This section investigates several estimators of the EUT parameters by employing the most famous estimation methodologies in the literature. Here, we consider methodologies such as the maximum likelihood, the maximum product space, the least-square, and the weighted-least-square.

Let $Y_1, Y_2, \ldots, Y_n$ is a set of independently and identically EUT distributed random variables with parameter θ and α and $y_1, y_2, \ldots, y_n$ display their realizations. With this assumption, the likelihood function of the $y_1, y_2, \ldots, y_n$ measurements, let us call $L(\theta, y_1, y_2, \ldots, y_n)$, is written as

$$L(\theta, y_1, y_2, \ldots, y_n) = \prod_{i=1}^{n} \alpha\theta\left(-y_i^{-\theta-1}\right)\left(y_i^{\theta} - 1\right)\left(e^{1-y_i^{-\theta}} y_i^{-\theta}\right)^{\alpha}$$

and the corresponding logarithmic likelihood function is

$$\begin{aligned} \ln L(\theta, y_1, y_2, \ldots, y_n) &= -\alpha \sum_{i=1}^{n} y_i^{-\theta} + (\theta - \alpha\theta) \sum_{i=1}^{n} \ln(y_i) \\ &+ \sum_{i=1}^{n} y_i^{-\theta} \\ &+ \sum_{i=1}^{n} \ln\left(\theta e^{1-y_i^{-\theta}} y_i^{-2\theta-1}\right. \\ &\left. - \theta e^{1-y_i^{-\theta}} y_i^{-\theta-1}\right) \\ &+ \alpha n + n \ln(\alpha) - n. \end{aligned} \tag{12}$$

Hence, we obtain the following score functions by taking the first derivatives of the parameters θ and α and equating them to zero.

$$\delta \ln L(\theta, y_1, y_2, \ldots, y_n) \tag{13}$$

$$+\sum_{i=1}^{n}\frac{\theta e^{1-y_i^{-\theta}}y_i^{-3\theta-1}\ln(y_i)}{\theta e^{1-y_i^{-\theta}}y_i^{-2\theta-1}-\theta e^{1-y_i^{-\theta}}y_i^{-\theta-1}}=0.$$

$$\frac{\delta lnL(\theta,y_1,y_2,\ldots,y_n)}{\delta\alpha}=-\sum_{i=1}^{n}y_i^{-\theta}-\theta\sum_{i=1}^{n}ln(y_i)+\frac{n}{\alpha}+n \qquad (14)$$
$$=0.$$

The maximum likelihood estimators of the parameters θ and α are obtained from the simultaneous solution of the score functions (13) - (14). Here, utilizing simple procedures will not yield the analytical solution to the score functions (13)-(14). However, we may quickly arrive at the maximum likelihood estimates of the parameters θ and α by utilizing a numerical approach like Newton's method or employing software like Octave's (Eaton et al., 2019) "fmincon" function or "mle" function of R (Team, 2013).

By adhering to the notations of (Swain et al, 1988), we, now, investigate the least-squares estimators of unknown parameters of EUT distribution. Let $y_{(1)},y_{(2)},\cdots,y_{(n)}$ ordered measurements and $P_j=\frac{j}{n+1}$ displays the value of empirical distribution function for j^{th} observation. Then, considering the cdf of the EUT distribution given by (4) the least-squares estimator of the parameters θ and α are obtained by minimizing the utility function

$$U_{LSE}=\sum_{j=1}^{n}\left(F\left(y_{(j)},\theta,\alpha\right)-P_j\right)^2,$$

$$U_{LSE}=\sum_{j=1}^{n}\left(\left(e^{1-y_{(j)}^{-\theta}}y_{(j)}^{-\theta}\right)^{\alpha}-P_j\right)^2,$$

with respect to parameters θ and α. This optimization problem can be easily solved by employing a numerical method.

The weighted least-squares estimator of the parameters θ and α can be obtained by minimizing

$$U_{WLSE} = \sum_{j=1}^{n} \frac{(n+1)^2(n+2)}{j(n-j+1)} \left(\left(e^{1-y_{(j)}^{-\theta}} y_{(j)}^{-\theta} \right)^{\alpha} - P_j \right)^2,$$

with respect to θ and α.

Now, we investigate the maximum product space estimators of the EUT parameters. The maximum product space estimation method was first discussed by (Ranneby, 1984). Based on (Ranneby, 1984) notation, maximum product space estimators of the EUT parameters θ and α can be obtained by maximizing the utility function

$$U_{MPS} = \sum_{j=1}^{n+1} \ln\left[F\left(y_{(j)}, \theta, \alpha\right) - F\left(y_{(j-1)}, \theta, \alpha\right) \right]. \tag{15}$$

with respect to parameters θ and α . Considering the cdf (4), we have

$$U_{MPS} = \sum_{j=1}^{n+1} \ln\left[\left(e^{1-y_{(j)}^{-\theta}} y_{(j)}^{-\theta} \right)^{\alpha} - \left(e^{1-y_{(j-1)}^{-\theta}} y_{(j-1)}^{-\theta} \right)^{\alpha} \right], \tag{16}$$

where $F\left(Y_{(0)}, \theta, \alpha\right) \equiv 0$, and $F\left(Y_{(n+1)}, \theta, \alpha\right) \equiv 1$. Equation (23) can be easily maximized by utilizing the Fmincon function of the Octave (Eaton et al., 2019).

SIMULATION STUDY

This section's goal is to quantitatively analyze the efficiencies of the estimators obtained in the previous section. With this aim, we run some Monte-Carlo simulations. We use two criteria to compare the estimators: Bias and mean square error given by

$$MSE = \frac{1}{k} \sum_{i=1}^{k} (\tau - \hat{\tau}_i)^2$$

and

$$Bias = \frac{1}{k} \sum_{i=1}^{k} \hat{\tau}_i - \tau,$$

respectively, where k is the repetition of the simulation.. We sets the parameter's values as $\theta = (0.5, 1.0, 2.0, 5.0)$ and $\alpha = (0.5, 1.0, 2.0)$ in

simulations iterated 1000 times. The simulated results for $n = 50,100,150$ are figured in Tables 2-5.

Table 2: Simulated results for $\theta = 0.5$ and $\alpha = 0.5, 1.0, 2.0$

			θ			α		
α	Method	n	$\hat{\theta}$	Bias $\hat{\theta}$	MSE $\hat{\theta}$	$\hat{\alpha}$	Bias $\hat{\alpha}$	MSE $\hat{\alpha}$
0.5	MLE	50	0.5241	0.0241	0.0244	0.5133	0.0133	0.0034
	LSE		0.5344	0.0344	0.0278	0.4971	-0.0029	0.0047
	WLSE		0.5301	0.0301	0.0278	0.5011	0.0011	0.0047
	MPSE		0.5234	0.0234	0.0243	0.5140	0.0140	0.0036
	MLE	100	0.5074	0.0074	0.0112	0.5077	0.0077	0.0016
	LSE		0.5131	0.0131	0.0123	0.5005	0.0005	0.0025
	WLSE		0.5105	0.0105	0.0123	0.5031	0.0031	0.0025
	MPSE		0.5075	0.0075	0.0113	0.5075	0.0075	0.0017
	MLE	150	0.5024	0.0024	0.0071	0.5041	0.0041	0.0010
	LSE		0.5072	0.0072	0.0086	0.4998	-0.0002	0.0015
	WLSE		0.5048	0.0048	0.0086	0.5017	0.0017	0.0015
	MPSE		0.5024	0.0024	0.0071	0.5042	0.0042	0.0010
1.0	MLE	50	0.5002	0.0002	0.0058	1.0306	0.0306	0.0152
	LSE		0.5058	0.0058	0.0067	1.0016	0.0016	0.0200
	WLSE		0.5035	0.0035	0.0067	1.0091	0.0091	0.0200
	MPSE		0.5001	0.0001	0.0059	1.0320	0.0320	0.0158
	MLE	100	0.4985	-0.0015	0.0029	1.0087	0.0087	0.0062
	LSE		0.5011	0.0011	0.0031	0.9970	-0.0030	0.0091
	WLSE		0.4999	-0.0001	0.0031	1.0013	0.0013	0.0091
	MPSE		0.4985	-0.0015	0.0029	1.0089	0.0089	0.0065
	MLE	150	0.5017	0.0017	0.0017	1.0117	0.0117	0.0048
	LSE		0.5032	0.0032	0.0020	1.0037	0.0037	0.0067
	WLSE		0.5026	0.0026	0.0020	1.0065	0.0065	0.0067
	MPSE		0.5018	0.0018	0.0018	1.0116	0.0116	0.0049
2.0	MLE	50	0.5007	0.0007	0.0013	2.0828	0.0828	0.0607
	LSE		0.5035	0.0035	0.0014	2.0294	0.0294	0.0808

	WLSE		0.5025	0.0025	0.0014	2.0410	0.0410	0.0808
	MPSE		0.5004	0.0004	0.0013	2.0871	0.0871	0.0641
	MLE		0.4992	-0.0008	0.0007	2.0202	0.0202	0.0253
	LSE	100	0.5006	0.0006	0.0008	1.9892	-0.0108	0.0370
	WLSE		0.5000	0.0000	0.0008	1.9989	-0.0011	0.0370
	MPSE		0.4992	-0.0008	0.0007	2.0174	0.0174	0.0261
	MLE		0.4995	-0.0005	0.0004	2.0196	0.0196	0.0160
	LSE	150	0.4998	-0.0002	0.0005	2.0035	0.0035	0.0236
	WLSE		0.4996	-0.0004	0.0005	2.0099	0.0099	0.0236
	MPSE		0.4994	-0.0006	0.0004	2.0184	0.0184	0.0163

Table 3: Simulated results for $\theta = 1.0$ and $\alpha = 0.5, 1.0, 2.0$

			θ			α		
α	Method	n	$\hat{\theta}$	Bias $\hat{\theta}$	MSE $\hat{\theta}$	$\hat{\alpha}$	Bias $\hat{\alpha}$	MSE $\hat{\alpha}$
0.5	MLE		1.0139	0.0139	0.0899	0.5119	0.0119	0.0032
	LSE	50	1.0354	0.0354	0.1107	0.4985	-0.0015	0.0045
	WLSE		1.0278	0.0278	0.1107	0.5012	0.0012	0.0045
	MPSE		1.0137	0.0137	0.0906	0.5117	0.0117	0.0034
	MLE		1.0026	0.0026	0.0467	0.5026	0.0026	0.0015
	LSE	100	1.0090	0.0090	0.0514	0.4958	-0.0042	0.0021
	WLSE		1.0048	0.0048	0.0514	0.4986	-0.0014	0.0021
	MPSE		1.0018	0.0018	0.0469	0.5029	0.0029	0.0015
	MLE		1.0066	0.0066	0.0275	0.5055	0.0055	0.0011
	LSE	150	1.0157	0.0157	0.0320	0.4991	-0.0009	0.0014
	WLSE		1.0112	0.0112	0.0320	0.5012	0.0012	0.0014
	MPSE		1.0065	0.0065	0.0275	0.5054	0.0054	0.0011
1.0	MLE		1.0069	0.0069	0.0231	1.0340	0.0340	0.0149
	LSE	50	1.0156	0.0156	0.0257	1.0022	0.0022	0.0190
	WLSE		1.0128	0.0128	0.0257	1.0094	0.0094	0.0190
	MPSE		1.0065	0.0065	0.0231	1.0347	0.0347	0.0161
	MLE		1.0002	0.0002	0.0107	1.0185	0.0185	0.0069
	LSE	100	1.0075	0.0075	0.0117	1.0034	0.0034	0.0091
	WLSE		1.0041	0.0041	0.0117	1.0083	0.0083	0.0091

	MPSE		1.0000	0.0000	0.0107	1.0189	0.0189	0.0070
	MLE	150	0.9966	-0.0034	0.0080	1.0073	0.0073	0.0046
	LSE		0.9997	-0.0003	0.0087	0.9967	-0.0033	0.0065
	WLSE		0.9979	-0.0021	0.0087	1.0014	0.0014	0.0065
	MPSE		0.9962	-0.0038	0.0080	1.0077	0.0077	0.0048
2.0	MLE	50	0.9976	-0.0024	0.0052	2.0662	0.0662	0.0519
	LSE		1.0027	0.0027	0.0059	2.0029	0.0029	0.0770
	WLSE		1.0006	0.0006	0.0059	2.0195	0.0195	0.0770
	MPSE		0.9973	-0.0027	0.0052	2.0650	0.0650	0.0564
	MLE	100	0.9996	-0.0004	0.0028	2.0255	0.0255	0.0262
	LSE		1.0012	0.0012	0.0031	1.9951	-0.0049	0.0374
	WLSE		1.0005	0.0005	0.0031	2.0066	0.0066	0.0374
	MPSE		0.9996	-0.0004	0.0028	2.0255	0.0255	0.0267
	MLE	150	1.0020	0.0020	0.0017	2.0125	0.0125	0.0161
	LSE		1.0033	0.0033	0.0019	1.9952	-0.0048	0.0234
	WLSE		1.0027	0.0027	0.0019	2.0018	0.0018	0.0234
	MPSE		1.0019	0.0019	0.0017	2.0128	0.0128	0.0162

Table 4: Simulated results for $\theta = 2.0$ and $\alpha = 0.5, 1.0, 2.0$

			θ			α		
α	Method	n	$\hat{\theta}$	Bias $\hat{\theta}$	MSE $\hat{\theta}$	$\hat{\alpha}$	Bias $\hat{\alpha}$	MSE $\hat{\alpha}$
0.5	MLE	50	2.0482	0.0482	0.3288	0.5137	0.0137	0.0035
	LSE		2.1058	0.1058	0.4017	0.4963	-0.0037	0.0053
	WLSE		2.0798	0.0798	0.4017	0.5017	0.0017	0.0053
	MPSE		2.0472	0.0472	0.3315	0.5137	0.0137	0.0038
	MLE	100	2.0085	0.0085	0.1852	0.5058	0.0058	0.0014
	LSE		2.0223	0.0223	0.2069	0.4984	-0.0016	0.0020
	WLSE		2.0153	0.0153	0.2069	0.5011	0.0011	0.0020
	MPSE		2.0069	0.0069	0.1850	0.5060	0.0060	0.0014
	MLE	150	2.0174	0.0174	0.1122	0.5039	0.0039	0.0010
	LSE		2.0264	0.0264	0.1242	0.4995	-0.0005	0.0017
	WLSE		2.0211	0.0211	0.1242	0.5012	0.0012	0.0017
	MPSE		2.0170	0.0170	0.1124	0.5039	0.0039	0.0011
1.0	MLE	50	2.0144	0.0144	0.0868	1.0222	0.0222	0.0130

	LSE		2.0356	0.0356	0.0959	0.9919	-0.0081	0.0176
	WLSE		2.0272	0.0272	0.0959	1.0001	0.0001	0.0176
	MPSE		2.0136	0.0136	0.0866	1.0237	0.0237	0.0138
	MLE		2.0130	0.0130	0.0487	1.0140	0.0140	0.0064
	LSE	100	2.0203	0.0203	0.0532	1.0009	0.0009	0.0089
	WLSE		2.0171	0.0171	0.0532	1.0055	0.0055	0.0089
	MPSE		2.0126	0.0126	0.0487	1.0149	0.0149	0.0066
	MLE		2.0074	0.0074	0.0302	1.0089	0.0089	0.0047
	LSE	150	2.0133	0.0133	0.0346	0.9971	-0.0029	0.0065
	WLSE		2.0104	0.0104	0.0346	1.0026	0.0026	0.0065
	MPSE		2.0073	0.0073	0.0302	1.0090	0.0090	0.0048
2.0	MLE		2.0084	0.0084	0.0244	2.0661	0.0661	0.0548
	LSE	50	2.0194	0.0194	0.0272	2.0022	0.0022	0.0687
	WLSE		2.0150	0.0150	0.0272	2.0189	0.0189	0.0687
	MPSE		2.0085	0.0085	0.0246	2.0685	0.0685	0.0583
	MLE		1.9953	-0.0047	0.0109	2.0321	0.0321	0.0268
	LSE	100	1.9982	-0.0018	0.0120	2.0018	0.0018	0.0366
	WLSE		1.9968	-0.0032	0.0120	2.0122	0.0122	0.0366
	MPSE		1.9952	-0.0048	0.0108	2.0302	0.0302	0.0270
	MLE		1.9981	-0.0019	0.0075	2.0155	0.0155	0.0160
	LSE	150	2.0000	0.0000	0.0082	1.9942	-0.0058	0.0235
	WLSE		1.9989	-0.0011	0.0082	2.0025	0.0025	0.0235
	MPSE		1.9978	-0.0022	0.0075	2.0151	0.0151	0.0162

Table 5: Simulated results for $\theta = 5.0$ and $\alpha = 0.5, 1.0, 2.0$

			θ			α		
α	Method	n	$\hat{\theta}$	Bias $\hat{\theta}$	MSE $\hat{\theta}$	$\hat{\alpha}$	Bias $\hat{\alpha}$	MSE $\hat{\alpha}$
0.5	MLE		5.1305	0.1305	2.4130	0.5141	0.0141	0.0033
	LSE	50	5.2299	0.2299	2.6717	0.4962	-0.0038	0.0048
	WLSE		5.1929	0.1929	2.6717	0.5008	0.0008	0.0048
	MPSE		5.1319	0.1319	2.4053	0.5137	0.0137	0.0035
	MLE		5.0470	0.0470	1.0020	0.5081	0.0081	0.0017
	LSE	100	5.0937	0.0937	1.1820	0.5009	0.0009	0.0025
	WLSE		5.0662	0.0662	1.1820	0.5038	0.0038	0.0025

	MPSE		5.0446	0.0446	1.0025	0.5085	0.0085	0.0018
	MLE	150	5.0068	0.0068	0.7254	0.5053	0.0053	0.0013
	LSE		5.0688	0.0688	0.8224	0.4997	-0.0003	0.0018
	WLSE		5.0426	0.0426	0.8224	0.5014	0.0014	0.0018
	MPSE		5.0081	0.0081	0.7275	0.5053	0.0053	0.0013
1.0	MLE	50	5.0336	0.0336	0.5695	1.0313	0.0313	0.0145
	LSE		5.0719	0.0719	0.6230	1.0015	0.0015	0.0195
	WLSE		5.0573	0.0573	0.6230	1.0095	0.0095	0.0195
	MPSE		5.0308	0.0308	0.5662	1.0321	0.0321	0.0158
	MLE	100	4.9889	-0.0111	0.2734	1.0129	0.0129	0.0066
	LSE		4.9971	-0.0029	0.3046	0.9991	-0.0009	0.0092
	WLSE		4.9943	-0.0057	0.3046	1.0036	0.0036	0.0092
	MPSE		4.9892	-0.0108	0.2745	1.0130	0.0130	0.0067
	MLE	150	5.0330	0.0330	0.1883	1.0081	0.0081	0.0042
	LSE		5.0588	0.0588	0.2182	0.9965	-0.0035	0.0067
	WLSE		5.0465	0.0465	0.2182	1.0009	0.0009	0.0067
	MPSE		5.0344	0.0344	0.1896	1.0073	0.0073	0.0043
2.0	MLE	50	4.9900	-0.0100	0.1326	2.0726	0.0726	0.0618
	LSE		5.0075	0.0075	0.1509	2.0133	0.0133	0.0765
	WLSE		5.0001	0.0001	0.1509	2.0330	0.0330	0.0765
	MPSE		4.9888	-0.0112	0.1340	2.0755	0.0755	0.0649
	MLE	100	4.9975	-0.0025	0.0737	2.0282	0.0282	0.0268
	LSE		5.0053	0.0053	0.0825	2.0113	0.0113	0.0391
	WLSE		5.0015	0.0015	0.0825	2.0181	0.0181	0.0391
	MPSE		4.9977	-0.0023	0.0737	2.0288	0.0288	0.0272
	MLE	150	4.9988	-0.0012	0.0418	2.0193	0.0193	0.0162
	LSE		5.0068	0.0068	0.0465	1.9971	-0.0029	0.0225
	WLSE		5.0027	0.0027	0.0465	2.0065	0.0065	0.0225
	MPSE		4.9987	-0.0013	0.0419	2.0188	0.0188	0.0164

The suggested whole estimators for parameters θ and α display good estimate performance, as shown by the simulated results presented in Tables 2–5. Owing to the results in Tables 2–5, we draw the conclusion that all estimators are asymptotically consistent and unbiased because all estimators have lower Bias and lower MSE values as n grows.

Additionally, we concluded that the MLE estimators performs better than other estimators with a lower MSE value.

CONCLUSION

We, in this work, focus on the development of a novel probability model that can be used in modeling observations in the unit range. The newly developed distribution is an extended form of the Unit Teissier distribution called the Exponentiated Unit Teissier. The pdf and cdf of the mentioned distribution are obtained based on the Exponentiation method, taking into account the Unit Tiessier distribution as a base model. In addition to obtaining the survival, hazard, reserved hazard, and quantile functions of the EUT distribution, its moments, variance, and the distribution of order statistics are also extensively studied in the paper. Plots of the pdf and hazard function of the distribution are visualized with a set of figures for various values of the parameters. Considering the most widely used estimator-obtaining methods in the literature, various estimators of the shape and scale parameters of the newly developed distribution are obtained in the study. The estimation efficiencies of these estimators are also demonstrated by performing a series of Monte-Carlo simulation studies. According to the results of the conducted simulations, it can be concluded that maximum likelihood estimators of the parameters can be used effectively to estimate unknown parameters of the distribution. Furthermore, the newly constructed distribution may be regarded as an alternative model which can be applied to both symmetrical and right- or left-skewed observations found in the unit interval.

REFERENCES

1. Gupta, R. D., & Kundu, D. (2001). Exponentiated exponential family: an alternative to gamma and Weibull distributions. Biometrical Journal: Journal of Mathematical Methods in Biosciences, 43(1), 117-130.

2. Aryal, G. R., & Tsokos, C. P. (2011). Transmuted Weibull distribution: A generalization of theWeibull probability distribution. European Journal of pure and applied mathematics, 4(2), 89-102.

3. Merovci, F. (2013). Transmuted lindley distribution.Int. J. Open Problems Compt. Math, 6(2), 63-72.

4. Ashour, S. K., & Eltehiwy, M. A. (2015). Exponentiated power Lindley distribution. Journal of advanced research, 6(6), 895-905.

5. Mahdavi, A., & Kundu, D. (2017). A new method for generating distributions with an application to exponential distribution. Communications in Statistics-Theory and Methods, 46(13), 6543-6557.

6. Yilmaz, A., & Biçer, C. (2018). A new wrapped exponential distribution. Mathematical Sciences, 12(4), 285-293.

7. Biçer, H. D. (2019). Properties and Inference for a New Class of Generalized Rayleigh Distributions with an Application. Open Mathematics, 17(1), 700-715.

8. Demirci Biçer, H. (2019). Properties and inference for a new class of XGamma distributions with an application. Mathematical Sciences, 13(4), 335-346.

9. Biçer, C., & Yılmaz, A. (2022). Wrapped Two-Sided Lindley Distribution.Research & Reviews in Science and Mathematics.

10. Gómez-Déniz, E., Sordo, M. A., & Calderín-Ojeda, E. (2014). The Log–Lindley distribution as an alternative to the beta regression model with applications in insurance. Insurance: Mathematics and Economics, 54, 49-57.

11. Pourdarvish, A., Mirmostafaee, S. M. T. K., & Naderi, K. (2015). The exponentiated Topp-Leone distribution: Properties and application. Journal of Applied Environmental and Biological Sciences, 5(7), 251-256.

12. Yilmaz, A. (2016). The flexible skew Laplace distribution. Communications in Statistics-Theory and Methods, 45(23), 7053-7059.

13. Altun, E., & Hamedani, G. G. (2018). The log-xgamma distribution with inference and application. Journal de la Société Française de Statistique, 159(3), 40-55.

14. Mazucheli, J., Menezes, A. F. B., & Chakraborty, S. (2019). On the one

parameter unit-Lindley distribution and its associated regression model for proportion data. Journal of Applied Statistics,46(4), 700-714.

15. Ghitany, M. E., Mazucheli, J., Menezes, A. F. B., & Alqallaf, F. (2019). The unit-inverse Gaussian distribution: A new alternative to two-parameter distributions on the unit interval. Communications in Statistics-Theory and Methods, 48(14), 3423-3438.

16. Mazucheli, J., Menezes, A. F. B., Fernandes, L. B., De Oliveira, R. P., & Ghitany, M. E. (2020). The unit-Weibull distribution as an alternative to the Kumaraswamy distribution for the modeling of quantiles conditional on covariates. Journal of Applied Statistics, 47(6), 954-974.

17. Modi, K., & Gill, V. (2020). Unit Burr-III distribution with application. Journal of Statistics and Management Systems, 23(3), 579-592.

18. Demirci Biçer, H., & Biçer, C. (2022). Unit Ishita Distribution with Inference. Research & Reviews in Science and Mathematics.

19. Krishna, A., Maya, R., Chesneau, C., & Irshad, M. R. (2022). The Unit Teissier Distribution and Its Applications. Mathematical and Computational Applications, 27(1), 12.

20. Abramowitz, M., Stegun, I. A., & Romer, R. H. (1988). Handbook of mathematical functions with formulas, graphs, and mathematical tables.

21. Corless, R.M.; Gonnet, G.H.; Hare, D.E.G.; Jeffrey, D.J.; Knuth, D.E. On the Lambert W function. Adv. Comput. Math. 1996, 5, 329–359.

22. Eaton, J. W., Bateman, D., Hauberg, S., & Wehbring, R. (2019). GNU Octave version 4.0. 0 manual: a high-level interactive language for numerical computations. 2015. URL http://www. gnu. org/software/octave/doc/interpreter, 8, 13.

23. Team, R. C. (2013). R: A language and environment for statistical computing.

24. Swain, J. J., Venkatraman, S., & Wilson, J. R. (1988). Least-squares estimation of distribution functions in Johnson's translation system. Journal of Statistical Computation and Simulation, 29(4), 271-297.

25. Ranneby, B. (1984). The maximum spacing method. An estimation method related to the maximum likelihood method. Scandinavian Journal of Statistics, 93-112.

CHAPTER 6

ZERO RADIAL TIDES WORMHOLES IN F(R,Φ,X) THEORY

Erkan ERASLAN [1]

Melis ULU DOĞRU[2]

1 Çanakkale Onsekiz Mart University, School of Graduate Studies, Department of Physics. Çanakkale, TURKEY, erkan.eraslan@comu.edu.tr

2 Assoc. Prof. Dr., Çanakkale Onsekiz Mart University, Science Faculty, Department of Physics. Çanakkale, TURKEY, melisulu@comu.edu.tr

1. INTRODUCTION

Humans have tried to explain and understand the universe throughout its history. Many theories have been put forward describing the universe. Early theories were limited to the area that humans could see. The early ones of these theories were far from scientific discipline and based on myths. The first known depiction of the universe is the world map created by Babylonian priests. The universe is depicted as a tray floating in an ocean. This map, with the Euphrates in the middle, includes only the Mesopotamian region where Babylonians lived (Horowitz, 1988).

Anaximander was the first person to design the universe with observation and rational thinking. He thought of the earth as cylindrical in terms of shape. The earth hangs in the void. He used symmetrical circles. Later, Aristotle described the universe in a spherical way. Earth is located at the center of the universe. The universe consists of nested spheres. The innermost sphere is the earth, followed by the Moon, Mercury, Venus, Sun, Mars, Jupiter, Saturn and the outermost sphere of the stars. He divided the universe into two sub-lunar and superlunar. The superlunar sphere is immutable. All celestial bodies are fixed in their spheres. Switching between spheres is not allowed. Aristarchus put forward the first heliocentric theory. The sun is located in the center of the stellar sphere. All celestial bodies, including the earth, revolve around the sun. Later, Ptolemy put Aristotle's geocentric theory on a mathematical basis. According to him, all other celestial bodies revolve around the earth in circular motion. The sphere with the fixed stars is the end of the universe. He developed a system called the circle-centered mechanism to explain the retrograde motion of the planets. The Ptolemaic system was accepted for many years (Wolpert, 2002).

Copernicus reintroduced the heliocentric model of the universe belonging to Aristarchus. He proposed that the celestial spheres were circular and in perfect shape. Although it does not make these propositions with scientific methods, it is revolutionary. Brahe opposed the heliocentric model of the universe proposed by Copernicus. This model both did not fit Aristotelian physics and was inconsistent with his belief. Brahe collected data by observing the sky for many years. But these data dealt a great blow to Aristotelian physics. Later, Kepler explained planetary kinematics with three laws named after him. He abandoned circular orbits and proposed elliptical orbits. In the same period, Galileo deeply shook Aristotle's physics with his famous tower of Pisa experiments related to kinematics. He studied the movements of other planets in the solar system with the telescope he developed. By preparing the basis of kinematic laws with

falling body and oscillation experiments, he opened the doors of dynamical laws to Newton (Hawking, 2009).

Newton saw that Kepler's laws describe the acceleration field. He sensed this acceleration field as a force field from the dynamic viewpoint. He interpreted that this force field is a gravitational field and that both sun and the planets apply this force to each other because they appear symmetrical in terms of their masses. Newton was the first to suggest that this situation is valid in the entire universe (Özemre, 1982).

The main problem of gravity is to determine the field strength for a given mass distribution. For this, it is necessary to calculate the field strength by determining the gravitational potential from the Poisson equation. Classical Gravitation Theory has been successful in determining the orbits of planets and other celestial bodies. First Neptune, then Pluto was discovered only with the help of calculations. Despite all the successes of the Classical Theory of Gravitation, there have been some situations that it cannot explain. The main ones are; orbital motion of Mercury, direct deflection of light passing near celestial bodies, it is the phenomenon where the frequency of light decreases as it passes through a gravitational field. Einstein's General Theory of Relativity (GTR) explained these phenomena. GTR is based on equivalence principle, geodetic principle and general covariance principle (Özemre, 1982).

Cosmological observations in the past years reveal the inadequacies of GTR in explaining the universe (Filippenko & Riess, 1988). A need has arisen for alternative theories for the different phases of the universe that could explain the early inflation and late expansion. In addition, these theories must be related to dark matter and dark energy structures.

This study includes the investigation of Zero Radial Tides (ZRT) wormholes within the scope of $f(R,\Phi,X)$ theory, which is one of the alternative gravity theories. This study is planned as follows: In Section 2, $f(R,\Phi,X)$ theory is presented. In Section 3, ZRT wormholes and cosmic matter form are defined. In Section 4, ZRT wormholes solutions are given within the scope of $f(R,\Phi,X)$ theory.

2. AN ALTERNATIVE GRAVITATION THEORY: $f(R,\Phi,X)$ GRAVITY

Defining an effective theory of gravity and explaining all phases and structure of the universe with a single theory is still main problem of

today's cosmology. The cosmological constant term, which was not added to the field equations as an expected result of tensor algebra and variational calculus in GTR, is an extra term that describes the expanding dynamism of the universe in a limited way. The limited success of this extra term has prompted the search for such terms to be added to the Einstein Tensor in field equations due to the nature of mathematics and physics. Therefore, recent studies have applied to differences in defining the Lagrangian density, which is used to describe the matter-area-geometry relationship. This difference has led to the proposition of many alternative gravitational theories. $f(R,\Phi,X)$ theory is one of the alternative gravity theories. In addition, it is a hybrid theory influenced by $f(R,\Phi,X)$ theory, $f(R)$ theory and k-essence theories. $f(R,\Phi,X)$ theory is considered by the action (Hwang ve Noh, 2002; Tsujikawa, 2007):

$$S = \frac{1}{16\pi G}\int \sqrt{-g}\, f(R,\Phi,X)\, d^4x + S_m \qquad (1)$$

where S_m represents action of matter. R, Φ, X denote Ricci scalar, scalar potential and the kinetic term, respectively. In this theory, the awareness of a function, not Ricci scalar itself, which would naturally add the term cosmological constant, is one of the considerations. As in scalar-tensor theories, it is thought that scalar field is a factor affecting the geometry of the universe in order to bring the scalar field contribution, which is responsible for the early expansion, to the field equations. Also, it has been taken into account, together with others, that kinetic factors may contribute to validity in different scales and due to the expanding structure. X kinetic term is defined as:

$$X(\phi) = -\frac{1}{2}[\partial^\alpha\phi\partial_\alpha\phi]\xi \qquad (2)$$

here ξ parameter can be processed as +1 or -1. The sign of the constant is determined by the canonical and/or non-canonical scalar fields. In this study, we consider ξ =1. In addition, as the GTR action is known as:

$$S = \frac{1}{16\pi G}\int \sqrt{-g}Rd^4x + S_m, \qquad (3)$$

From equation (3), GTR field equations are produced as:

$$R_{ik} - \frac{1}{2}g_{ik}R + \Lambda g_{ik} = \chi T_{ik}. \qquad (4)$$

In f(R,Φ,X) theory, unlike GTR, field equations are defined as follows:

$$FG_{ik} - \frac{1}{2}(f - RF)g_{ik} - \nabla_i\nabla_k F + g_{ik}\nabla_\alpha\nabla^\alpha F - \frac{\varepsilon}{2}H(\nabla_i\phi)(\nabla_k\phi) = T_{ik}. \qquad (5)$$

Here $F \equiv \frac{df}{dR}$ and $H \equiv \frac{df}{dX}$, ∇_i indicates the covariant derivative. As seen in equation (4), the left side represents the geometric structure and the right side represents the matter structure. In addition to the field equations of the GTR, the terms of $-\frac{1}{F}\nabla_i\nabla_k F$, $\frac{1}{F}g_{ik}\nabla_\alpha\nabla^\alpha F$, $-\frac{1}{F}\frac{\varepsilon}{2}H(\nabla_i\phi)(\nabla_k\phi)$ and $-\frac{1}{F}\frac{1}{2}(f-RF)g_{ik}$ come to the left side as the contribution of the $f(R)$ and k-essence theories, and to the right side as the contribution of the $\frac{1}{F}$ factor $f(R)$ theory. Since scalar field propagates in the form of waves, it is expected that the scalar field will satisfy the wave equation in scalar tensor theories. Klein-Gordon wave equation for the $f(R,\Phi,X)$ theory is given by:

$$\nabla_i\left(H\nabla^i\phi\right)+\varepsilon N=0 \tag{6}$$

where $N \equiv \frac{df}{d\phi}$ defined as (Tsujikawa, 2007).

2. ZERO RADIAL TIDES (ZRT) WORMHOLES

Wormholes are structures that are thought to connect two different space-times like a bridge. It was first put forward by Einstein and Rosen in 1935. As a result of eliminating singularities in Schwarzschild solution, it provides a solution without singularity and horizon. Because wormholes combine two different space-times, they are frequently encountered in studies such as time and space travel. It is thought that there are numerous wormholes on the Planck scale in the universe (Lemos et al, 2003). These wormholes are so small that it is impossible to pass through them. However, these wormholes can reach a passable size if supported by exotic materials (Morris & Thorne, 1988). The metric that defines the ZRT wormholes geometry is:

$$ds^2=-dt^2+\left(1-\frac{b(r)}{r}\right)^{-1}dr^2+r^2(d\theta^2+sin^2\theta d\phi^2). \tag{7}$$

These wormholes do not have or move any tide in the radial direction. The supporting cosmic matter form may be fluid with impaired anisotropy. Energy-Momentum tensor is defined as:

$$T_{ik}=(p+\rho)u_iu_k+pg_{ik} \tag{8}$$

where ρ energy density, p pressure and u_i comoving vectors specifies. Wormholes can also be a way of crossing into other universes, due to their ability to connect different regions of space-time. For this, they need to be supplemented with exotic substances. In order for the wormhole to be passable, the throat radius of the wormhole is assumed to be in the range

of $r_0 \leq r < +\infty$. The redshift function must have finite values everywhere, while the shape function must satisfy the following values (Aygün, 2007);

$$b(r_0) = r_0, \tag{9}$$

$$b(r_0)' < 1, \tag{10}$$

$$b(r_0) < r, r > r_0. \tag{11}$$

Lorentzian wormholes must satisfy Eqs.(9)-(11) to be traversable. If the structure of a wormhole has conformal, rotating, charged and similar equipment, the traversability conditions differ from these equations. The next section examines solutions for both types of ZRT wormholes.

3. ZRT WORMHOLES in $f(R, \Phi, X)$ THEORY

The field equations for perfect fluid with the ZRT wormholes space-time and Klein-Gordon Equation are obtained from Eqs. (5)-(8) as follows:

$$(-6r^2F'' - 3r^2\epsilon H{\Phi'}^2)\big(r - b(r)\big) + \big(3r^2b(r)' + 4r^2 - 7rb(r)\big)F' + 4Fb(r)'r - 8Fb(r) + 2r^3(3p - 5\rho) = 0, \tag{12}$$

$$(-2rF'' - r\epsilon H{\Phi'}^2)\big(r - b(r)\big) + \big(b(r)'r - 4r + 3b(r)\big)F' + 4b(r)'F - 6r^2(p - \rho) = 0, \tag{13}$$

$$2r\big(r - b(r)\big)H'\Phi' + (2 - 3b(r) - b(r)' + 2r)H\Phi' + 2r\big(r - b(r)\big)H\Phi'' + 2\epsilon Nr^2) = 0. \tag{14}$$

Here, prime indicates the partial derivative with respect to the radial coordinate *r*. A joint solution of Eqs. (12)-(14) 's is given as:

$$F(r) = C_1, \tag{15}$$

$$N(r) = C_2C_3X(r)^{C_3-1}, \tag{16}$$

$$H(r) = \frac{C_1b(r)'r - 3b(r)}{{\Phi'}^2\epsilon r^2(r - b(r)}\quad , \tag{17}$$

$$\rho(r) = \frac{C_1(b(r)'r + b(r))}{2r^3(w+1)}\quad , \tag{18}$$

$$p(r) = \frac{wC_1(b(r)'r + b(r))}{2r^3(w+1)}. \tag{19}$$

As is commonly known, isotropic fluid cosmic matter satisfies Equation of State which shows that pressure and density are directly proportional (*w* is the proportionality coefficient). The Equation of State is taken into account in the solutions. As can be seen, obtained values of $p(r)$ and $\rho(r)$ change according to state of $b(r)$ function. Therefore, it is possible to review several sub-states in more detail with the shape function, which points to different wormhole models.

(i) Zero Density Wormholes

Zero density wormholes are a type of wormhole that was investigated by Kuhfittig and Visser at different times and associated with Hayward black holes (Kuhfittig, 2014; Visser, 1996). The shape function of zero density wormholes, which has gained importance with studies showing that singularity in black holes can transform into the mass of the matter source of the wormhole, is $b(r) = r_0$. Here, r_0 indicates the minimum throat radius of the wormhole. The wormhole geometry obtained when we consider the shape function as $b(r) = r_0$ is given in Fig 1.

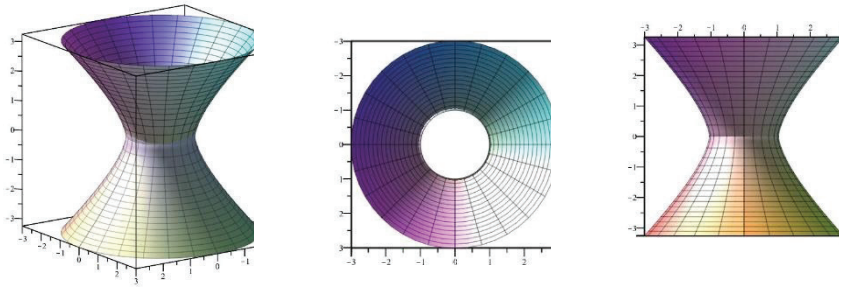

(a) General View (b) Top View (c) Side View

Fig.1. ZRT Wormholes in the case of zero density condition such as $b(r) = r_0$, $(C_1 = 1)$.

In this case, density and pressure given by Eqs. (18)-(19) are obtained as $\rho(r) = \frac{C_1 r_0}{2r^3(w+1)}$ and $p(r) = \frac{wC_1 r_0}{2r^3(w+1)}$, respectively. The pressure and energy density changes of fluid filling ZRT wormholes in the case of $b(r) = r_0$ for the positive and negative values of *w* are shown in Fig. 2 and Fig. 3.

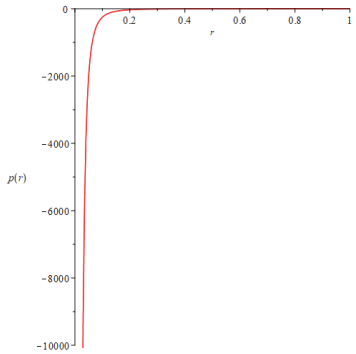

(a)

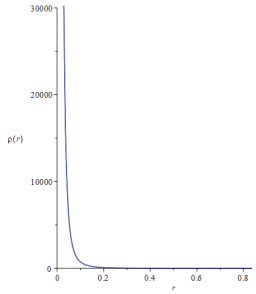

(b)

Fig.2. (a) Pressure and (b) Energy Density of ZRT Wormholes in the case of zero density condition such as $b(r) = r_0$, ($C_1 = 1$ $w = -\frac{1}{3}$).

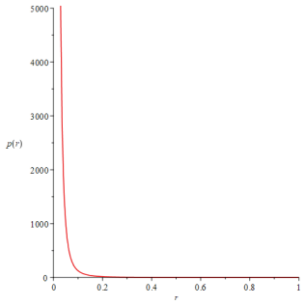

(a)

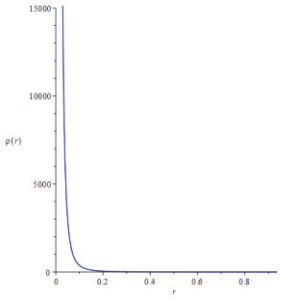

(b)

Fig.3. (a) Pressure and (b) Energy Density of ZRT Wormholes in the case of zero density condition such as $b(r) = r_0$, ($C_1 = 1$ $w = \frac{1}{3}$).

(ii) Visser Kar Dadhich Wormholes

Visser Kar Dadhich wormholes use a small amount of exotic matter to create traversable wormholes. All considered models are special Schwarzschild Blackhole models. The shape function of Visser Kar Dadhich wormholes is defined as $b(r) = 2m$ (Visser *et. al.,* 2003). Here, m indicates the small mass of the exotic matter filling with wormhole. The

wormhole geometry obtained when we consider the shape function as $b(r) = 2m$ is given in Fig 4.

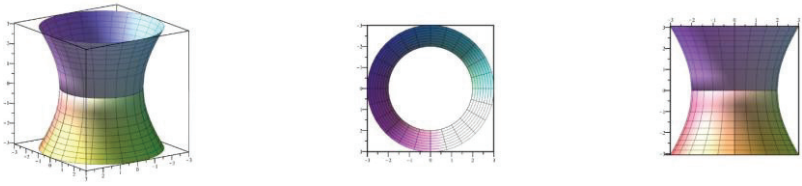

(a) General View (b) Top View (c) Side View

Fig.4. ZRT Wormholes in the case of Visser Kar Dadhich condition such as $b(r) = 2m$, $(C_1 = 1)$.

In this case, density and pressure given by Eqs. (18)-(19) are obtained as $\rho(r) = \frac{2mC_1}{2r^3(w+1)}$ and $p(r) = \frac{w2mC_1}{2r^3(w+1)}$, respectively. The pressure and energy density changes of fluid filling ZRT wormholes in the case of $b(r) = 2m$ for the positive and negative values of *w* are shown in Fig. 5 and Fig. 6.

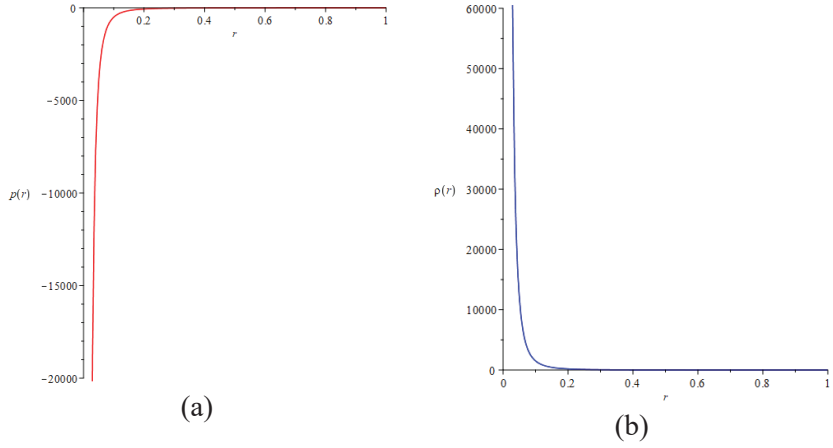

(a) (b)

Fig. 5. (a) Pressure and (b) Energy Density of ZRT Wormholes in the case of Visser Kar Dadhich condition such as $b(r) = 2m$, $(C_1 = 1\ w = -\frac{1}{3})$.

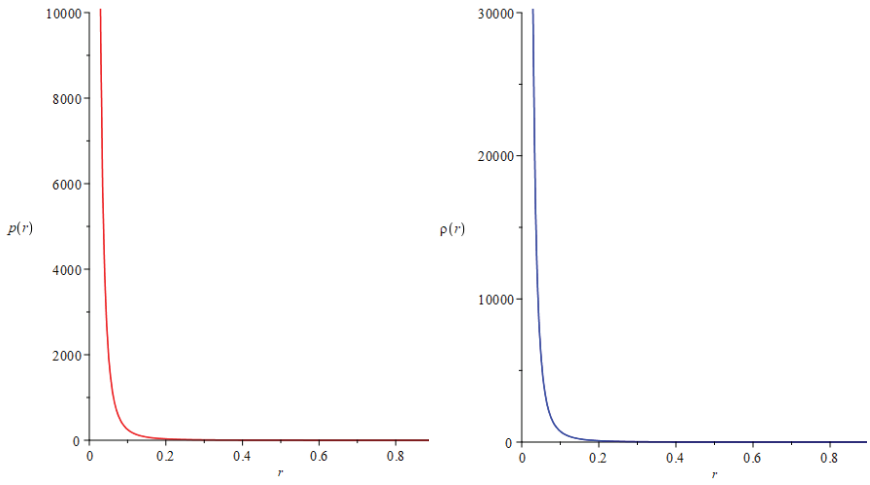

(a) (b)

Fig. 6. (a) Pressure and (b) Energy Density of ZRT Wormholes in the case of Visser Kar Dadhich condition such as $b(r) = 2m$, $(C_1 = 1\ w = \frac{1}{3})$.

(iii) ZRT Wormholes with $b(r_0) = r^n$

In this part, a shape function that increases exponentially with radial coordinate is used. The exponent of the radial coordinate directly affects whether the resulting wormhole is traversable. While the wormhole geometry obtained when we consider the shape function as $b(r) = r^n$ and $0 < n < 1$, is given in Fig 7, another wormhole geometry obtained when we consider the shape function as $(r) = r^n$ and $1 < n$ is given in Fig 8.

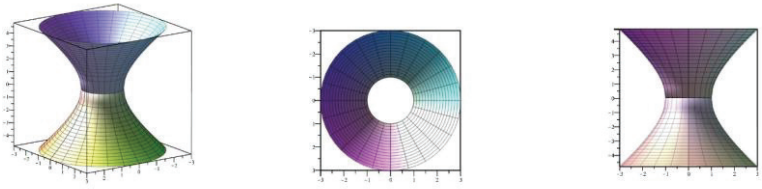

(a) General View (b) Top View (c) Side View

Fig.7. ZRT Wormholes in the case of $b(r) = r^n$, $(C_1 = 1, n = \frac{1}{2})$.

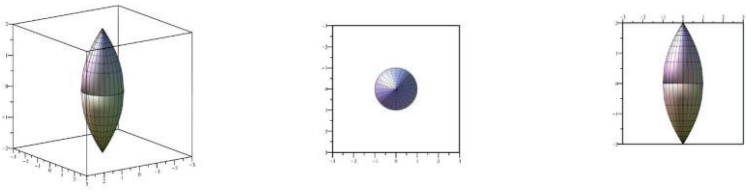

(a) General View (b) Top View (c) Side View

Fig.8. ZRT Wormholes in the case of $b(r) = r^n$, $(C_1 = 1, n = 2)$.

As it is clear from Fig.7, general traversable wormhole model can be defined that satisfies field equations of the theory without having a throat singularity. Traversable wormholes that allow this solution also provide Eqs. (9)-(11). For this type of wormholes models, which is a static and Lorentzian model, when omega is negative in the Equation of State, the matter filling the geometry becomes a negative pressure fluid.

In this case, density and pressure given by Eqs. (18)-(19) are obtained as $\rho(r) = \frac{C_1 r^{n(n+1)}}{2r^3(w+1)}$ and $p(r) = \frac{wC_1 r^{n(n+1)}}{2r^3(w+1)}$, respectively. If *w* is negative, the pressure and energy density change, which indicates the exotic matter that supports traversability, is shown in the Fig.9. It is understood that this type of wormhole model can only be valid for $w < 0$ in the range of $0 < n < 1$ because of the shape function that provides the traversability conditions. On the other hand, if *w* is positive, the pressure and energy density change, which indicates the normal matter that violates traversability, is shown in the Fig.10. It is understood that this type of wormhole model can only be valid for $w > 0$ in the range of $1 < n$ because of the shape function that violates the traversability conditions.

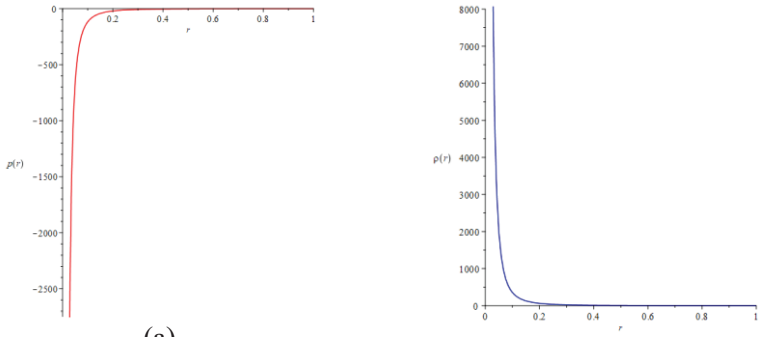

(a) (b)

Fig. 9. (a) Pressure and (b) Energy Density of ZRT Wormholes in the case of $b(r) = r^n$, ($w = -\frac{1}{3}, n = \frac{1}{2}$).

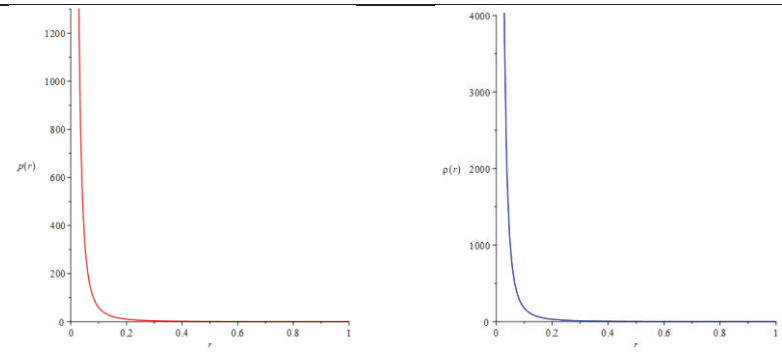

Fig. 10. (a) Pressure and (b) Energy Density of ZRT Wormholes in the case of $b(r) = r^n$, ($w = \frac{1}{3}, n = 2$).

5. CONCLUSION

In this study, alternative gravitational theories, one of the most fundamental problems that have been researched throughout the history of cosmology but still have not found an answer, are mentioned. In today's cosmology, attention has been drawn to the theory of gravity, which has just been proposed. The basic equations of the $f(R, \Phi, X)$ theory are remembered. Wormholes, which are thought to connect two independent regions in the universe with a tube, have been taken into account. Fluid distribution, which is considered as the source of ZRT wormholes, has been investigated within the scope of $f(R, \Phi, X)$ theory. The obtained

solutions of field equation are gained for traversable and non-traversable wormhole geometries. As a result, $f(R,\Phi,X)$ theory allows the distribution of exotic matter as a source for geometrically traversable wormholes. On the other hand, it supports that normal matter can be matter source for the wormhole geometry that has lost its traversability feature. In this context, the idea that $f(R,\Phi,X)$ theory supports previously obtained solutions in the literature and can be accepted as a coherent theory of gravity is supported.

6. ACKNOWLEDGEMENT

This study is a part of the master's thesis titled with "f(R, Φ, X) Theory" prepared by Erkan Eraslan and was supported by Çanakkale Onsekiz Mart University Scientific Research Projects Coordination Unit. Project Number: 4201.

7. REFERENCES

Aygün, M. (2007). Kurt delikleri, karanlık enerji ve madde ilişkileri.

Einstein, A., & Rosen, N. (1935). The particle problem in the general theory of relativity. *Physical Review*, *48*(1), 73.

Filippenko, A. V., & Riess, A. G. (1998). Results from the high-z supernova search team. *Physics Reports*, *307*(1-4), 31-44.

Hawking, S. (2009). Galileo and the birth of modern science. *American Heritage's Invention & Technology*, *24*(1), 36.

Hwang, J. C., & Noh, H. (2002). Cosmological perturbations in a generalized gravity including tachyonic condensation. Physical Review D, 66(8), 084009

Horowitz, W. (1988). The Babylonian map of the world. *Iraq*, *50*, 147-165.

Kuhfittig, P. (2014), Aditi J. of Mathematical Physics, 5, 25-34.

Lemos, J. P., Lobo, F. S., & de Oliveira, S. Q. (2003). Morris-Thorne wormholes with a cosmological constant. *Physical Review D*, *68*(6), 064004.

Morris, M. S., Thorne, K. S., & Yurtsever, U. (1988). Wormholes, time machines, and the weak energy condition. *Physical Review Letters*, *61*(13), 1446.

Özemre, A. Y. (1982). *Gravitasyonun rölativist teorileri*. İÜ.

Tsujikawa, S. (2007). Matter density perturbations and effective gravitational constant in modified gravity models of dark energy. Physical Review D, 76(2), 023514.

Visser, M. (1996). Lorentzian wormholes: from Einstein to Hawking, New York, SpringerVerlag.

Visser, M., Kar, S. and Dadhich,N. (2003). Traversable Wormholes with Arbitrarily Small Energy Condition Violations. *Phys. Rev. Lett.* 90, 201102.

Wolpert, L. (2002). *Science and mathematics in ancient Greek culture*. Oxford University Press on Demand.

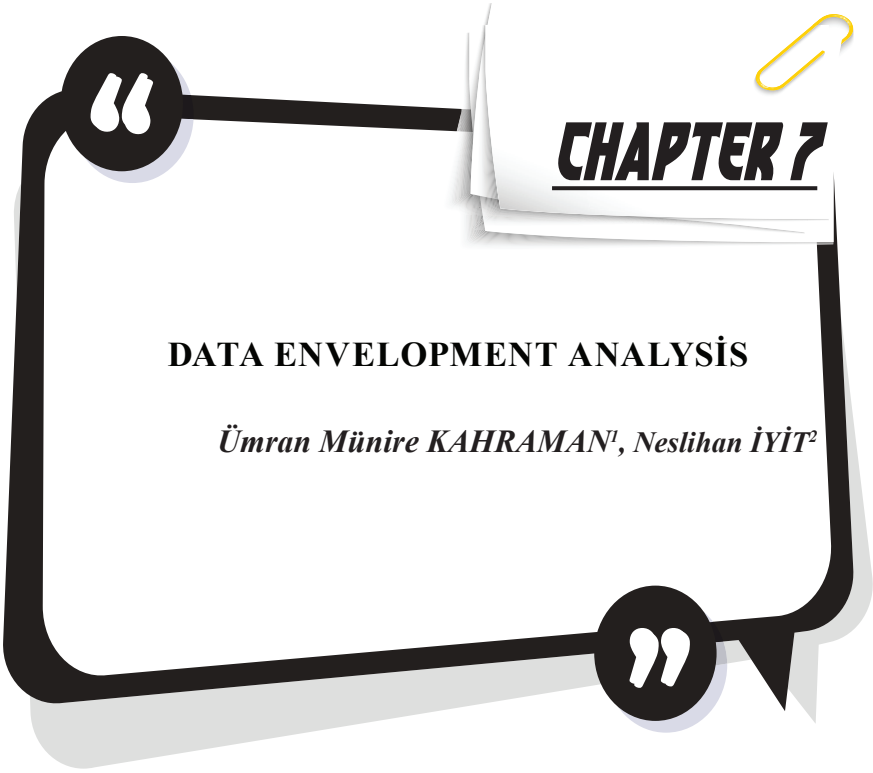

CHAPTER 7

DATA ENVELOPMENT ANALYSİS

Ümran Münire KAHRAMAN[1], Neslihan İYİT[2]

1 Assist.Prof., Department of Business, Faculty of Political Science, Necmettin Erbakan University, Konya, Türkiye, ukahraman@erbakan.edu.tr, ORCID ID: 0000-0002-9840-0461

2 Corresponding Author: Assoc.Prof.Dr., Department of Statistics, Faculty of Science, Selcuk University, Konya, Türkiye, niyit@selcuk.edu.tr,

ORCID ID: 0000-0002-5727-6441

1. Introduction

Data envelopment analysis (DEA), a non-parametric performance measurement method, allows measuring the performance of different organizations taken as Decision Making Units (DMU) at the same time using various input and output variables. By using these inputs and outputs with mathematical programming, the objective function for each DMU is optimized and a solution set that optimizes the efficiency as a measure of performance is determined.

The calculation of the efficiency of DMUs is based on the principle of dividing the weighted sum of the outputs by the weighted sum of the inputs. The efficiency calculated with DEA method will be an indicator of pruductivity in the mean of performance.

After the concept of technical efficiency emerged in the field of economics, Farrel (1957) used the concept of efficiency instead of productivity. And then Charnes et al. (1978) developed a linear programming (LP) problem and the dual of the LP problem as the basis for DEA (Cooper et al., 2011). By using DEA method, the relative effectiveness of a feature is measured, that is, the effectiveness of DMUs is compared to each other using the same inputs and outputs features.

As a result of linear programming, DMUs with an objective function equal to 1 are determined as effective. On the other hand, DMUs with an objective function not equal to 1 are tried to be compared to one of the efficiency value equals to one. Thus, the actions to be taken to activate the inefficient units are determined (Banker, 1992). Efficiency reviews are conducted for commercial firms, government agencies, nonprofits, educational institutions, police forces, hospitals and military units.

2. DEA Mathematical Programming Models

For DEA, the CCR (Charnes – Cooper – Rhodes) model, some additional models based on the CCR model, the BCC (Banker - Charnes – Cooper) model and the additive model are methods based on mathematical programming.

2.1. CCR Ratio Model

The model developed by Charnes et al. (1978) considers the proportional model for maximizing the efficiency when there are n number

of DMUs in the DEA method. Maximizing the efficiency, which is the ratio of the weighted sum of the outputs to the weighted sum of the inputs, can be expressed as a function of the weights;

$$\max f_o(u,v) = \frac{\sum_{r=1}^{s} u_r y_{ro}}{\sum_{i=1}^{m} v_i x_{io}} \quad (1)$$

Here, x_{io} is the i^{th} input amount $(i = 1,2,\dots,m)$ for the o^{th} DMU, and y_{ro} shows the output amount for $r = 1,2,\dots,s$. u_r and v_i are the weights of the outputs and inputs, respectively (Cooper et al., 2011).

Charnes and Cooper (1962) created an input-oriented model by transforming linear programming to determine the relative efficiency of a $\text{DMU}_j = DMU_o$ for $j = 1,2,\dots,n$. The LP problem given in Eq. (1) is taken as the objective function as follows (Cooper et al., 2011);

$$max \ \sum_{r=1}^{s} \mu_r y_{ro}$$

subject to

$$\sum_{r=1}^{s} \mu_r y_{rj} - \sum_{i=1}^{m} v_i x_{ij} \le 0, j = 1,2,\dots,n \quad (2)$$

$$\sum_{i=1}^{m} v_i x_{io} = 1$$

$$\mu_r \ge 0, r = 1,2,\dots,s$$

$$v_i \ge 0, i = 1,2,\dots,m$$

where μ_r represents the transformed output weights. The dual form of the LP problem is also as follows (Talluri, 2000; Lotfi et al., 2020);

$$minQ$$

subject to

$$\sum_{j=1}^{n} x_{ij}\lambda_j - Qx_{io} \le 0, j = 1,2,\dots,n \quad (3)$$

$$\sum_{r=1}^{s} y_{rj}\lambda_j \ge y_{ro}$$

$$\lambda_j \geq 0$$

where, Q is the efficiency score and λ_j's are dual variables.

2.2. BCC Ratio Model

BCC model is emerged by Banker et al. (1984) and Banker and Thrall (1992) by adding the convexity constraint to the CCR model. The BCC model includes the concept of returns to scale (RTS).

A proportional increase in inputs leading to a less increase in output is called a decreasing RTS, and a proportional increase in inputs leading to a greater increase in output is called an increasing RTS. CCR model depends on the assumption of constant RTS. On the other hand, BCC model depends on changeable RTS.

LP problem according to BCC model can be given as follows (Cooper et al., 2011);

$$max \ \sum_{r=1}^{s} \mu_r y_{ro} - u_o$$

subject to

$$\sum_{r=1}^{s} \mu_r y_{rj} - \sum_{i=1}^{m} v_i x_{ij} - u_o \leq 0, j = 1,2,\dots,n \qquad (4)$$

$$\sum_{i=1}^{m} v_i x_{io} = 1$$

$$\mu_r \geq \varepsilon$$

$$v_i \geq \varepsilon$$

u_o free in sign

If the optimal solution obtained as a result of the BCC model is interpreted by comparing with the CCR model, the scale efficiency can be revealed (Oruç, 2008). However, the u_o variable is interpreted according to its received value. A positive value of u_o indicates decreasing RTS, a

negative value of u_o indicates increasing RTS, and a value of zero indicates constant returns to scale (Özgür, 2007).

2.3. Additive Model

For some DMU_os, having slacks on inputs and outputs will lead to weak efficiency. It is undesirable as it can bring alternative optimal solutions with weak efficiency. The additive model expresses the slacks to maximize with a LP problem. Thus, the situation of weak efficiency in terms of both inputs and outputs is eliminated. Unlike the proportional model, the efficiency score cannot be calculated for DMU_os as a result of the additive model (Cooper et al., 2011).

3. Input or Output Orientation in Data Envelopment Analysis

DEA models can be examined in two groups as input-oriented and output-oriented. Input-oriented implementation is about cost reduction for a production variable in inefficient DMUs. With the reductions that can be made on the inputs, it is aimed to ensure efficiency without causing a change in the output level.

Output-oriented applications, similar to input-oriented applications, are studies based on improving the performance for the output variable. If no change can be made on the input's amounts, it is expected to be able to obtain more outputs with the same level of inputs.

4. Stages and Implementation of Data Envelopment Analysis

In this section, the steps to perform a DEA application will be explained by applying on a dataset.

4.1. Identification of Decision Making Units

DMUs should be units in which the same input and output values can be determined, included in the same market conditions. The number of inputs and outputs are important for the number of DMUs in DEA. Since the weights assigned to the inputs and outputs are free, the number of DMUs is recommended as $n \geq 2(m + s)$ so that the DEA can discriminate the efficiency values well.

In the application part of this study, a simulated data set is determined as DMUs, inputs and outputs.

4.2. Identifying Inputs and Outputs

There are no model restriction or measuring unit constraints on the inputs and outputs to be used to measure the effectiveness of the DMUs in DEA method. However, the fact that the inputs and outputs consist of very different quantities such as ratios and high-value variables affect the solution results of DEA and this situation may lead to inconsistency. For this reason, the inputs and outputs in the DEA method should not differ much in size.

The data set consisting of 3 inputs and 3 outputs for 15 DMUs is given in Table 1.

Table 1. The Data Set of Inputs and Outputs for DMUs in DEA Implementation

	Outputs			**Inputs**		
DMUs	y_1	y_2	y_3	x_1	x_2	x_3
DMU1	223018934	232643535	6576420	25015	38382438	357761365
DMU2	150262839	158354333	2558265	16956	21316946	231440818
DMU3	123838377	147712375	2703042	15615	19238711	212539905
DMU4	6317	0	1655	29	46771	54960
DMU5	158878192	161827908	4528712	14000	30654582	271016470
DMU6	9200350	8794868	175380	1784	1520266	12454162
DMU7	9621503	11441272	114915	1488	1289866	15393509
DMU8	16136281	17605982	125194	3611	2532793	23818856
DMU9	1098668	1030266	5220	225	194908	1508704
DMU10	49832658	56363829	941799	9640	7799401	79727390
DMU11	177359976	204257243	4701206	24756	35960981	311625913
DMU12	154274856	172624217	2932795	18366	26118547	252819538
DMU13	23155134	21843075	217609	3816	2279593	32850738
DMU14	31901763	28412441	541966	5550	3912064	48476955
DMU15	21064781	25599230	296233	4001	3663014	38807717

4.3. Relative Efficiency Measurement with Data Envelopment Analysis

In this section, the LP problems created for the input-oriented CCR, CCR Dual and BCC models for the dataset and their results are given. The analyzes are made using the codes prepared by Lotfi et al. (2020) with the RStudio program.

4.3.1. CCR Ratio Model Application

The LP problem given by Eq. (2) is formed based on the data given in Table 1 for DMU1 as follows;

max 223018934μ1 + 232643535μ2 + 6576420μ3 subject to (5)

223018934μ1+232643535μ2+6576420μ3-25015v1-38382438v2-357761365v3<=0

150262839μ1+158354333μ2+2558265μ3-16956v1-21316946v2-231440818v3<=0

123838377μ1+147712375μ2+2703042μ3-15615v1-19238711v2-212539905v3<=0

6317μ1+0μ2+1655μ3-29v1-46771v2-54960v3<=0

158878192μ1+161827908μ2+4528712μ3-14000v1-30654582v2-271016470v3<=0

9200350μ1+8794868μ2+175380μ3-1784v1-1520266v2-12454162v3<=0

9621503μ1+11441272μ2+114915μ3-1488v1-1289866v2-15393509v3<=0

16136281μ1+17605982μ2+125194μ3-3611v1-2532793v2-23818856v3<=0

1098668μ1+1030266μ2+5220μ3-225v1-194908v2-1508704v3<=0

49832658μ1+56363829μ2+941799μ3-9640v1-7799401v2-79727390v3<=0

177359976μ1+204257243μ2+4701206μ3-24756v1-35960981v2-311625913v3<=0

154274856μ1+172624217μ2+2932795μ3-18366v1-26118547v2-252819538v3<=0

23155134μ1+21843075μ2+217609μ3-3816v1-2279593v2-32850738v3<=0

31901763μ1+28412441μ2+541966μ3-5550v1-3912064v2-48476955v3<=0

21064781μ1+25599230μ2+296233μ3-4001v1-3663014v2-38807717v3<=0

25015v1+38382438v2+357761365v3=1

v1>=0, v2>=0, v3>=0, μ1>=0, μ2>=0, μ3>=0

The dual form of the input-oriented CCR model given by Eq. (3) for DMU1 can be given as follows;

min Q
subject to (6)

25015 Q – 25015 λ1- 16956 λ2 - 15615 λ3 - 29 λ4 - 14000 λ5- 1784 λ6 - 1488 λ7 – 3611 λ8- 225 λ9 – 9640 λ10 – 24756 λ11 – 18366 λ12 – 3816 λ13 – 5550 λ14- 4001 λ15 >=0
38382438 Q - 38382438 λ1- 21316946 λ2- 19238711 λ3- 46771 λ4- 30654582 λ5- 1520266 λ6- 1289866 λ7- 2532793 λ8- 194908 λ9- 7799401 λ10- 35960981 λ11- 26118547 λ12- 2279593 λ13- 3912064 λ14- 3663014 λ15 >=0
357761365 Q - 357761365 λ1- 231440818 λ2- 212539905 λ3- 54960 λ4- 271016470 λ5- 12454162 λ6- 15393509 λ7- 23818856 λ8- 1508704 λ9- 79727390 λ10- 311625913 λ11- 252819538 λ12- 32850738 λ13- 48476955 λ14- 38807717 λ15 >=0
223018934 λ1+ 150262839 λ2+ 123838377 λ3+ 6317 λ4+ 158878192 λ5+ 9200350 λ6+ 9621503 λ7+ 16136281 λ8+ 1098668 λ9+ 49832658 λ10+ 177359976 λ11+ 154274856 λ12+ 23155134 λ13+ 31901763 λ14+ 21064781 λ15 >=223018934

232643535 λ1+ 158354333 λ2+ 147712375 λ3+ 0 λ4+ 161827908 λ5+ 8794868 λ6+ 11441272 λ7+ 17605982 λ8+ 1030266 λ9+ 56363829 λ10+ 204257243 λ11+ 172624217 λ12+ 21843075 λ13+ 28412441 λ14+ 25599230 λ15 >=232643535
6576420 λ1+ 2558265 λ2+ 2703042 λ3+ 1655 λ4+ 4528712 λ5+ 175380 λ6+ 114915 λ7+ 125194 λ8+ 5220 λ9+ 941799 λ10+ 4701206 λ11+ 2932795 λ12+ 217609 λ13+ 541966 λ14+ 296233 λ15 >=6576420
λ1>=0, λ2>=0, λ3>=0, λ4>=0, λ5>=0, λ6>=0, λ7>=0, λ8>=0, λ9>=0, λ10>=0, λ11>=0, λ12>=0, λ13>=0,
λ14>=0, λ15>=0

4.3.2. BCC Ratio Model Application

In order to reveal the existence of variable RTS, BCC model in Eq. (4) is obtained by adding the u_o variable to the CCR ratio model in Eq. (2).

4.3.3. CCR and BCC Ratio Model Results

The efficiency scores calculated for the CCR ratio model and the estimations of the weight values of the inputs and outputs are given in Table 2. The efficiency scores obtained for the CCR dual ratio model are also the same.

Table 2. CCR Ratio Model Results for Inputs, Outputs and Efficiency Scores in DEA

DMUs	μ_1	μ_2	μ_3	v_1	v_2	v_3	Efficiency Scores
DMU1	0.00000000	0.00000000	0.00000003	0.00000030	0.00000001	0.00000000	0.97699
DMU2	0.00000000	0.00000000	0.00000004	0.00000229	0.00000001	0.00000000	1
DMU3	0.00000000	0.00000000	0.00000007	0.00000064	0.00000002	0.00000000	1
DMU4	0.00000000	0.00000000	0.00001820	0.00015822	0.00000000	0.00000032	1
DMU5	0.00000001	0.00000000	0.00000001	0.00001329	0.00000000	0.00000000	1
DMU6	0.00000011	0.00000000	0.00000000	0.00000000	0.00000000	0.00000008	1
DMU7	0.00000004	0.00000005	0.00000000	0.00000039	0.00000008	0.00000006	1
DMU8	0.00000003	0.00000003	0.00000000	0.00000022	0.00000004	0.00000004	1
DMU9	0.00000090	0.00000000	0.00000000	0.00000000	0.00000000	0.00000066	0.985763
DMU10	0.00000000	0.00000002	0.00000014	0.00000137	0.00000001	0.00000001	0.99386
DMU11	0.00000000	0.00000000	0.00000003	0.00000124	0.00000000	0.00000000	0.970682

DMU12	0.00000000	0.00000001	0.00000000	0.00002270	0.00000000	0.00000000	0.994297
DMU13	0.00000004	0.00000000	0.00000000	0.00000000	0.00000003	0.00000003	1
DMU14	0.00000002	0.00000000	0.00000053	0.00000463	0.00000012	0.00000001	1
DMU15	0.00000000	0.00000003	0.00000025	0.00000985	0.00000000	0.00000002	0.895069

The dual variable values obtained as a result of the CCR dual ratio model estimations are shown in Table 3.

Table 3. Dual Variables of CCR Dual Ratio Model in DEA

DMUs	DMU1	DMU2	DMU3	DMU4	DMU5	DMU6
λ1	1.0000	0.0000	0.0000	0.0000	0.0000	0.0000
λ2	0.0000	1.0000	0.0000	0.0000	0.0000	0.0000
λ3	0.0000	0.0000	1.0000	0.0000	0.0000	0.0000
λ4	0.0000	0.0000	0.0000	1.0000	0.0000	0.0000
λ5	0.0000	0.0000	0.0000	0.0000	1.0000	0.0000
λ6	0.0000	0.0000	0.0000	0.0000	0.0000	1.0000
λ7	0.0000	0.0000	0.0000	0.0000	0.0000	0.0000
λ8	0.0000	0.0000	0.0000	0.0000	0.0000	0.0000
λ9	0.0000	0.0000	0.0000	0.0000	0.0000	0.0000
λ10	0.0000	0.0000	0.0000	0.0000	0.0000	0.0000
λ11	0.0000	0.0000	0.0000	0.0000	0.0000	0.0000
λ12	0.0000	0.0000	0.0000	0.0000	0.0000	0.0000
λ13	0.0000	0.0000	0.0000	0.0000	0.0000	0.0000
λ14	0.0000	0.0000	0.0000	0.0000	0.0000	0.0000
λ15	0.0000	0.0000	0.0000	0.0000	0.0000	0.0000

DMU15	DMU14	DMU13	DMU12	DMU11	DMU10	DMU9	DMU8	DMU7
0.0010	0.0000	0.0000	0.0000	0.6046	0.0583	0.0000	0.0000	0.0000
0.0000	0.0000	0.0000	0.5046	0.0000	0.0000	0.0000	0.0000	0.0000
0.0000	0.0000	0.0000	0.5937	0.0000	0.0000	0.0000	0.0000	0.0000
0.0000	0.0000	0.0000	0.0000	0.0000	0.2727	0.0000	0.0000	0.0000
0.0000	0.0000	0.0000	0.0310	0.0000	0.0000	0.0000	0.0000	0.0000
0.4015	0.0000	0.0000	0.0000	0.9911	1.3044	0.1194	0.0000	0.0000
1.9088	0.0000	0.0000	0.0000	4.7969	2.7366	0.0000	0.0000	1.0000
0.0000	0.0000	0.0000	0.0000	0.0000	0.0000	0.0000	1.0000	0.0000
0.0000	0.0000	0.0000	0.0000	0.0000	0.0000	0.0000	0.0000	0.0000
0.0000	0.0000	0.0000	0.0000	0.0000	0.0000	0.0000	0.0000	0.0000
0.0000	0.0000	0.0000	0.0000	0.0000	0.0000	0.0000	0.0000	0.0000
0.0000	0.0000	0.0000	0.0000	0.0000	0.0000	0.0000	0.0000	0.0000
0.0000	0.0000	1.0000	0.0000	0.0000	0.0000	0.0000	0.0000	0.0000
0.0000	1.0000	0.0000	0.0000	0.0000	0.0000	0.0000	0.0000	0.0000
0.0000	0.0000	0.0000	0.0000	0.0000	0.0000	0.0000	0.0000	0.0000

BCC ratio model efficiency measurement results for DMUs are given in Table 4 where RTS are obtained by estimating the weights for inputs and outputs.

Table 4. BCC Ratio Model Results for Inputs, Outputs and Efficiency Scores in DEA

DMUs	μ_1	μ_2	μ_3	v_1	v_2	v_3	Efficiency Scores	u_o
DMU1	0.00000000	0.00000000	0.00000003	0.00000008	0.00000001	0.00000000	0.97699	-0.00102
DMU2	0.00000000	0.00000000	0.00000004	0.00000229	0.00000001	0.00000000	1	0
DMU3	0.00000000	0.00000000	0.00000007	0.00000064	0.00000002	0.00000000	1	0
DMU4	0.00000000	0.00000000	0.00001820	0.00015822	0.00000000	0.00000032	1	0
DMU5	0.00000001	0.00000000	0.00000001	0.00001329	0.00000000	0.00000000	1	0
DMU6	0.00000011	0.00000000	0.00000000	0.00000000	0.00000000	0.00000008	1	0
DMU7	0.00000004	0.00000005	0.00000000	0.00000039	0.00000008	0.00000006	1	0
DMU8	0.00000003	0.00000003	0.00000000	0.00000022	0.00000004	0.00000004	1	0
DMU9	0.00000090	0.00000000	0.00000000	0.00000239	0.00000000	0.00000066	1	0.016191
DMU10	0.00000000	0.00000001	0.00000013	0.00000064	0.00000002	0.00000001	1	-0.00339
DMU11	0.00000000	0.00000001	0.00000000	0.00000000	0.00000000	0.00000000	0.988778	-0.15727
DMU12	0.00000000	0.00000001	0.00000001	0.00002008	0.00000000	0.00000000	1	-0.05013
DMU13	0.00000004	0.00000000	0.00000000	0.00000000	0.00000003	0.00000003	1	0
DMU14	0.00000002	0.00000000	0.00000053	0.00000463	0.00000012	0.00000001	1	0
DMU15	0.00000000	0.00000004	0.00000000	0.00000828	0.00000000	0.00000002	0.918305	-0.02637

4.4. Reviews for the Input-Oriented Model

According to the results obtained from CCR dual ratio model, effective DMUs for ineffective units and the dual variable values given in Table 3 can be examined. The values of x_i^* for comparisons calculated by $x_i^* = \sum_{j=1}^{n} \lambda_j x_{ij}$ are given in Table 5.

Table 5. Target Input Values for Inefficiency DMUs in Input-Oriented DEA

DMUs	x_1^*	x_2^*	x_3^*
DMU1	25015	38382438	357761365
DMU2	16956	21316946	231440818
DMU3	15615	19238711	212539905
DMU4	6317	0	1655
DMU5	14000	30654582	271016470
DMU6	1784	1520266	12454162
DMU7	1488	1289866	15393509
DMU8	3611	2532793	23818856
DMU9	213.0379509	181543.9201	1487224.862
DMU10	9580.812619	7751514.474	79237882.18
DMU11	24030.19837	30900409.52	302489598.8
DMU12	18261.26598	23129243.2	251377808.3
DMU13	3816	2279593	32850738
DMU14	5550	3912064	48476955
DMU15	3581.170451	3110237.927	34735578.45

References

[1] Banker R.D. Charnes A. Cooper W.W. Some models for estimating technical and scale ınefficiencies in data envelopment analysis. Management Science. 1984; 30(9): 1078-1092.

[2] Banker R.D. Selection of efficiency evaluation models. Contemporary Accounting Research. 1992; 9(1): 343-355. https://doi.org/10.1111/j.1911-3846.1992.tb00885.x .

[3] Banker R.D. Thrall R.M. Estimation of returns to scale using data envelopment analysis. EJOR. 1992; 62(1): 74-84.

[4] Charnes A. Cooper W.W. Chance constraints and normal deviates. Journal of the American Statistical Association. 1962; 57(297): 134-148. https://doi.org/10.1080/01621459.1962.10482155 .

[5] Charnes A. Cooper W.W. Rhodes E. Measuring the efficiency of decision making unit. European Journal of Operational Research. 1978; 2(6): 429-444. https://doi.org/10.1016/0377-2217(78)90138-8.

[6] Cooper W.W. Seiford L.M. Zhu J. Handbook on data envelopment analysis. International Series in Operations Research & Management Science. 2nd ed. New York: Springer; 2011. https://doi.org/10.1007/978-1-4419-6151-8.

[7] Farrell M.J. The measurement of productive efficiency. Journal of the Royal Statistical Society: Series A (General). 1957; 120(3): 253-281.

[8] Lotfi F.H. Ebrahimnejad A. Vaez-Ghasemi M. Moghaddas Z. Data envelopment analysis with R. Studies in Fuzziness and Soft Computing. 1st ed. Switzerland: Springer Cham; 2020. https://doi.org/10.1007/978-3-030-24277-0 .

[9] Oruç K.O. Güngör İ. Bulanık veri zarflama analizi modellerinin karşıla ştırılması: Sınırlandırılmış veriler için. Suleyman Demirel University Jo urnal of Faculty of Economics & Administrative Sciences. 2010; 15(2): 417-442.

[10] Özgür E. Katılım bankalarının finansal etkinliği. Afyon Kocatepe Univ ersity Journal of the Faculty of Economics and Administrative Sciences . 2008; 10 (1): 159-175.

[11] Talluri S. Data envelopment analysis: models and extensions. Decision Line. 2000; 31: 8-11.